REGULATION OF CALCIUM INFLUX AND REACTIVE OXYGEN SPECIES PRODUCTION DURING INFECTION OF LEGUMES BY RHIZOBIA

SARAH SHAILES

A thesis submitted to the University of East Anglia for the degree of Doctor of Philosophy

John Innes Centre

January 2014

Contents

Publications

During the course of this project the following manuscript has been prepared:

Shailes, S. and Oldroyd, G.E.D (In press). Nod factor-induced calcium signaling in legumes.

Biological Nitrogen Fixation (Ed. De Brujin, F.J.), Wiley/Blackwell. *Includes material from Chapter 1.*

ABSTRACT

Nod factor (NF) can induce two separate calcium responses in legume root hairs. Nuclear-associated calcium spiking is central to the symbiosis signalling (Sym) pathway, which is necessary for the activation of genes required for nodule formation and bacterial infection. In addition NF activates a tip-focused calcium influx, which is less-well studied but is thought to be involved in bacterial infection. NF also activates ROS transient production at the tip of root hair cells. In this thesis I used fluorescent probes (Ca^{2+}-sensitive Cameleons YC2.1 and YC3.6 and the ROS-sensitive CM-H_2DCFDA dye) to characterise the NF-induced calcium influx and ROS transient responses in *Medicago truncatula.* Along with being spatially and temporally co-incident, the responses require similar concentrations of NF to be activated, are inhibited by the NADPH oxidase inhibitor diphenyleneiodonium and are dependent on the NF receptor NFP but independent of the Sym pathway components DMI1 and DMI2. These results suggest the NF-induced calcium influx and ROS transient are part of a common signalling pathway during bacterial infection.

ROP signalling is associated with ROS production and calcium influx during developmental root hair elongation. I assessed the role of ROPs during rhizobial infection in *M. truncatula* and found a ROP-activating protein, *MtGAP1,* was upregulated in root hairs during bacterial infection and is involved in normal root hair curling and infection thread development. Two pieces of evidence directly link ROP signalling with the NF-induced calcium influx: *gap1* mutants were hypersensitive for induction of the calcium influx, and there was a reduction in the number of calcium influx responses in *ROP9* RNAi knockdown lines. Drawing parallels between developmental root hair elongation and bacterial infection I propose a model for the regulation of ROP signalling by NF leading to root hair curling, the activation of the calcium influx and ROS transient, and infection thread formation.

ACKNOWLEDGEMENTS

LIST OF TABLES

LIST OF FIGURES

Continued overleaf

LIST OF ABBREVIATIONS

Abbreviation	Definition
AM	Arbuscular mycorrhizal
ADP	Adenosine 5'-diphosphate
ATP	Adenosine 5'-triphosphate
AVG	L-a-(2-aminoethoxyvinyl) glycine
BHQ	2',5'-di(tert-butyl)-1,4-benzohydroquinone
BLAST	Basic local alignment search tool
BNM	Buffered nodulation medium
CaM	Calmodulin
CBL	Calcineurin-B-like
CCaMK	Calcium/calmodulin-dependent protein kinase
CDPK	Calcium-dependent protein kinase
cDNA	Complementary deoxyribonucleic acid
CFP	Cyan fluorescent protein
CM-H$_2$DCFDA	5-(and-6)-chloromethyl-2',7'-dichlorodihydrofluorescein diacetate
CPA	Cyclopiazonic acid
CT	Threshold cycle
DMI	Does not make infections
DMSO	Dimethyl sulphoxide
DPI	Diphenyleneiodonium
DWA	Dionised water agar
EDTA	Ethylenediaminetetraacetic acid
ENOD	Early nodulin
ER	Endoplasmic reticulum
ERN	Ethylene response factor required for nodulation
FP	Fahraeus plant medium
FRET	Förster resonance energy transfer
F$_1$	Offspring from a genetic cross

Abbreviation	Definition
F_2, F_3...	Offspring of F_1, offspring of F_2...
GEF	Guanine exchange factor
GAP	GTPase-activating protein
h	Hour
H_2O_2	Hydrogen peroxide
IP_3	Inositol triphosphate
LNP	Lectin nucleotide phosphohydrolase
MCA	Medicago Ca^{2+} ATPase
MES	2-(N-morpholino)ethanesulfonic acid
mM	Millimolar
MW	Molecular weight
Myc-LCOs	Mycorrhizal lipochitooligosaccharide
NF	Nod factor
NIN	Nodule inception
nM	Nanomolar
nm	Nanometre
NS-Myc-LCO	Non-sulphated mycorrhizal lipochitooligosaccharide
NSP	Nodulation signalling pathway
O_2^-	Superoxide
PAMP	Pathogen associated molecular pattern
PCR	Polymerase chain reaction
PIP-2	Phosphatidylinositol 4,5-bisphosphate
PLC	Phospholipase C
pM	Picomolar
PLD	Phospholipase D
ROP	Rho of Plants GTPase
ROS	Reactive oxygen species
RNAi	Ribonucleic acid interference
mRNA	Messenger ribonucleic acid
SERCA	Sarco/endoplasmic reticulum Ca^{2+}-ATPase
Sym	Common symbiosis pathway

Continued overleaf

Abbreviation	Definition
TF	Transcription factor
T_1	Offspring of transformed plants
T_2	Offspring of T_1 generation
X-gal	5 bromo-4-chloro-3-indoyl-β-D-galactopyranoside
YFP	Yellow fluorescent protein
µg	microgram
µl	microlitre
µM	micromolar
µm	micrometre
µmol	micromole

CHAPTER 1: GENERAL INTRODUCTION

1.1 Calcium signalling in plants

In plants, calcium is a ubiquitous signal involved in a number of developmental processes including pollen tube and root hair apical growth, regulation of stomatal aperture and responses to abiotic and biotic stresses (Dodd et al., 2010, Feijo et al., 2001, Foreman et al., 2003, McAinsh et al., 1995). A calcium signal can consist of a single elevation in free calcium ions (Ca^{2+}) within a cellular compartment, for example the sustained elevations of free Ca^{2+} in the cytoplasm and nucleus caused by the recognition of pathogen associated molecular patterns (PAMPs) during innate plant defence (Dodd et al., 2010). The signal can also exhibit oscillatory behaviour, such as the tip-focused Ca^{2+} gradients in pollen tubes and root hair cells, which oscillate with the same period as the oscillations in cell growth (Feijo et al., 2001, Monshausen et al., 2008). In *Arabidopsis thaliana* root hairs the oscillations in Ca^{2+} have a period of about 30 seconds but Ca^{2+} oscillations can have a much longer period; for example oscillations with a period of 24 hours are involved in circadian clock regulation (Love et al., 2004). Calcium signals can activate downstream signalling pathways via regulation of Ca^{2+}-binding proteins, including CALCIUM-DEPENDENT PROTEIN KINASESs (CDPKs), Calmodulins (CaMs) and the CALCINEURIN-B-LIKE (CBL) phosphatases (Harper et al., 2004). The activation of these signalling pathways can lead to changes in gene expression and/or physiological changes in cells.

Calcium signalling is involved in the establishment of symbioses between members of the legume family of plants and nitrogen-fixing bacteria known as rhizobia. Legume-rhizobia symbioses start with an exchange of signals. Prior to any physical contact, the plant releases flavonoids into the soil. The rhizobia respond by producing lipochitooligosaccharides called Nod factors (NFs) (Denarie et al., 1996, Long, 1996, Spaink et al., 1991). NFs are first perceived by the legume at the root epidermis and are capable of activating two different calcium responses in root hairs; nuclear-localised calcium oscillations (spiking) and a tip-focused calcium influx.

1.2 Overview of legume-rhizobia symbiosis

Globally, the availability of nitrogen and phosphorus limit plant growth, resulting in the widespread use of chemical fertilisers in agriculture. Many plants have overcome these limitations through symbiotic interactions with soil microbes. The most widespread symbiotic interactions are with mycorrhizal fungi that provide the plant with nutrients including phosphate in exchange for carbon. Arbuscular mycorrhizal (AM) symbioses have existed for over 400 million years and are found in 70-80% of land plant species (Parniske, 2008b). In addition to forming symbioses with mycorrhizal fungi, many members of the legume family of flowering plants, including the crop plants pea (*Pisum sativum*) and soybean (*Glycine max*), are capable of forming symbioses with nitrogen-fixing bacteria known collectively as rhizobia. The bacteria are housed in specialised organs in the plant roots called nodules, which provide a low oxygen environment to maximise nitrogen-fixation by the rhizobia. The development of a successful symbiosis requires the co-ordination of nodule organogenesis with infection of the rhizobia into the plant root.

In many legumes, including the model plants *Medicago truncatula* and *Lotus japonicus,* rhizobia infect into the root through root hair cells (Figure 1.1). After rhizobia attach to the surface of growing root hairs, the root hairs curl to entrap rhizobia within an infection pocket. During this process the rhizobia divide resulting in a small, but growing population. The next stage is the initiation of the infection thread, started by the invagination of plant cell membrane. This requires the degradation of cell wall by NODULATION PECTATE LYASE (NPL) (Xie et al., 2012). The infection thread extends to guide the dividing rhizobia down through the root hair cell and into the cortical layers of the root. The progression of the growing infection thread down to the base of the root hair cell is preceded by movement of the nucleus, which is normally found at the tip of growing root hair cells, but travels to the base of root hair cells during bacterial infection (Lloyd et al., 1987, Rae et al., 1992). The close association of the tip of the infection thread and the nucleus is likely to be for the production and delivery of new cell membrane and wall materials to the growing tip. Periodically the tip of the infection thread can be free of rhizobia, suggesting that infection thread growth does not always require direct contact from the rhizobia (Fournier et al., 2008).
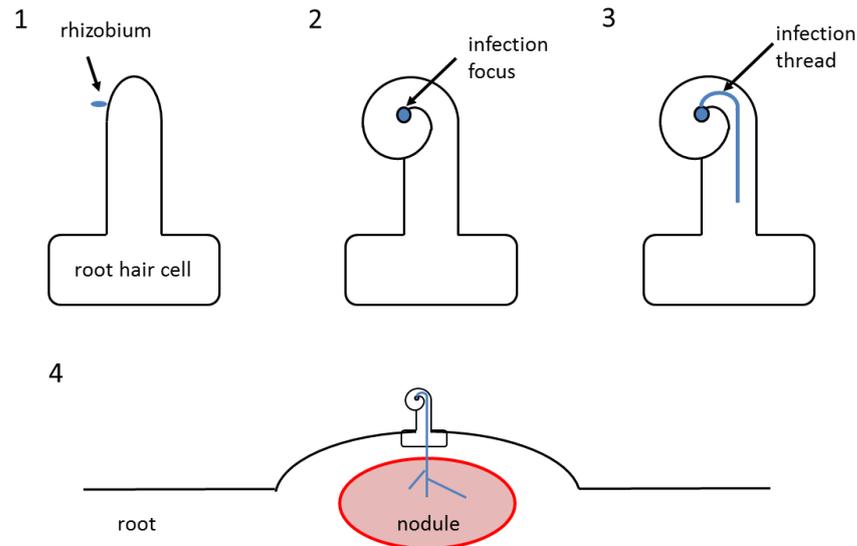
Figure 1.1: The stages of rhizobial infection into the *Medicago truncatula* root.

[1] A Rhizobium attaches near to the tip of a root hair cell. **[2]** The root hair curls entrapping the dividing rhizobia in a pocket known as an infection focus. **[3]** The infection thread initiates from an invagination of the plant cell membrane and elongates to guide the dividing rhizobia down through the root hair cell towards the cortical layers of the root. **[4]** In the cortex, host cells divide to make a nodule primordium. When the infection thread reaches the cortex it branches (ramifies) to enable the rhizobia to infect cells within the nodule primordium.

NF is required for bacterial infection but it is not sufficient. When legumes are inoculated with exopolysaccharide-deficient *Sinorhizobium meliloti* mutants, the infection threads abort in root hair cells (Pellock et al., 2000). *M. truncatula* roots treated with wildtype (exopolysaccharide-producing) rhizobia more strongly express genes involved in translation and protein degradation, and have lower expression of defence-related genes than roots treated with exopolysaccharide-deficient rhizobia (Jones et al., 2008, Jones and Walker, 2008). This suggests that exopolysaccharides are signals that promote bacterial infection by preparing the cells for invasion and downregulating defence responses.

Alongside bacterial infection, cortical cells in the root divide to produce nodule primordia. Once an infection thread reaches a nodule primordium it branches (ramifies) to enable the bacteria to infect into cells in the nodule. Once they have infected into cells within the nodule they differentiate into bacteroids, which are specialised for nitrogen fixation. As the rhizobia differentiate into bacteroids the *Nod* genes (including Nod factor synthesis genes) are switched

off (Marie et al., 1992, Marie et al., 1994). The bacteroids are fully surrounded by plant membranes that are specialised for nutrient exchange between the bacteroid and the plant cell. Together, a bacteroid and its surrounding plant membrane are referred to as a symbiosome. Within the nodule a low oxygen environment is maintained because rhizobial nitrogenase is inhibited by oxygen-binding to its metal cofactors. ATP is required for nitrogen fixation so the bacteroids express a cytochrome oxidase (cbb$_3$) with a high affinity for O$_2$ (Mandon et al., 1994, Preisig et al., 1993) to enable them to carry out respiration in a low oxygen environment.

1.3 Calcium spiking

In legumes, after NF addition there is a delay of 10-15 minutes before calcium spiking starts around the nuclear region of legume root hair cells (Ehrhardt et al., 1996, Miwa et al., 2006a). Use of both nuclear-targeted and nuclear-excluded calcium reporters confirms that the spiking originates from the periphery of the nucleus and can be observed both in the nucleoplasm and the nuclear-associated cytoplasm, suggesting that the nuclear envelope and nuclear-associated endoplasmic reticulum (ER) are the calcium sources (Capoen et al., 2011, Sieberer et al., 2009). The response can be activated by NF concentrations as low as 10^{-12} M and can also be activated by chitin oligomers, NF analogues and mycorrhizal-produced Lipochitooligosaccharides (Myc-LCOs) (Genre et al., 2013, Oldroyd et al., 2001a, Walker et al., 2000). Once activated by NF, calcium spiking is very robust and can be observed in a root hair cell for many hours (Miwa et al., 2006b, Walker et al., 2000). In *Medicago truncatula* the spikes have a period of around 90 seconds, although this can vary over the course of the spiking response and between cells (Kosuta et al., 2008, Miwa et al., 2006b, Sun et al., 2007).

Calcium spiking is central to the common symbiosis (Sym) signalling pathway required to form symbioses with rhizobia and mycorrhizal fungi (Figure 1.2). The pathway has a core set of genetic components required for both symbioses that are involved with generating, or "encoding" the calcium spiking response and "decoding" it to lead to the activation of downstream genes. Downstream of calcium decoding, differential transcription factors induce genes required for nodule formation and bacterial infection in the rhizobial symbiosis, or to facilitate fungal infection during the AM symbiosis. During nodulation, genes induced by the Sym pathway include *EARLY NODULIN11* (*ENOD11)* and the transcription factors *NODULE*

INCEPTION (*NIN)* and *ETHYLENE RESPONSE FACTOR REQUIRED FOR NODULATION1* (*ERN1)* (Journet et al., 2001, Marsh et al., 2007, Middleton et al., 2007, Schauser et al., 1999).
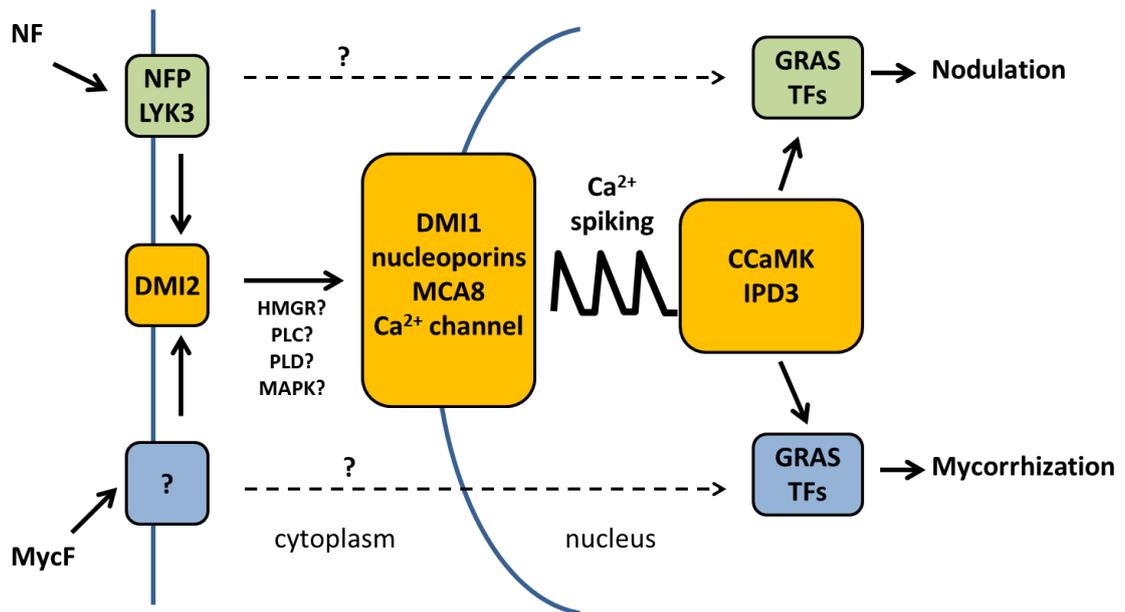
Figure 1.2: The Sym pathway.

The Sym pathway (shown in orange) is shared between nodulation and mycorrhization. NFs from rhizobia are perceived by NOD FACTOR PERCEPTION (NFP) and LYSM RECEPTOR-LIKE KINASE 3 (LYK3) at the plasma membrane and mycorrhization factors (MycF) are perceived by currently unidentified receptors. The signals from both symbionts activate DOESN'T MAKE INFECTIONS 2 (DMI2) also located at the plasma membrane and then nuclear calcium spiking is mediated by the cation channel DMI1, nucleoporins, the Ca^{2+}-ATPase MCA8 and an unidentified calcium channel. Downstream of calcium spiking CALCIUM-CALMODULIN-DEPENDENT PROTEIN KINASE (CCaMK) is activated and with its interacting partner, INTERACTING PROTEIN OF DMI3 (IPD3) promotes appropriate gene expression for either nodulation or mycorrhization via activation of GRAS transcription factors (TFs). Parallel signalling may also be involved.

In *Lotus japonicus* calcium spiking is dependent on the NF receptors NOD FACTOR RECEPTOR 5 (NFR5) and NFR1 of the LysM receptor kinase-like family (Miwa et al., 2006a). In *M. truncatula* the homologues are NFP and LYK3 respectively, but interestingly only NFP is required for NF-induced calcium spiking (Ben Amor et al., 2003, Smit et al., 2007, Wais et al., 2000). Another plasma membrane component, a LRR-receptor kinase called DMI2/SymRK is required for NF induction of calcium spiking and is required for both rhizobial and mycorrhizal symbioses (Endre et al., 2002, Stracke et al., 2002, Wais et al., 2000). It is likely that these receptors act in a complex to bind NF and activate downstream signalling.

1.3.1 Secondary messengers: linking Nod factor (NF) recognition at the plasma membrane with nuclear calcium spiking

From the plasma membrane the signal generated by NF recognition must be relayed to the nucleus probably via by secondary messengers, to generate calcium spiking, but the mechanism for this is unclear. There is evidence for the involvement of phospholipase C (PLC) and phospholipase D (PLD) in the Sym pathway. Inositol trisphosphate (IP$_3$) along with diacylglycerol (DAG) are the products of phosphatidylinositol 4,5-bisphosphate (PIP-2) hydrolysis by phospholipase C (PLC) and the PLC inhibitor U73122 blocks both NF-induced calcium spiking and *pENOD11-GUS* expression (Engstrom et al., 2002, Pingret et al., 1998). PLD can catalyse the conversion of DAG to phosphatidic acid, which can also act as a signal molecule. NF activates PLD activity in legumes (den Hartog et al., 2001, den Hartog et al., 2003) and a PLD inhibitor n-butanol inhibits both calcium spiking and *pMtENOD11-GUS* expression suggesting PLD may also be involved in the Sym pathway (Charron et al., 2004, Sun et al., 2007).

Interestingly, the G-protein agonist mastoparan (or its synthetic analogue Mas7) can activate calcium oscillations similar to NF-induced calcium spiking and can induce *pMt-ENOD11-GUS* expression (Pingret et al., 1998, Sun et al., 2007). However, there are some differences in NF and Mas7-induced calcium spiking signatures. Mas7 leads to calcium oscillations with a slower initial release of calcium, greater period variability and the oscillations are not confined to the nucleus but can be observed all over the cell (Sun et al., 2007). Unlike the NF response, it is independent of *NFP* and *DMI2*, suggesting it either acts downstream of these receptors or by an independent mechanism. Several monomeric G-proteins have been identified as having roles in nodulation including members of the ROP (Rho of Plants) GTPase family and a Rab GTPase (Blanco et al., 2009, Ke et al., 2012). *L. japonicus* ROP6 is able to bind to NFR5 and the gene is expressed in nodules and infection threads after inoculation with *Mesorhizobium loti* (Ke et al., 2012). In *ROP6* RNA interference (RNAi) lines, infection thread development into the cortex was impaired and few nodules were formed (Ke et al., 2012). G-proteins can activate multiple signalling pathways including IP$_3$ production and in pollen tube tips PIP-2 accumulation is dependent on ROP-GTPases (Kost et al., 1999). Mastoparan activates PLC and PLD in the legume *Vicia sativa* (den Hartog et al., 2001). Altogether these results suggest that NF receptor activation could result in the activation of ROP-GTPases leading to the production of IP$_3$ and DAG to activate calcium spiking in the nucleus. However, there is no direct evidence for IP$_3$ induction of calcium spiking and mastoparan-induced calcium release during the

activation of plant mitogen-activated protein kinase (MAPK) signalling occurs independently of G-proteins (Miles et al., 2004) so care should be taken in interpreting these Mas7 results.

Multiple secondary messengers may be interacting in a signalling pathway so even if IP_3/DAG are involved in generating NF-induced calcium spiking, it is possible that other secondary messengers are also required. The MAP kinase kinase SYMRK-INTERACTING PROTEIN (SIP2) interacts with DMI2/SymRK (Chen et al., 2012a). In *L. japonicus SIP2* RNAi plants produced fewer nodules and three nodulation marker genes including *NIN* were downregulated suggesting a MAPK signalling cascade may be involved in generating calcium spiking. An enzyme known as HMGR1 (3-hydroxy-3-methylglutaryl coenzyme A reductase1) also interacts with MtDMI2 (Kevei et al., 2007). HMGRs catalyse the production of mevalonate, a precursor required for isoprenoid biosynthesis. Treatment with lovastatin, an HMGR inhibitor led to reduced numbers of nodules in *M. truncatula* plants inoculated with *Sinorhizobium meliloti,* and *MtHMGR* RNAi lines produced fewer nodules than wildtype suggesting that mevalonate is required for nodule formation (Kevei et al., 2007). It may be that mevalonate is required for the production of isoprenoid compounds such as cytokinins or phytosteroids but it is also possible that mevalonate or a downstream compound is acting as a secondary messenger to relay the NF signal to the nucleus to activate calcium spiking.

1.3.2 Generating calcium spiking: the nuclear envelope machinery

Once the NF signal reaches the nucleus there are several genes that are required to induce calcium spiking. *Medicago truncatula DMI1* encodes a protein that localises preferentially to the inner nuclear membrane with structural similarity to the pore domain of MthK, a calcium-activated potassium channel in *Methanobacterium thermoautotrophicum* (Ane et al., 2004, Capoen et al., 2011, Charpentier et al., 2008, Edwards et al., 2007, Imaizumi-Anraku et al., 2005, Miwa et al., 2006a, Riely et al., 2007, Venkateshwaran et al., 2008, Wais et al., 2000). In *L. japonicus* there are two homologues of *DMI1* required for calcium spiking known as *CASTOR* and *POLLUX* (Charpentier et al., 2008). CASTOR has ion channel activity *in vitro* with preferential mobilisation of potassium*,* and POLLUX can complement a potassium ion (K^+)-transport-deficient yeast mutant, providing evidence that they are functional K^+-permeable channels (Charpentier et al., 2008). Although *M. truncatula* has a gene orthologous to *CASTOR*, it is not required for calcium spiking. *L. japonicus castor* and *pollux* mutants can be complemented by *DMI1* suggesting that *DMI1* in *M. truncatula* can fulfil the roles of both

CASTOR and *POLLUX*. (Venkateshwaran et al., 2012). *NUCLEOPORIN85* (*NUP85*), *NUP133* and *NENA* encode subunits of the nucleopore and are also required for NF induction of calcium spiking (Groth et al., 2010, Miwa et al., 2006a, Saito et al., 2007). These proteins possibly function in the transport of membrane proteins to the inner nuclear membrane (Groth et al., 2010, Kanamori et al., 2006, Saito et al., 2007), and obvious substrates would be DMI1, POLLUX and CASTOR.

For the initiation of a calcium spike, where the Ca^{2+} concentration in the nucleus and the nuclear-associated cytoplasm increase, Ca^{2+}-permeable channels must be present in the nuclear membrane to allow calcium release from the nuclear periplasm (Figure 1.3). The genetic identity of the channel is still unknown. Its absence among nodulation mutants identified in several forward genetic screens conducted over the last two decades suggests that there may be multiple different genes involved or they may have other roles in development.

To return the calcium released into the nucleus and the nuclear-associated cytoplasm back to its store, a Ca^{2+}-pump is required that actively transports calcium across the nuclear membrane against its electrochemical gradient. A role for plant type IIA [SERCA (SARCO/ENDOPLASMIC RETICULUM Ca^{2+}-ATPase)] Ca^{2+}-ATPases was suggested by an inhibitor cyclopiazonic acid (CPA) and two activators, gingerol and butylated hydroxynanisole, that can block calcium spiking (Capoen et al., 2009, Capoen et al., 2011, Engstrom et al., 2002). RNA interference (RNAi) of a nuclear-localized SERCA Ca^{2+}-ATPase [MEDICAGO Ca^{2+} ATPase (MCA8)] resulted in a large reduction in the number of root hair cells with NF-induced calcium spiking (Capoen et al., 2011). MtMCA8 is localized to the nuclear membranes, but has no preference for the inner or outer membranes. This location coupled with the phenotype of RNAi suggests MCA8 acts to return Ca^{2+} to the nuclear envelope during NF- induced calcium spiking.

1.3.3 Modelling calcium spiking

To further understand how the NF-induced calcium oscillations in the nucleus may be generated, Granqvist *et al.* (2012) developed a mathematical model to simulate the oscillations. It consists of three membrane components: a Ca^{2+}-activated K^+ channel (based on DMI1), a voltage-gated Ca^{2+}-permeable channel and a Ca^{2+}-pump (based on MCA8) (Figure 1.3). Assuming that the nuclear membrane potential is more negative on the nucleoplasmic side than in the nuclear envelope lumen the model can simulate self-sustaining calcium

oscillations in the nucleoplasm similar to those experimentally observed in *M. truncatula*. However, the calcium oscillations in this model continue indefinitely, suggesting additional components or activities are required for the cessation of the response.
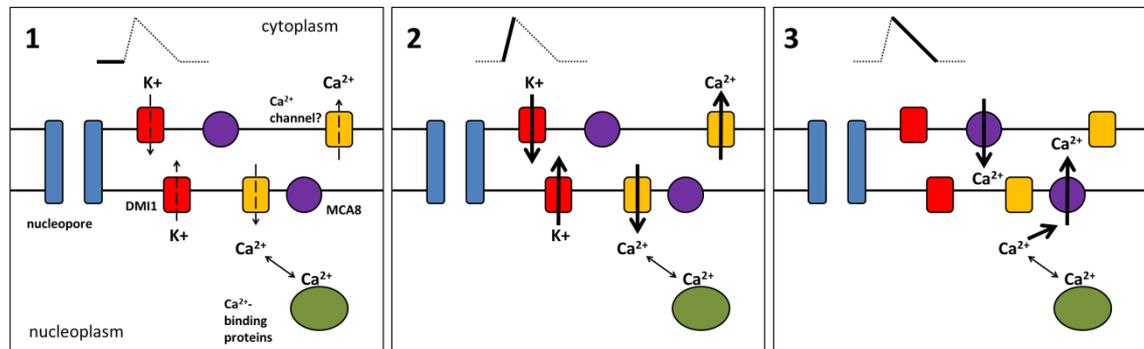
Figure 1.3: Model of calcium spike generation at the nuclear membranes.

[1] Prior to the start of a calcium spike the membrane potential is negative on the nucleoplasmic side close to the potassium resting potential and DMI1 (shown in red) is weakly conducting potassium. This drives a transient influx of Ca^{2+} through the Ca^{2+}-permeable channel (yellow) into the nucleoplasm leading to the depolarization of the membrane until it reaches the calcium equilibrium potential. **[2]** The conductivity of DMI1 increases, resulting in the flow of potassium ions down their electrochemical gradient into the nuclear lumen. This hyperpolarizes the inner nuclear membrane, generating the large Ca^{2+} flow into the nucleoplasm that forms the upwards part of the calcium spike. **[3]** Once the membrane returns to the potassium ion equilibrium potential the K^+ and Ca^{2+} currents almost cease and the downwards part of the calcium spike is formed by the action of MCA8 (purple) returning calcium ions to the nuclear envelope lumen. Since the electrochemical gradient of Ca^{2+} is so large once the membrane potential returns to the starting value the conductance of the voltage-activated Ca^{2+}-permeable channel increases leading to a transient release of Ca^{2+} that restarts the cycle. The frequency and shape of calcium spikes can be modulated by altering concentrations of calcium-binding proteins (green) in the nucleus.

The addition of Ca^{2+}-binding proteins, which act as Ca^{2+} buffers, improves the ability of the model to simulate calcium spiking. By altering buffer concentrations they can stop the oscillations or alter the period of the oscillations, to simulate the observed variation in experimental data. When the model was set up with high levels of unbound Ca^{2+}-binding proteins at the start, rapid calcium oscillations preceded the regular spiking pattern. This is very similar to experimental observations where, in about 50% of cases calcium spiking appeared to start with a rapid oscillatory phase before the regular spiking pattern was established (Granqvist et al., 2012). Experimentally adding additional NF after the induction of calcium spiking led to a short stage of rapid oscillations before the regular spiking pattern

resumed in *M. truncatula* root hair cells, suggesting NF may increase calcium buffering capacity in the nucleus by regulating Ca^{2+}-binding proteins.

While the model can simulate calcium oscillations it is not without its limitations. For simplicity only the nucleoplasm and the nuclear membrane lumen are included and within those compartments it does not include any spatial information. Nevertheless, it proposes a mechanism for how a relatively small number of genetic components can generate robust calcium spiking and predicts that Ca^{2+}-binding proteins are important modulators. It indicates that the currently unidentified Ca^{2+}-permeable channel could be voltage-gated, although a ligand-gated or a dual-regulated channel could also be possible (Granqvist et al., 2012).

The function of the cation channel DMI1 can also be hypothesized using the model. It could be acting to counter-balance the flow of the positively-charged Ca^{2+} into the nucleoplasm when Ca^{2+}-permeable channels are activated, or alternatively it could directly trigger the activation of a voltage-gated calcium channel by polarizing the inner nuclear membrane potential. Charpentier *et al.* (2013) predicted that calcium spiking is only initiated when DMI1 and the calcium channel are activated simultaneously with DMI1 conductance dependent on the membrane potential and Ca^{2+} concentration (Figure 1.3). It indicates that although the main function of DMI1 is to act as a counter-ion channel, initial low-level K^+ conductance is required to activate a transient calcium ion flux. In turn this activates both DMI1 and the Ca^{2+}-permeable channel by depolarisation of the nuclear membrane. The conclusions from the model are supported by the following evidence: the homology of DMI1 to a Ca^{2+}-activated K^+-permeable channel, DMI1 interferes with galactose-induced cytosolic calcium transient increases in yeast cells and when expressed in HEK (Human Embryonic Kidney) cells is sufficient to drive calcium-induced calcium release (Edwards et al., 2007, Peiter et al., 2007, Venkateshwaran et al., 2008). This all indicates the ability of DMI1 to coordinate calcium channels in diverse cell types. From the model it seems possible that the calcium spiking machinery could be primed for activation even in the absence of NF, suggesting DMI1 or the Ca^{2+}-permeable channel may be negatively regulated and NF perception releases them enabling calcium spiking to be initiated.

It is still not clear whether the calcium spiking in the nucleoplasm and the nuclear-associated cytoplasm is a consequence of calcium fluxes across both the inner and outer nuclear membrane, or due to calcium fluxes across only one side with Ca^{2+} flowing from the nucleoplasm to the cytoplasm or *vice versa* through nuclear pores to generate the spiking response on the other side. So far using current imaging techniques it has not yet been

possible to distinguish between these scenarios (Capoen et al., 2011). However, modelling suggests that diffusion through the nuclear pore is insufficient to explain calcium release inside and outside the nucleus. Calcium spiking in the nucleoplasm has a clear function since this is where the downstream components of the Sym pathway including the Calcium/Calmodulin – dependent Kinase (CCaMK) and transcription factors such as NODULATION SIGNALLING PATHWAY1 (NSP1) and NSP2 are located (Hirsch et al., 2009, Kalo et al., 2005, Levy et al., 2004, Mitra et al., 2004, Riely et al., 2007). The question remains whether calcium spiking in the nuclear-associated cytoplasm is just a consequence of the presence of machinery on the inner and outer nuclear membranes and/or the permeability of calcium through nuclear pores, or whether it has a biologically relevant function in nodulation.

1.3.4 Decoding calcium spiking in the nucleus

Mutants defective for CCaMK retain calcium spiking but lack NF-induced gene expression and nodulation suggesting CCaMK is positioned downstream of calcium spiking (Levy et al., 2004, Mitra et al., 2004, Miwa et al., 2006a) and likely acts to decode this signal. CCaMK has a kinase domain at the N-terminal end, a calmodulin (CaM)-binding domain/autoinhibitory domain and three Ca^{2+}-binding EF hand motifs, making it highly unusual as it is capable of perceiving both free Ca^{2+} and Ca^{2+}-bound to calmodulin (Patil et al., 1995). The kinase and CaM-binding domains have sequence similarity to Calmodulin-dependent Protein Kinase II (CaMKII) in animals, which is capable of frequency-dependent activation by calcium, making CCaMK a good candidate for the decoding of calcium spiking (De Koninck and Schulman, 1998, Patil et al., 1995).

There are several gain-of-function mutations in CCaMK, including truncated "kinase only" forms and point mutations of the threonine at position 271 (T271) in *M. truncatula* (or equivalent in other species). These result in the activation of nodulation gene expression and spontaneous nodule formation even in the absence of rhizobia (Gleason et al., 2006, Hayashi et al., 2010, Takeda et al., 2012, Tirichine et al., 2006). These gain-of-function mutations demonstrate that CCaMK activation is sufficient to activate downstream components of the Sym pathway and also that T271 has a crucial role in the regulation of the protein. CCaMK kinase activity can be regulated by autophosphorylation and mutations of the equivalent threonine residue in *Lilium longiflorum* CCaMK resulted in lower levels of autophosphorylation and substrate phosphorylation, supporting a role for T271 in regulation (Sathyanarayanan et

al., 2001). In *L. japonicus* Sym pathway mutants that are unable to produce calcium spiking, expression of autoactive CCaMK T265D and T265I (equivalent to T271) variants restored nodulation and AM colonisation demonstrating that the primary purpose of generating nuclear calcium spiking is the activation of CCaMK (Hayashi et al., 2010, Madsen et al., 2010). However, the infection process was delayed and was less efficient with fewer functional nodules, probably due to deregulated CCaMK activity and ectopic expression, especially in the case of CCaMK^{T265D}, which was expressed under control of a constitutive promoter.

The CaM-binding and EF hand domains appear to play different roles in the activation of CCaMK. Calmodulin binding to CCaMK decreases phosphorylation of CCaMK (Takezawa et al., 1996). The autoinhibitory domain of CCaMK overlaps with the CaM-binding domain so CaM-binding may release autoinhibition of the protein (Patil et al., 1995). The Ca^{2+}-binding affinities to calmodulin and that of calmodulin binding to CCaMK suggest that CaM-binding to CCaMK may only occur at significant levels at the higher concentrations of Ca^{2+} generated by calcium spiking (Swainsbury et al., 2012). In contrast, the affinities of calcium binding to the EF hands suggests that at basal Ca^{2+} concentrations before calcium spiking starts some of the EF hands may be occupied by calcium. Ca^{2+} binding to the EF hands negatively regulates CCaMK by promoting phosphorylation of T271, whereas CaM binding to CCaMK blocks T271 phosporylation to activate CCaMK (Miller et al., 2013). Therefore the EF hands and the CaM-binding domain provide CCaMK with mechanisms for sensing both high and low levels of calcium to faciliate the switch from the inactive to active state during calcium spiking (Figure 1.4).

Point mutations in T271 and the CaM-binding domain of CCaMK have provided some insights into the mechanism of activation of the protein. Interestingly, both phospho-ablative (T-A) and phospho-mimic (T-D) mutations in T271 result in spontaneous nodule formation in legumes (Gleason et al., 2006, Takeda et al., 2012, Tirichine et al., 2006). A possible explanation of how these "opposite" mutations could have the same phenotypes has been provided by homology modelling of *L. japonicus* CCaMK with *Caenorhabditis elegans* CaMKII (Shimoda et al., 2012). This homology modelling predicted that CCaMK residue T271 forms a hydrogen bond network with neighbouring residue R323 in the CaM-binding/autoinhibitory domain. According to the model, mutation or phosphorylation of T271 would disrupt the hydrogen bond network, weakening the link between the kinase and CaM-binding/autoinhibitory domain, thus preventing effective autoinhibition even in the absence of Ca^{2+} (Shimoda et al., 2012). However, this model is not consistent with the evidence that EF hands negatively regulate

CCaMK via phosphorylation of T271 (Miller et al., 2013). Building on the *L. japonicus* CCaMK homology model, and developing their own for *M. truncatula* CCaMK, Miller et al., (2013) predicted a different hydrogen bond network with bonds forming between phosphorylated T271, R323 (two bonds) and S322. In the model both unphosphorylated T271 and the phospho-mimic T271D substitution only formed one hydrogen bond with R323 (Miller et al., 2013). Therefore, this model predicts that phosphorylation of T271 stabilises the inactive state of the protein, which is consistent with the experimental data, and also accounts for the autoactivity of both phospho-ablative and phospho-mimic T271 mutants. This suggests that calcium-binding to the EF hands at low calcium concentrations promotes autophosphorylation of T271 to stabilise the inactive state of CCaMK (Figure 1.4).

CCaMK can be negatively regulated by phosphorylation of residues in the CaM-binding domain (Figure 1.4). The *ccamk-14* mutant in *L. japonicus* has a serine to asparagine mutation at position 337 (equivalent of S343 in *M. truncatula*) that causes uncoupling of infection and nodule organogenesis (Kosuta et al., 2011, Liao et al., 2012). The mutant is defective in mycorrhizal infection and during rhizobial infection produces more infection threads in the epidermis but the infection threads are impaired in progression through to the cortex, although nodule formation is unaffected (Kosuta et al., 2011). The phospho-mimic variant CCaMK^{S337D} is unable to complement *ccamk-1,* suggesting CCaMK^{S337D} is not active. A neighbouring serine residue in *M. truncatula,* S344, also negatively regulates CCaMK activation when phosphorylated (Routray et al., 2013). A phosphor-mimic S344D mutation reduced CaM-binding to CCaMK and impaired CCaMK interaction with IPD3 (Routray et al., 2013). The S344D mutation also suppressed spontaneous nodule formation in the phosphor-ablative T271A mutant. This indicates that phosphorylation of S344 can occur after the activation of CCaMK and inactivate it. Unlike its neighbouring residue (S343), the phosphomimic S344D mutation blocked both the formation of nodules and reduced colonisation by AM fungi (Routray et al., 2013), suggesting that CCaMK activity may be fine-tuned by the differential phosphorylation of individual residues in the CaM-binding domain.

CCaMK interacts with and phosphorylates IPD3 (CYCLOPS in *L. japonicus*), a protein of unknown function with two nuclear localisation signal motifs and a C-terminal coiled-coil motif thought to mediate protein-protein interactions (Messinese et al., 2007, Yano et al., 2008). *IPD3/CYCLOPS* is required for both rhizobial and AM infection (Yano et al., 2008). Although the mechanisms are currently unclear, CCaMK/IPD3 complex activation and recruitment of several GRAS transcription factors including *NSP1, NSP2* and *REQUIRED FOR ARBUSCULAR*

MYCORRHIZATION 1 (RAM1) are involved in the activation of specific nodulation or mycorrhizal gene expression (Gobbato et al., 2012, Heckmann et al., 2006, Kalo et al., 2005, Smit et al., 2005).
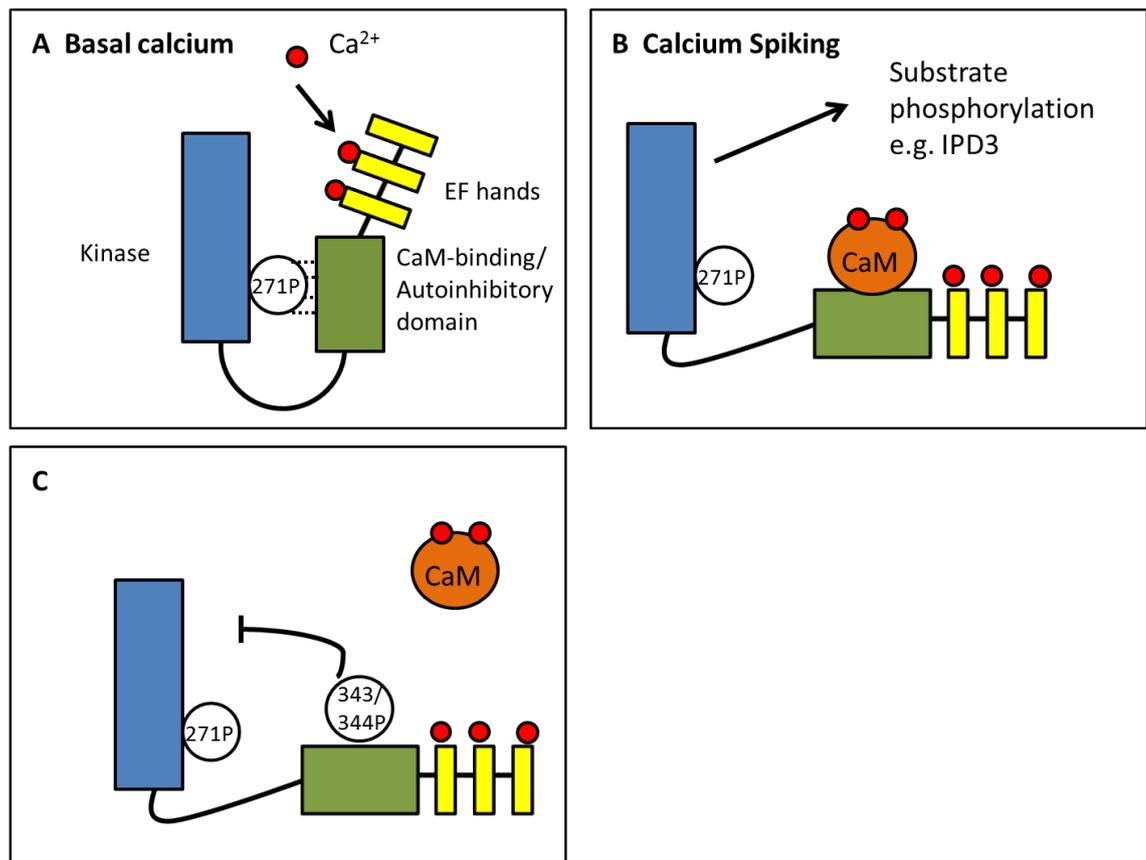
Figure 1.4: Model of CCaMK regulation.

[A] Inactive CCaMK with a hydrogen bond network linking the kinase and CaM-binding/autoinhibitory domains. At basal calcium concentrations some of the EF hands are occupied by calcium ions, promoting Threonine 271 phosphorylation to drive the hydrogen-bond network, deactivating CCaMK. **[B]** At the onset of calcium spiking higher Ca^{2+} concentrations result in full occupancy of the EF hands and calcium-bound to calmodulin (CaM). CaM binds to the CaM-binding domain, inducing a conformational change that releases the inhibition of the kinase domain, resulting in phosphorylation of CCaMK targets (e.g. IPD3/CYCLOPS). **[C]** Inactivation of CCaMK by phosphorylation of serines 343-344 in the CaM-binding domain, which prevents CaM binding and restores autoinhibition of the kinase domain by association with the CaM-binding/autoinhibitory domain.

1.3.5 Do calcium spiking signatures encode specificity between nodulation and mycorrhization?

One of the most interesting questions regarding Sym pathway function is how activation of a shared signalling pathway can result in the differential outputs required to establish either the rhizobial or mycorrhizal symbiosis. Either specificity must be encoded within the pathway itself or a parallel pathway exists that modulates the output of the Sym pathway to induce the appropriate changes in gene expression. If specificity is encoded within the pathway it would

29

be expected that the calcium spiking signatures would be different between the symbioses and CCaMK would be capable of differential activation, as is CaMKII in animal systems (De Koninck and Schulman, 1998).

The concept of different calcium spiking signatures is supported by mathematical analyses of calcium spiking signatures in *M. truncatula* produced by NFs and the mycorrhizal fungus *Rhizophagus irregularis* (previously *Glomus intraradices*). Kosuta et al. (2008) found that the duration of a mycorrhizal-induced calcium spike was shorter than a NF-induced spike and there were also differences in shape. However, this experimental set up was not optimal because when using the fungus it is impossible to determinate when the plant root first perceives the fungus and the concentrations of the then unidentified diffusible signal factors dubbed "Myc factors". Using a different experimental set up Sieberer et al. (2012) studied calcium spiking signatures during the progression of infection of rhizobia and mycorrhizal fungi. They found that for both symbioses cortical cells switched from low frequency calcium oscillations prior to the microbes reaching the cell to high frequency oscillations during apoplastic entry. The high frequency oscillations appeared to be similar in both symbioses so it seems likely during the infection process at least calcium oscillations do not encode symbiont specificity. Myc-LCOs and chitin oligomers from fungal exudates that are capable of activating calcium spiking have recently been identified and if mathematical analyses of these calcium spiking signatures with those produced by NFs is carried out it may lead to some clarification (Genre et al., 2013, Maillet et al., 2011).

Instead of spike duration and shape encoding specificity, CCaMK could be differentially activated by the number of calcium spikes that occur. In *M. truncatula* NF-induced calcium spiking only leads to *ENOD11* expression after about 36 individual spikes have occurred (Miwa et al., 2006b). It could be possible that during AM colonisation a different number of calcium spikes occur, perhaps due to differences in nuclear Ca^{2+}-binding protein concentrations that terminate spiking sooner or later than during nodulation.

CCaMK activation does not appear to be associated with differential induction of symbiotic specific responses. The autoactive CCaMK$^{1-314}$ (kinase only) variant activated both the nodulation marker *NIN* and mycorrhizal marker subtilase (*SbtM1*) expression when expressed in *L. japonicus* (Takeda et al., 2012). Interestingly, *SbtM1* is expressed in multiple cell layers in CCaMK$^{1-314}$ expressing plants and is associated with the formation of fungal infection-like structures, but *NIN* expression is restricted to the epidermis (Takeda et al., 2012). However the *snf1* mutant, which expresses autoactive CCaMK^{T265I} induced nodulation specific gene

expression but not AM-specific gene expression, indicating that the phosphorylation status of threonine 265 may be important in activating rhizobial associated responses (Takeda et al., 2011).

At this stage it seems unlikely that differences in calcium spiking responses can allow CCaMK to discriminate between the rhizobia and AM fungi and instead alternative signalling may define the specificity of the response. There is evidence for the existence of parallel signalling pathways in NF signalling. The Sym pathway mutants *dmi1, dmi2* and *dmi3* retain root hair deformation and the NF-induced calcium influx (Miwa et al., 2006a). An autoactive CCaMK variant induces spontaneous nodule formation in NF receptor mutants but does not support bacterial infection (Hayashi et al., 2010). These results suggest that there are parallel signalling pathways downstream of the NF receptors that mediate rhizobial infection alongside the Sym pathway.

1.4 The calcium influx

In addition to calcium spiking, NF treatment also induces a calcium influx into the cytoplasm that originates in the tip of root hair cells (Miwa et al., 2006a, Shaw and Long, 2003a, Walker et al., 2000). Using ion selective electrodes Felle et al. (1998) were able to detect the calcium influx occurring within seconds of NF addition with Ca^{2+} moving into the cytoplasm from the extracellular matrix. To initiate the calcium influx response higher concentrations of NF must be used than those required to initiate calcium spiking, with 10^{-9} M required for half maximal induction and 10^{-8} M typically used to induce the response reliably (Felle et al., 2000, Miwa et al., 2006a, Shaw and Long, 2003a). Non-sulphated NFs and chitin oligomers, which are able to activate calcium spiking, do not activate the calcium influx suggesting it has higher NF stringency (Felle et al., 1999a, Miwa et al., 2006a, Shaw and Long, 2003a, Walker et al., 2000). In addition to being temporally and spatially separate it is also possible to genetically separate calcium spiking and the calcium influx. Both responses are dependent on the NF receptor *NFP (*in *L. japonicus NFR5* and *NFR1*) but the Sym pathway mutants *dmi1* and *dmi2* both retain the calcium influx response (Ben Amor et al., 2003, Miwa et al., 2006a). Altogether these results suggest that the calcium influx is involved in a parallel pathway independent of calcium spiking. However, Shaw and Long (2003a) reported that the calcium influxes observed in *dmi1* and *dmi2* after NF addition appeared to be shorter in duration than in wildtype *M. truncatula,* so it is possible that *DMI1* and *DMI2* can modulate the calcium influx.

The requirement for higher concentrations of NF and the higher stringency suggest the calcium influx may be involved in bacterial infection (Miwa et al., 2006a, Shaw and Long, 2003a). In the early stages of establishment of the symbiosis before rhizobia attach to the root surface the NF concentrations perceived by the plant are likely to be low, but presumably high enough to activate calcium spiking to induce early nodulation gene expression. When rhizobia attach to root hair cells (Figure 1.1) and as they divide within the infection foci and infection threads the local NF concentrations on the plant membrane surface are likely to rise, perhaps to the threshold required for calcium influx activation. Thus, the calcium influx could be associated with root hair curling and/or infection thread formation.

The infection process also has more stringent requirements for NF than induction of the Sym pathway, demonstrated by the *nodO/nodE* double mutant of *Rhizobium leguminosaurum* bv. *viciae*, which induces root hair deformation and many infection foci on vetch but rarely forms infection threads (Walker and Downie, 2000). The *nodO* gene encodes a secreted protein that is capable of forming cation-selective pores in membranes (Sutton et al., 1994) and restoration of it or *nodE* (involved in attachment of acyl groups to NF) rescued infection thread development by the mutant, suggesting that an ion flux across the plant membrane induced by NodO could compensate for defective NF structures.

Rhizobia with a mutation in *nodL* produce NFs missing an O-linked acetyl group on the N-acylated glucosamine residue (Ardourel et al., 1994). *Medicago sativa* inoculated with *nodL* rhizobia produce nodules but there is a delay in bacterial infection with a lower frequency of root hair curling and infection thread formation (Ardourel et al., 1994). The absence of the O-linked acetyl group on *nodL* NF results in a marked reduction in the activation of the calcium influx but does not affect activation of calcium spiking, providing further evidence for the involvement of the calcium influx in bacterial infection (Morieri et al., 2013). Along with *nodE,* the *nodL* infection phenotype indicates the presence of different receptor complexes that have different NF stringencies for the activation of calcium spiking and the calcium influx.

1.4.1 A role for the apyrase LECTIN NUCLEOTIDE PHOSPHOHYDROLASE (LNP) in NF-induced calcium signalling

Calcium spiking and the calcium influx are both dependent on *LNP*. *LNP* antisense lines in *L. japonicus* did not form nodules or infection threads and the lines were defective for calcium spiking and the calcium influx, but maintained root hair deformation (Roberts et al., 2013). LNP

has apyrase (hydrolysis of phophoanhydride bonds of nucleoside triphosphates and diphosphates) activity. It is found on the surface of root hairs and is activated by NF-binding (Etzler et al., 1999, Etzler et al., 2000). ADP treatment partially rescued Soybean *LNP (GS52)* RNAi lines, which are defective for nodule development and infection, suggesting ADP may have a role in promoting nodulation (Govindarajulu et al., 2009).

Extracellular ATP is a signal molecule involved in a wide range of processes in plants including root gravitropism, growth, pollen germination and stress responses (Jeter et al., 2004, Kim et al., 2006, Song et al., 2006, Steinebrunner et al., 2003, Tang et al., 2003, Wu et al., 2007). In *A. thaliana*, high or very low levels of extracellular ATP or ADP can inhibit root hair elongation (Clark et al., 2010). ATP and ADP are able to induce increases in cytosolic free Ca^{2+} in plants (Demidchik et al., 2003, Demidchik et al., 2009, Demidchik et al., 2011, Jeter et al., 2004). In root cells ATP treatment induced NADPH oxidase-dependent ROS production triggering an elevation in cytosolic free Ca^{2+} (Demidchik et al., 2009). Extracellular ATP is a well-established signal in animals, and is perceived by purinoreceptors on the cell surface (Burnstock, 2007). No homologues of animal purinoreceptors have been found in plants, but recently a plant ATP receptor has been identified (Choi et al., 2014). DORN1 (DOES NOT RESPOND TO NUCLEOTIDES 1) is a lectin receptor kinase that binds ATP. It is required for ATP-induced elevation in cytoplasmic free Ca^{2+}, mitogen-activated protein kinase activation, and gene expression (Choi et al., 2014). It is possible that during nodulation LNP regulates extracellular ADP/ATP levels to modulate NF-induced calcium responses.

1.4.2 The calcium influx is spatially and temporally coincident with other NF responses including transient reactive oxygen species (ROS) production

At the tip of a legume root hair after NF addition there is an efflux of chloride ions, intracellular alkalisation and plasma membrane depolarisation, all occurring a few seconds after the calcium influx (Ehrhardt et al., 1992, Felle et al., 1996, Felle et al., 1998, Kurkdjian, 1995). The Ca^{2+} inhibitor nifedipine inhibits these responses and the responses can be mimicked by treatment with the calcium ionophore A32187 and the Ca^{2+}-ATPase inhibitor 2,5-di(t-butyl)-1,4-benzohydroquinone (BHQ), providing further evidence that the calcium influx acts upstream of these responses (Felle et al., 1998, Felle et al., 1999b). After membrane depolarisation there is an efflux of K^+ from the cell and membrane repolarisation. Like the calcium influx, the membrane depolarisation is not induced by non-sulphated NFs or chitin

oligomers and is dose-dependent with a maximal response produced at $10^{-8}/10^{-7}$ M NF (Ehrhardt et al., 1992, Felle et al., 1996, Shaw and Long, 2003a). Felle et al. (1998) suggested a model where the NF–induced calcium influx acts as a secondary messenger leading to the activation of the chloride efflux and intracellular alkalinisation, perhaps by inhibition of proton pumps, to generate the membrane depolarisation. They also suggested that membrane repolarisation is achieved by the efflux of potassium ions through K^+-permeable channels, which is activated once the membrane potential becomes more positive than the potassium equilibrium potential.

Other responses to NF also occur at the tip of root hair cells. Within 3-6 minutes of NF addition cytoskeletal changes occur in legumes (Cárdenas et al., 1998, Weerasinghe et al., 2003, Weerasinghe et al., 2005). The cytoskeletal changes precede NF-induced root hair deformation where the root hairs start to swell, bend and branch. There is also a transient increase in reactive oxygen species (ROS) production starting around one minute after NF addition with ROS levels restored to normal levels by around three minutes (Cárdenas et al., 2008, Shaw and Long, 2003b). Chitin oligomers were unable to produce the response, and the fungal elicitor chitin produced a larger, more sustained increase in ROS production more like the ROS burst seen during PAMP recognition in plant defence. Pretreatment of root hair cells with diphenyleneiodonium (DPI), an inhibitor of NADPH oxidases and other flavin-containing enzymes, inhibited the response, suggesting that the main source of the ROS may be from NADPH oxidases (Cárdenas et al., 2008). During the apical growth of root hair cells and pollen tubes, Ca^{2+}, protons and ROS interact to drive polar growth so it is possible that during nodulation the transient ROS production may be involved with the calcium influx and intracellular alkalinisation that lead to membrane depolarisation (Foreman et al., 2003, Monshausen et al., 2007, Monshausen et al., 2008). Although the ROS transient appears to be occurring later than the calcium influx and membrane depolarisation, these processes have not been measured concurrently and the differences may be associated with technical differences in the experiments.

Reactive oxygen species can as signal molecules in plants and there is evidence that ROS levels are regulated throughout the nodulation process (Apel and Hirt, 2004). Increased superoxide production can be detected in infection threads formed during the *M. sativa-S. meliloti* symbiosis, and there is an accumulation of hydrogen peroxide during nodule development and bacterial infection (Rubio et al., 2004, Santos et al., 2001). A ROS-sensitive peroxidase [RHIZOBIUM-INDUCED PEROXIDASE (RIP1)] is induced by NF treatment, suggesting that ROS

levels are regulated by NFs (Cook et al., 1995, Ramu et al., 2002). ROS levels in *M. truncatula* roots start to decline 30-60 minutes after NF treatment (Lohar et al., 2007, Shaw and Long, 2003b). The response can be activated by 100 pM NF but is not activated by sulphated chitotetraose or non-sulphated NFs. The decline was absent in *nfp* mutants but was present in Sym pathway mutants, suggesting it is involved in a separate signalling process. Exogenous ROS treatment prevented NF-induced root hair swelling and branching, suggesting that the ROS decline is involved in root hair deformation, perhaps by preventing the activation of plant defence responses (Lohar et al., 2007). It seems likely that the transient ROS increase and the later, more gradual decline in ROS may have separate signalling roles in nodulation.

1.4.3 Calcium and ROS signalling in root hairs: lessons from apical growth

Gradients of Ca^{2+}, pH and ROS production are required for apical growth of root hairs (Foreman et al., 2003, Herrmann and Felle, 1995, Jones et al., 1995). These gradients oscillate with the same period but out of phase with oscillations in rate of cell expansion (Monshausen et al., 2007, Monshausen et al., 2008). Ca^{2+} influxes across the plasma membrane at the tip of cells are responsible for the calcium gradient (Herrmann and Felle, 1995, Very and Davies, 2000). The *A. thaliana rhd2* mutant lacks the tip-focused Ca^{2+} gradient, tip ROS production and has stunted roots and short root hair cells (Foreman et al., 2003, Schiefelbein and Somerville, 1990, Wymer et al., 1997). *RHD2* encodes a plasma membrane NADPH oxidase [RESPIRATORY BURST OXIDASE HOMOLOGUE C (AtRBOHC)] and ROS treatment to *rhd2* roots raised cytoplasmic Ca^{2+} levels in the root hairs and restored cell expansion but this was not limited to the tip, suggesting the sub-cellular localisation of ROS production is important for appropriate polar cell expansion (Foreman et al., 2003). Although NADPH oxidases produce in ROS as superoxide (O_2^-) on the external surface of the cell, O_2^- is highly reactive and is rapidly converted to hydrogen peroxide (H_2O_2), which can enter cells via plasma membrane water channels (aquaporins) (Bienert et al., 2007, Dynowski et al., 2008, Hooijmaijers et al., 2012). Therefore, NADPH oxidase-mediated ROS production can lead to ROS increases both inside and outside cells. The annexin AtANN1 has been proposed to be a ROS-dependent Ca^{2+} permeable channel involved in root hair growth (Laohavisit et al., 2012). *A. thaliana ann1* mutants have short root hairs and lack the ROS-dependent Ca^{2+} permeable conductance, and *AtAnn1* can mediate a ROS-dependent Ca^{2+} permeable conductance across lipid bilayers (Laohavisit et al., 2012).

Plant NADPH oxidases (RBOHs) contain calcium-binding EF-hand motifs and Ca^{2+} have been shown to regulate their activity *in vitro*, suggesting a positive-feedback loop between Ca^{2+} and ROS is involved in regulating apical growth (Keller et al., 1998, Sagi and Fluhr, 2001, Takeda et al., 2008). Elevation of the pH of the external medium surrounding *rhd2-1* mutants to 6.0 restored normal root growth along with the tip-focused Ca^{2+} gradient (Monshausen et al., 2007). However, the mutants had lower ROS levels in root hairs and lacked the oscillations in ROS production at the tip, suggesting either pH lies downstream of ROS or that they may act together to regulate root hair growth.

The Ca^{2+} gradients are thought to provide directional regulation of apical growth by regulating exocytosis and actin reorganisation (He et al., 2006, Rato et al., 2004). Alongside any signalling roles, ROS and pH may also directly regulate cell wall structure. ROS are involved in peroxidative-cross linking of cell wall polysaccharides and pH is involved in cell expansion (Bibikova et al., 1998, Cosgrove, 1999, Kerr and Fry, 2004, Kjellbom et al., 1997). Artificially raising the pH of the external medium surrounding *A. thaliana* roots to 8.0 or application of ROS arrested root tip growth, whereas decreasing the external pH to 4.5, or treatment with the ROS scavenger MCLA (methoxylated *Cypridina luciferin* analogue) caused root tip bursting, suggesting ROS and a rise in apoplastic pH promote cell wall hardening during the slower growth phases.

Root hair apical growth is co-ordinated by ROP (RHO OF PLANTs) GTPases, which associate with the plasma membrane at the apex of the cell (Figure 1.5). There are 11 members of the ROP GTPase family in *A. thaliana* and they are involved in processes including abscisic acid (ABA) responses, pollen tube growth, cell shape formation and the low oxygen response (Craddock et al., 2012). ROP GTPases switch between an activate state when they are bound to GTP and an inactive state when they are bound to GDP (Figure 1.5). ROPs are regulated by RopGEFs (GUANINE EXCHANGE FACTORS), which exchange the GDP for GTP to return the ROP to its active state, RopGAPs (GTPase ACTIVATING PROTEINS), which promote the intrinsic GTPase activity of the ROP to inactivate it, and RhoGDIs (GDP DISSOCIATION INHIBITOR), which sequester ROPs in the cytosol to prevent them being activated by the RopGEFs (Berken and Wittinghofer, 2008, Bos et al., 2007, Carol et al., 2005, Kost, 2008). The *A. thaliana supercentipede1 (scn1)* mutant is defective in a RhoGDI and develops multiple root hair initials (Carol et al., 2005). *AtROP2* is mis-localised in this mutant demonstrating the importance of the regulation of ROP GTPase subcellular localisation for regulation of polar growth. In *A. thaliana ROP* genes can have redundant and non-redundant functions and *AtROP2, AtROP4*

and *AtROP6* are involved in root hair apical growth (Duan et al., 2010, Jones et al., 2002, Jones et al., 2007, Molendijk et al., 2001, Yang et al., 2007). *AtROP2* and *AtSCN1* are required for AtRBOHC-mediated ROS production during root hair growth (Carol et al., 2005, Jones et al., 2007). The FERONIA (FER) receptor-like kinase lies upstream of ROP signalling during root hair growth, interacting with AtRopGEF1 (Duan et al., 2010).
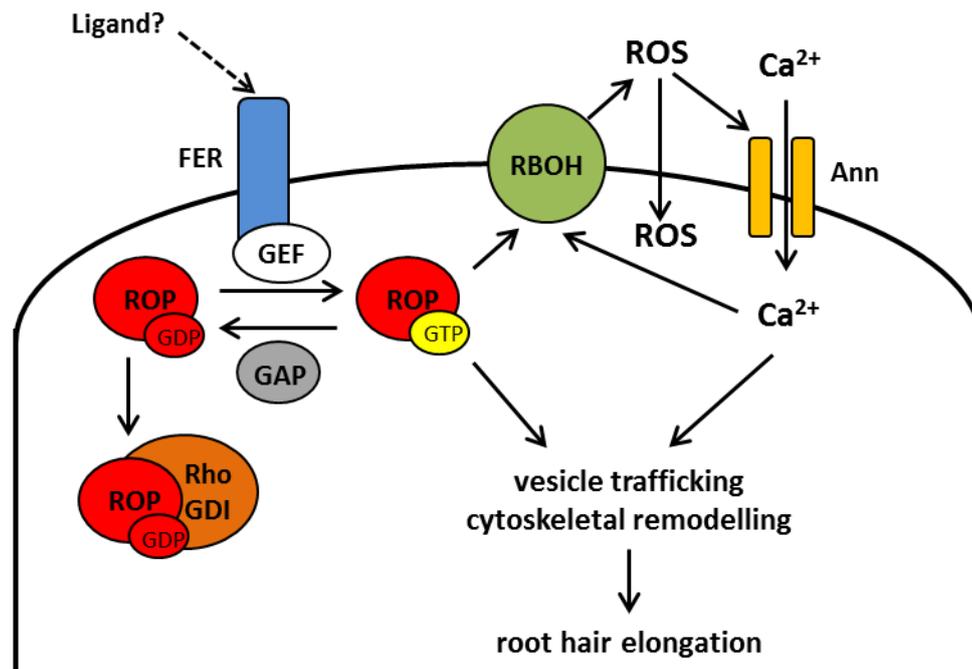
Figure 1.5: ROP signalling during developmental root hair elongation.

The FER receptor-like kinase is activated resulting in the activation of RopGEFs, which promote ROP signalling activity by exchanging ROP-bound GDP for GTP. ROP signalling is negatively regulated by RopGAPs, which assist the intrinsic GTPase activity of the ROPs to return them to the GDP-bound state, and the RhoGDIs, which bind to the ROP-GDP bound state and remove them from the plasma membrane. Together, the activities of RopGEFs, RopGAPs and RopGDIs maintain a zone of active ROP GTPases at the tip of the growing cell, which results in the localised activation of RBOH-dependent ROS production and Ca^{2+} influx through annexins (Ann) and/or other Ca^{2+}-permeable channels to generate tip gradients of ROS and Ca^{2+}. ROS in the form of H_2O_2 can enter cells through plasma membrane aquaproins. ROP signalling and the tip calcium gradient regulate vesicle trafficking and cytoskeletal remodelling at the tip leading to root hair elongation.

Regulation of polar growth is essential during rhizobial infection to mediate root hair curling around attached bacteria and the development of the infection thread. It seems likely that the mechanisms for regulating the processes for root hair growth may have been co-opted for rhizobial infection. NF treatment induces root hair elongation, but unlike apical growth this is independent of ethylene, indicating that if NF can activate the apical growth machinery it does so downstream of the ethylene receptors (Oldroyd et al., 2001b). Spot inoculation of NF to the surface of *M. truncatula* root hairs is sufficient to alter the axis of polar growth to generate root hair curling (Esseling et al., 2003). Recently evidence has been emerging of the involvement of ROP GTPase signalling in nodulation. Three *M. truncatula* ROP GTPase genes are up-regulated in roots and root hairs after inoculation with *S. meliloti* (Liu et al., 2010). RNAi knockdown of *MtROP9* inhibited a NF-induced ROS response and resulted in the formation of fewer nodules (Kiirika et al., 2012). In *Lotus japonicus LjROP6* is up-regulated after inoculation with *M. loti* and the protein interacts with the NF receptor NFR5 *in planta* (Ke et al., 2012) (Figure 1.6). *LjROP6* RNAi lines showed an inhibition of infection thread growth through the cortex suggesting ROP6 may promote infection thread development from the epidermis into the cortex, perhaps through regulation of the cytoskeleton (Ke et al., 2012). The RNAi lines also produced fewer nodules and the early nodulation genes *NIN* and *ENOD40* are down-regulated compared to wildtype after inoculation with *S. meliloti.* These results indicate that either *LjROP6* may be involved in the Sym pathway or it may lie in a parallel pathway, perhaps primarily involved in regulating infection but with a role in positive feedback of the Sym pathway as part of the co-ordination of nodule development and bacterial infection.

Part of the function of ROP GTPases in nodulation may involve the regulation of NADPH-dependent ROS production. The *MtRBOHA* gene is upregulated in nodules during the *M. truncatula-S. meliloti* symbiosis and expression of *MtRBOHA* appears to be restricted to the nitrogen-fixing zone of the nodules (Marino et al., 2011). Plants inoculated with *S. meliloti* mutant strains *nitrogen fixationH* (*nifH)* and *bacteroid developmentA* (*bacA),* which are unable to form functioning nodules, had lower *MtRBOHA* expression and *MtRBOHA* RNAi lines had lower nitrogen fixation activity in nodules (Marino et al., 2011). Coinciding with the decline in ROS after NF treatment, *MtRBOH2* and *MtRBOH3* are transiently down-regulated at one hour in an NFP-dependent manner in *M. truncatula* (Lohar et al., 2007). Another member, *PvRBOHB* is expressed in several tissues including developing nodules and in infected root hairs in *Phaseolus vulgaris* (Montiel et al., 2012). RNAi lines had reduced ROS production, fewer nodules and the infection threads were impaired in progression from the epidermal cells into the cortex. The few nodules that formed in the *PvRBOHB* RNAi lines had infection threads that

were wider and more irregular in shape, indicating that *PvRBOHB* is involved in infection thread development. It would be very interesting to know if any of the ROP GTPases or RBOHs that are involved in bacterial infection are also required for the induction of the calcium influx.

In summary, drawing on parallels between rhizobial infection in legumes and polar root hair growth in *A. thaliana* it seems likely that NF induction of the calcium influx is mediated by ROP GTPase signalling (Figure 1.6). At the root hair tip, perception of NFs by the NF receptors NFR5/NFR1 leads to the activation of ROP6, which could promote RBOH-dependent ROS production. The ROS production may promote cell wall remodelling and/or the activation of the calcium influx and membrane depolarisation. In *A. thaliana* ROP GTPases are master regulators of polar growth, so in legumes the calcium influx may be involved in ROP GTPase regulation of cytoskeletal rearrangement and vesicle trafficking leading to root hair curling and infection thread formation.
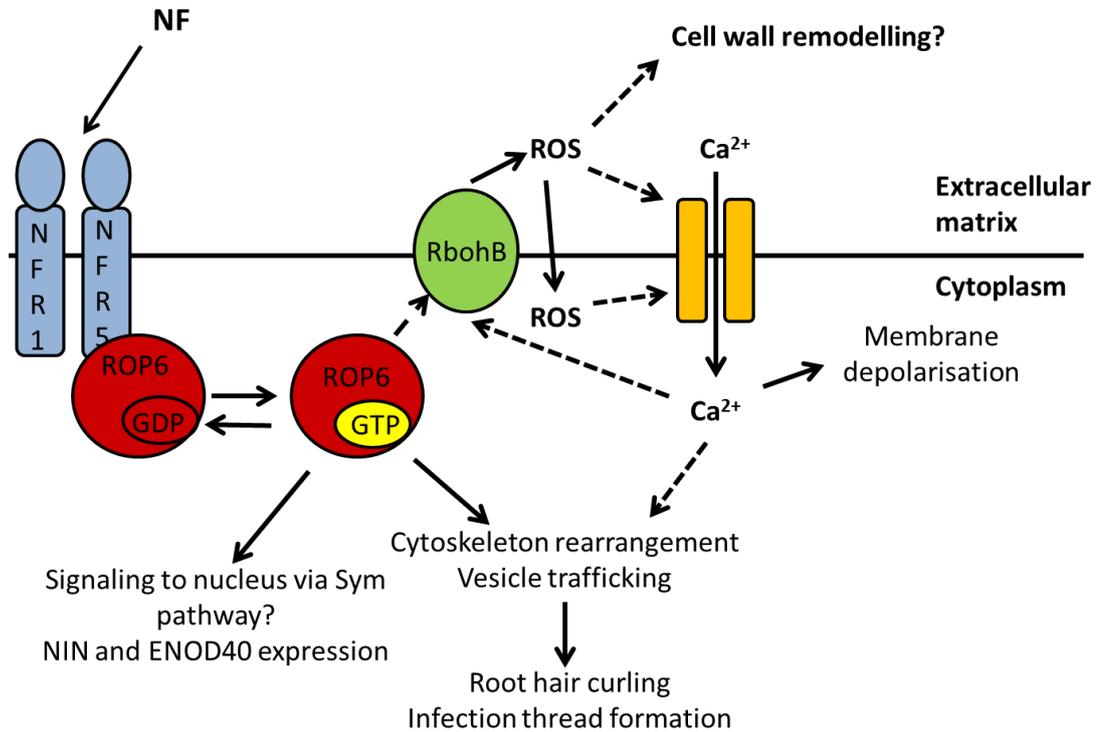
Figure 1.6: Initiation of the NF-induced calcium influx.

ROP6 signalling is activated by NF binding to ROP6-interacting partner NFR5. ROP6 activates RBOH activity producing ROS, promoting cell wall remodelling and activating a calcium influx. Ca^{2+} and ROP GTPases regulate cytoskeleton rearrangement and vesicle trafficking to generate root hair curling around attached rhizobia and regulate infection thread formation. ROP6 also induces *NIN* and *ENOD40* gene expression, perhaps via the Sym pathway. Cycling of ROP GTPases between GDP and GTP bound states by RopGEFs and RopGAPS (not shown) and sequestering in the cytoplasm by RhoGDIs ensure ROP activity can be appropriately localised to drive new membrane formation in the appropriate location and direction.

1.5 Research objectives

The NF-induced nuclear calcium spiking and tip-focused calcium influx are separate calcium signals with different roles in legume-rhizobia symbioses. The focus of this project was to further characterize the calcium influx and the NF-induced ROS transient, and investigate whether they are part of a common signalling pathway involved in bacterial infection, perhaps regulated by ROP GTPases. To do this, new tools for imaging Ca^{2+} and ROS in *M. truncatula* were developed and discussed in Chapter 3. In Chapter 4 a pharmacological approach was taken to identify new components required for the calcium influx and ROS transient. Next, a selection of *M. truncatula* nodulation and bacterial infection mutants were phenotyped for Ca^{2+} and ROS responses in Chapter 5. Finally, in Chapter 6 a reverse genetics approach was used, based on the parallels between developmental polar root hair growth and bacterial infection, to identify a *ROPGAP* gene (regulator of ROP GTPase) that modulates bacterial infection and the calcium influx. These different approaches provide insights into the signalling pathways involved in establishing the legume-rhizobia symbioses.

CHAPTER 2: MATERIALS AND METHODS

2.1 Plant Material

All *Medicago truncatula* lines used are listed in Table 2.1. Jemalong A17 or R108-1 were used as wild type for all experiments as appropriate.

Table 2.1: Plant Material

Line	Background	Description	Source (if applicable)
Jemalong A17		Wild type	Van den Bosch and Stacey (2003)
dmi1-1	A17	Single point mutation G1264A at 5' splice site at third intron leading to missplicing of *DMI1* mRNA	Giles Oldroyd, JIC
dmi2-1	Jemalong A5	Frame shift mutation leading to a premature stop codon in *DMI2*	Giles Oldroyd, JIC
nfp-1	A17		Ben Amor et al. (2003)
nin-1	A17	Fast neutron deletion allele at position 1850-1861 in *NIN*	Marsh et al. (2007)
skl	A17	Single point mutation (Q894stop) in *MtSkl1*	Penmetsa and Cook (1997)
hcl-1	A17	Point mutation (G2443A) in *LYK3*	Wais et al. (2000)
rit-1	A17	Fast neutron deletion-insertion allele resulting in truncated *RIT1*	Miyahara et al. (2010)
bit1-1	A17	Deletion of *ERN1* gene and 4 adjacent genes	Middleton et al. (2007)
R108-1		Wild type	Hoffmann et al. (1997)

Continued overleaf

Line	Background	Description	Source (if applicable)
YC2.1	R108-1	Transgenic line carrying YC2.1 gene under control of 35S promoter	Miwa et al. (2006b)
NF0457 (**cbs1-2**)	R108-1	*Tnt1* insertion line with insertion in an exon of *CBS1*	Jeremy Murray, JIC
NF10271 (**gap1-1)**	R108-1	*Tnt1* transposon insertion line with insertion in an exon of *MtGAP1*	Samuel Roberts Noble Foundation, USA
NF11438 (**gap1-2)**	R108-1	*Tnt1* transposon insertion line with insertion in an exon of *MtGAP1*	Samuel Roberts Noble Foundation, USA
A17 YC3.6	A17	Transgenic line carrying YC3.6 gene under control of 35S promoter	This study
R108 YC3.6	R108-1	Transgenic line carrying YC3.6 gene under control of 35S promoter	This study

2.2 Bacterial Strains

All bacterial strains used are listed in Table 2.2.

Table 2.2: Bacterial strains

Strain	database no.	Plasmid	Resistance	Description	Source
DH5 α	25	-	-	*Escherichia coli*	J. A. Downie, JIC
YC3.6	XP464	pcDNA3	Amp, Neo	DH5α strain containing pcDNA3 plasmid with YC3.6 under control of 2x35S promoters	(Nagai et al., 2004)
pB7WG2	1178	pB7WG2	Sp/Str	*E. coli* expressing pB7WG2 binary vector: 35S promoter and terminator, BASTA plant selection	(Karimi et al., 2002)
AGL1	X234	-	-	*disarmed Agrobacterium tumefaciens*	J.A. Downie, JIC
pK7GWIWG2(II)-dsRED	1350	pK7GWIWG2(II)-dsRED	Sp/Str	*A. rhizogenes* QUA1 carrying pK7GWIWG2(II) plasmid containing dsRED plant expression marker	(Kiirika et al., 2012)
ROP9i	1351	pK7GWIWG2(II)-dsRED	Sp/Str	As pK7GWIWG2(II)-dsRED but with *MtROP9* sequence in sense and antisense orientations between attR1 and attR2	(Kiirika et al., 2012)
Sm 2011	A1371	-	Str	Wildtype *Sinorhizobium meliloti* 2011	J. Dénarié, INRA-CNRS

continued overleaf

Strain	database no.	Plasmid	Resistance	Description	Source
Sm 2011 lacZ	D5190	pXLGD4	Str & Tet	Wildtype *S. meliloti* expressing *lacZ* gene	J.A. Downie, JIC
Sm 1021	19	-	-	Wildtype *S. meliloti* 1021	(Meade et al., 1982)
Sm SL44 (nodΔD1 ABC)			Tet	*S meliloti* nodΔD1ABC mutant.	J.A. Downie JIC

2.3 Media

The composition of the media used for plant and bacterial growth is given in table 2.3.

Table 2.3: Media used for plant and bacterial growth

Solution	Composition (for 1 l)
Rhizobium complete medium (TY)	5 g Difco tryptone, 3 g Difco yeast extract, 1.325 g $CaCl_2$ [containing 15 g LabM No.1 agar (Formedium, UK) for solid medium].
Luria-Bertani (LB)	10.0 g tryptone, 5.0 g yeast extract, 5.0 g NaCl, [containing 10.0 g Lab M No.1 agar (Formedium, UK) for solid medium].
SOC	20.0 g tryptone, 5.0 g yeast extract, 0.58 g NaCl, 0.19 g KCl, 2.03 g $MgCl_2$, 2.46 g $MgSO_4.7H_2O$, 3.6 g glucose.
Water agar (DWA)	1.5 % (w/v) Lab M No. 1 agar (Formedium, UK, pH 5.7 (adjusted with KOH).

Solution	Composition (for 1 l)
Fahraeus plant medium (FP)	0.1 g $CaCl_2$. $2H_2O$, 0.12 g $MgSO_4$, 0.01g $KHPO_4$, 0.150 g $NaHPO_4.12H_2O$, 5 mg ferric citrate, 2.86 g H_3BO_3, 2.03 g $MnSO_4$, 0.22 g $ZnSO_4.7H_2O$, 0.08 g $CuSO_4.5H_2O$, 0.08 g $H_2MoO_4.4H_2O$, pH 6.3-6.7. For solid medium 0.5% (w/v) LabM No. 1 agar was added.
Modified FP	FP medium containing 0.5 mM NH_4NO_3
Buffered nodulation medium (BNM)	390 mg MES, 344 mg $CaSO_4.2H_2O$, 0.125 g KH_2PO_4, 122 mg $MgSO_4.7H_2O$, 18.65 mg Na_2EDTA, 13.9 mg $FeSO_4.7H_2O$, 4.6 mg $ZnSO_4.7H_2O$, 3.1 mg H_3BO_3, 8.45 mg $MnSO_4.H_2O$, 0.25 mg $Na_2MoO_4.2H_2O$, 0.016 mg $CuSO_4.5H_2O$, 0.025 mg $CoCl_2.6H_2O$, pH 6.5. For solid medium 11.5 % (w/v) LabM No. 1 agar (Formedium) was added.
Medicago mix (compost)	6:6:1 Mix of Levington F2 compost, John Innes No. 2 compost and 4 mm grit.
Terragreen: Sand	1:1 mix of terragreen (Oil-dry UK ltd, UK) and sharp sand (BB Minerals, UK)

2.4 Growth selection of bacteria and *Medicago truncatula*

Antibiotics were used for selection of growth of bacteria and *Medicago truncatula*. Stock solutions of antibiotics were dissolved in water followed by sterilisation through filtration with a 0.2 µm filter, except for tetracycline, which was dissolved in ethanol. The final concentrations of antibiotics used for bacteria were kanamycin 50 µg/ml; tetracycline 5 µg/ml; spectinomycin 200 µg/ml (50 µg/ml for *Agrobacterium tumefaciens*), streptomycin 200-400 µg/ml, rifampicin 20 µg/ml. All antibiotics were supplied by Sigma (UK) except for kanamycin (Formedium, UK).

For selection of transformed *M. truncatula* roots or plants the final concentration of kanamycin used was 25 µg/ml. The concentration of ammonium glufosinate used was 3 mg/l.

2.5 Plasmids

The plasmids used in are listed in Table 2.4.

Table 2.4: Plasmids

Name	Description	Reference
pDONR201	Vector for gateway cloning. Kn^R	Clontech®
pB7WG2	Binary vector. Bacterial selection Sp/Str, Plant marker BASTA, 35S promoter and terminator.	(Karimi et al., 2002)
pB7WG2-YC3.6	pB7WG2 vector containing YC3.6 gene expressed behind the CaMV 35S promoter	This study

E. coli DH5α was used for construction of plasmids, using competent cell and heat shock transformation (Inoue et al., 1990). The resultant constructs were introduced into *Agrobacterium tumefaciens* by electroporation (see 2.12.8).

2.6 Chemicals

Oregon Green-dextran MW 10,000, Texas Red-dextran MW 10,000 and 5-(and-6)-chloromethyl-2',7'-dichlorodihydrofluorescein diacetate (CM-H$_2$DCFDA) dyes were supplied by Molecular Probes (Life Technologies, Eugene, USA). X-Gal (5 bromo-4-chloro-3-indoyl-β-D-galactopyranoside) was supplied by Formedium Ltd. (Norfolk, UK). All other chemicals were supplied by Sigma-Aldrich Ltd. (Poole, UK) unless otherwise stated.

Nod factors (NFs) purified from *Sinorhizobium meliloti* were obtained from Allan Downie (Morieri, 2010). The sulphated mycorrhizal lipochitooligosaccharide S-Myc-LCO [LCO-IV(C16:0,S)] and non-sulphated NS-Myc-LCO [LCO-IV(C18:1D9Z)], which were synthesised in E *E. coli*, were provided by Jean Denarie (Maillet et al., 2011).

2.7 *M. truncatula* seed sterilisation and plant growth

Seeds of *M. truncatula* were scarified using sandpaper and sterilised in commercial bleach solution (1:10 dilution) for two-three minutes and washed seven times with sterile deionised water. The seeds were then left in water to imbibe for 1-4 hours at room temperature. Subsequently, seeds were left for three days in plates with water agar (DWA) medium at 4°C in the dark.

2.7.1 On agar plates

Seedlings with 1-2 cm long roots were transferred to Fahraeus nitrogen-free plant agar medium (Fahraeus, 1957) agar (FP) plates containing 0.1 µM L-α-(2-aminoethoxyvinyl glycine) (AVG). AVG was added in order to prevent the inhibition of nodulation by ethylene accumulation in the roots. The region of the plates containing the roots was wrapped in black plastic and the plates were incubated vertically in a controlled environment (20°C/15°C, day/night cycles of 18/6 h with 32% relative humidity, 300 µmol m^{-2} s^{-1} light intensity).

2.7.2 In compost

Plants were germinated on DWA agar as described above, then the plates were placed upside down at room temperature overnight. Seedlings with 10-15 mm long roots were transferred to soil in Medicago Mix compost or terragreen:sand (Table 2.3). The plants were grown in a controlled environment room (20 °C, 16 h photoperiod) or a greenhouse and watered regularly. In the greenhouse additional heat was provided during the winter. For the first two-three days a clear glass lid was placed on top of the pots to protect the plants from drying out.

2.8 Cross fertilisation of *M. truncatula*

M. truncatula plants were grown in soil as described above (2.7). Once the plants started flowering cross fertilisation was carried out between the plants starting with the emasculation of a flower from a nodulation and/or bacterial infection mutant plant (female parent) using suction generated by a vacuum pump connected to a micropipette tip. Pollen from a YC3.6-expressing (male parent) flower was applied to the stigma of the female parent. After cross-fertilisation the stem holding the cross-fertilised flower was placed in a Falcon tube containing water covered with cotton wool to maintain a humid environment to prevent the flowers from

drying out. When a seed pod formed, the stem and pod were carefully removed from the Falcon tube and netting tied around them to enable the pod to mature and dry out. The F_1 progeny were screened for YC3.6 fluorescence using a fluorescence microscope and grown in Medicago mix compost. The F_2 progeny from the crosses were screened and the plants that had YC3.6 fluorescence and the desired mutant phenotype from the female parental line were kept and allowed to self-fertilise to produce seed. Experiments were carried out using the F_3 progeny.

2.9 Calcium imaging with Oregon Green

2.9.1 Plant preparation

Seedlings of *M. truncatula* were germinated and grown on FP+AVG agar plates overnight as described above. A small chamber was made on a 48 mm x 64 mm cover glass thickness no. 1.5 (Agar Scientific, Essex, UK) using high vacuum grease (Dow Corning, USA) and a seedling with a 2-3 cm long root was placed onto this and anchored in place using high vacuum grease and fragments of glass cover slips. The chamber was then filled with 200 µl of liquid FP medium.

2.9.2 Dye preparation

Oregon Green-dextran MW 10,000 and Texas Red-dextran MW 10,000 (Molecular Probes, Eugene, USA) were dissolved in sterile water to a final concentration of 5 mM. Texas Red (calcium-insensitive dye) was used as a reference to eliminate the background fluctuation. For each experiment, 1 µl 5x injection buffer [0.75 M KCl, 0.45 M 4-(2-hydroxyethyl)-1-piperazineethanesulfonic acid (HEPES), pH 7.0] was added to 4 µl of dye solution. Due to the higher fluorescence of Texas Red, 0.4 µl aliquots of Texas Red were added to 3.6 µl of Oregon Green, and then 1 µl 5x injection buffer was added to the mixed dye solution. The solution of dye was spun at 12,000 rpm in a microcentrifuge (Centrifuge 5424, Eppendorf) for one minute to remove any particulate matter and the upper solution was used for microinjection.

2.9.3 Needle Preparation

Thin needles for microinjection were made using Borosilicate Glass Capillaries (1B120F-4; World Precision Instruments Inc.) and a computer-controlled electrode puller (model P1000 Flaming/Brown Micropipette Puller, Sutter Instruments Ltd., USA). The optimized setting for

pulling very thin needles was a heat intensity setting of about 554 and a pulling force setting of about 52. The tips of these needles were examined under the light microscope and only needles with thin tips were selected for use in injection.

2.9.4 Microinjection

The microinjection system was essentially the same as that described by Wais et al. (2000). The needle was first loaded with about 0.2 µl of dye solution containing Oregon Green and Texas Red using a long thin pipette tip (Microloader; Eppendorf) and then the needle was back-filled with 10 µl of 1 M KCl. A prepared seedling (2.9.1) was placed on an inverted epifluorescence microscope. The reference electrode was placed into the FP medium in the bath. The needle was controlled by an electro-manipulator (PatchMan NP2; Eppendorf) and the tip of the needle was targeted to the apex of the growing root hair cells. The precise position of the needle tip was monitored by measuring the voltage through the needle. When the tip entered in the cytoplasm, the voltage changed slightly. Then dyes were injected into the root hair cell by iontophoresis using a direct current (DC) set at 10 nA. Injection proceeded until cells dimly fluoresced when viewed under illumination from a 100 W mercury bulb through a GFP filter block. After microinjection, root hairs were left at least 20 min before NF addition and only cells showing active cytoplasmic streaming were used for analysis. NFs were added in a small volume (2 µl) directly to the edge of the incubation chamber at the concentrations stated in the text.

2.9.5 Imaging by fluorescent microscopy

Fluorescence was imaged using a Nikon TE2000U inverted microscope coupled to a Hamamatsu Photonics digital CCD camera. An image splitter (Cairn Research, Faversham, Kent, UK) with optimised polychromatic mirror was used to monitor both Oregon Green and Texas red fluorescence and each image was sequentially collected every five seconds with a 1 s exposure using MetaFluor software. For Oregon Green the excitation wavelength was 488 nm and an 11 nm bandpass was selected using an Optoscan Monochromator (Cairn Research, Faversham, Kent, UK) with an emission filter of 545 ($\pm$ 15) nm. For Texas Red, an excitation wavelength of 570 nm was used and the fluorescence was monitored with an emission filter of 620 ($\pm$ 20) nm. After taking a series of images, the ratiometric traces were calculated by dividing Oregon Green fluorescence by that of Texas Red at each time point. Traces were generated using Microsoft Excel.

2.10 Calcium Imaging with Cameleon YC2.1/YC3.6

Seeds of the *M. truncatula* YC2.1 or YC3.6 transgenic lines were germinated, grown on FP+AVG plates overnight and placed in a small chamber filled with 200 µl of liquid FP as described above (2.9.1). CYAN FLUORESCENT PROTEIN (CYP) and YELLOW FLUORESCENT PROTEIN (YFP) fluorescence was imaged using a Nikon Eclipse Ti inverted fluorescence microscope coupled to a Qimaging RETIGA-SRV camera. A Nikon 40x working lens was used for imaging. The CFP component of YC2.1/YC3.6 was excited with a wavelength of 437 nm and an 11 nm bandpass using an Optoscan Monochromator (Cairn Research, Faversham, Kent, UK). Emitted fluorescence was separated by an image splitter with a dichroic mirror 515 nm, and then passed through an emission filter of 485 (± 20) nm for CFP fluorescence or 535 (± 15) nm for YFP fluorescence. Images were collected every one or five seconds with 750-1000 milliseconds exposure and analyzed using MetaFluor software. Traces were generated using Microsoft Excel.

For inhibitor treatments, seedlings were set up on the microscope ready for imaging prior to treatment with the chemical. Image acquisition commenced and the seedlings were incubated with the chemical for 15 minutes prior to the addition of 10 nM NF.

2.11 ROS imaging using CM-H_2DCFDA

On the day of use, CM-H_2DCFDA dye was dissolved in dimethyl sulphoxide (DMSO) to make a 100 mM stock solution. The dye was then diluted in liquid FP to a final concentration of 40 µM (containing 0.04% (w/v) DMSO). *M. truncatula* seeds were germinated and placed in a small chamber filled with 200 µl of liquid FP medium as described above (2.9.1). The prepared seedling was placed on the inverted fluorescence microscope and then the FP solution was replaced with 200 µl of the 40 µM dye solution. After 15 minutes the dye solution was removed and the chamber washed carefully three times using liquid FP, and then 200 µl liquid FP was added to the chamber. For treatment with diphenylenoidonium (DPI), 50 uM DPI [dissolved in DMSO, final concentration 0.2% (v/v)] was added to the chamber at this point. Root hairs were left at least 5 min before starting the imaging and NF added. Only cells that retained the dye within the cytoplasm and not the vacuole were included in the analysis. To check that any fluctuations in CM-H_2DCFDA fluorescence were not due to photo-oxidation or photo-bleaching, fluorescence intensities from a reference region away from the root hair cells

were also included to monitor background dye fluorescence. Any fluctuations in CM-H$_2$DCFDA intensity in the root hair cells that were also visible in the reference region were discounted from the analysis.

Fluorescence was imaged using a Nikon TE2000U inverted microscope coupled to a Hamamatsu Photonics digital CCD camera. The excitation wavelength was 488 nm with an 11 nm bandpass using an Optoscan Monochromator (Cairn Research, Faversham, Kent, UK). An emission filter of 535 with a 30 nm bandpass was used. Images were collected at one second intervals with 500 millisecond exposure. False colour mapping images of fluorescence insensity were generated using MetaFluor Software (Cairn, UK).

2.12 Physiological Techniques

2.12.1 Root and root hair length measurement

Seeds were sterilised and germinated on DWA plates as described in section 2.7. Seedlings with 10-20 mm long roots were placed on sterile filter paper on BNM agar in square (100 x 100 mm) plates. A second piece of filter paper was placed on top of the seedlings. Plates were incubated vertically in a growth chamber for approximately 72 hours (20°C/15°C, day/night cycles of 18/6 h with 32% relative humidity, 300 µmol m^{-2} s^{-1} light intensity).

To measure seedling root length photographs of the seedlings on agar plates were taken using a digital camera and root lengths measured using ImageJ software (National Institutes of Health, USA).

Root hair lengths were measured using seedlings placed on Fahraeus slides and viewed under a light microscope (Zeiss Axiophot) using a Zeiss 20 x objective lens. Working from the tip of the root, images were taken at the point where the root hairs first appear to be fully vacuolated at the tip (mature root hairs). Root hair lengths were measured from the images using ImageJ software (National Institutes of Health, USA).

2.12.2 Root hair deformation

Seeds were sterilised and germinated on DWA plates as described in section 2.7. Seedlings with 10-20 mm long roots were transferred to BNM + 0.1 µM AVG square (120 x 120 mm) agar plates and incubated vertically overnight in a growth chamber (20°C/15°C, day/night cycles of 18/6 h with 32% relative humidity, 300 µmol m^{-2} s^{-1} light intensity). The seedlings were then

transferred to Fahraeus slides filled with BNM solution containing 10 nM NF (negative controls had no NF added). After NF was added, the samples were left in the dark at room temperature for approximately 24 hours. Root hairs were examined under a light microscope and root hair deformation was scored without prior knowledge of the identity of the plant line (*i.e.* wildtype or mutant) or the treatment (NF or no treatment). Roots containing branching root hair cells were considered positive for this response. Images were taken using a light microscope (Zeiss Axiophot) with a QICAM 12-bit monochromatic camera (QImaging, UK).

2.12.3 Nodulation experiments

Seeds were sterilised and germinated on DWA plates as described in section 2.7. The plates were then transferred to room temperature overnight. The seedlings were then sown into terragreen:sand 1:1 mix and placed into a controlled environment room (20 °C/15 °C, 16 h photoperiod). After 6 days a culture of *S. meliloti* 2011 (2.2) was grown overnight in 5 ml TY broth at 28 °C with strepinomycin (2.4) with vigorous shaking until $0.3 < OD_{600} < 0.8$ (exponential phase). The culture was diluted in sterile deionised water to $OD_{600} = 0.001$ and this was used to water the plants. After a period of time (7, 10, 14 or 21 days) plants were dug up, the roots washed in water and the nodules counted.

2.12.4 Infection thread staining and quantification

M. truncatula seeds were sterilised and germinated on DWA plates as described in section 2.6. The plates were then transferred to room temperature and incubated overnight. Seedlings were placed on top of filter paper on BNM + 0.1 µM AVG square (120x120 mm) agar plates. A culture of *S. meliloti* 2011 *lacZ* (2.2) was grown overnight in 5 ml TY broth with streptinomycin and tetracycline (2.4) at 28 °C with vigorous shaking until $0.3 < OD_{600} < 0.8$ (exponential phase). The *S. meliloti* 2011 *lacZ* culture was diluted in sterile deionised water to $OD_{600} = 0.001$ and was used to inoculate the plants using an intranasal Mucosal Atomization (MADS) device (LMA, San Diego, USA) for even coverage (1 ml per plate) and another sterile filter paper placed on top. Plates were incubated in a growth chamber (20 °C/15 °C, day/night cycles of 18/6 h with 32 % relative humidity, 300 µmol m^{-2} s^{-1} light intensity).

After 6 days the roots were fixed in Z buffer (100 mM sodium phosphate pH 7.0, 10 mM KCl and 1 mM MgCl$_2$) containing 2.5% (w/v) glutaraldehyde under vacuum in a fume hood for 15-30 mins. Then fresh Z buffer with 2.5% (w/v) gluteraldyhde was added and the roots left for at least one hour at room temperature. The roots were then washed 3 times in Z buffer (no gluteraldehyde).

To stain the roots X-Gal staining solution was made up. For 1 ml: 880 μL Z buffer, 50 μl K$_3$[Fe(CN)$_6$] (potassium ferricyanide) 100 mM, 50 μl K$_4$[Fe(CN)$_6$] · 3H$_2$O (potassium ferrocyanide) 100 mM and 20 μl 5-bromo-4-chloro-3-ondolyl-beta-D-galactopyranosid (X-Gal) 4% (w/v) in dimethylformamide. The X-gal staining solution was added to the roots and incubated in the dark at 28 °C overnight.

The roots were washed in Z buffer with one quick wash followed by one for an hour. The stained roots were then placed in 5 ml fresh Z buffer with 2-3 drops of 0.5 M Na-EDTA to inhibit fungal growth.

Stained roots were viewed under a light microscope (Zeiss Axiophot) using a Zeiss 20X objective lens to quantify the infection events (represented by blue stained bacteria). The infection events were classified into three stages: infection foci, infection threads in the epidermis and ramifying infection threads in the cortex. Images were taken using a QICAM 12-bit monochromatic camera (QImaging, UK) using a RGB colour filter.

2.13 Molecular Biology Techniques

2.13.1 DNA extraction from plants

Genomic DNA extractions were carried out by Richard Goram (John Innes Centre) using DNeasy Plant kit 96 protocol (Qiagen, UK) as per manufacturer's instructions.

2.13.2 Plasmid extraction from bacteria

To prepare for extraction of plasmid DNA *E. coli* cultures were grown in LB broth with the appropriate antibiotic (2.2 and 2.4) at 37 °C for 12-16 h (to reach stationary phase) with vigorous shaking. Cultures of *Agrobacterium tumefaciens* were grown in TY broth with the appropriate antibiotic (2.2 and 2.4) at 28 °C for 2 days (to reach stationary phase with vigorous shaking. Extraction of plasmid DNA from *E. coli* and *A. tumefaciens* was carried out using a QIAprep Spin Miniprep Kit (Qiagen, UK), as per manufacturer's instructions.

2.13.3 Amplification of DNA by polymerase chain reaction (PCR)

DNA was amplified by PCR using 1 to 20 ng of template DNA in reaction volumes of 10-50 μl. For cloning purposes the Phusion polymerase (New England Biolabs, Hertfordshire) was used

as per manufacturer's instructions. For all other purposes GoTaq polymerase kit (Promega, Southampton) was used as per manufacturer's instructions, unless otherwise stated.

For genotyping of *Tnt1* insertion lines for insertions in *MtGAP1* and *CBS1* the primers used are listed in Table 2.5.

Table 2.5: **Primers used for genotyping insertions in *Tnt1* lines**

DNA target	Forward primer 5'-sequence-3'	Reverse primer 5'-sequence-3'
MtGAP1	AGGCTGCTCTTCTTGACTGG	TTCTCAACCGTGACCAGTGT
CBS1	CAAACTCGCGGTGTTTAATG	TTGGAAGACCCTGTTGAACC
Tnt1	TCCTTGTTGGATTGGTAGCC	CAGTGAACGAGCAGAACCTGTG

2.13.4 Agarose gel electrophoresis

DNA fragments were separated by electrophoresis in horizontal agarose gels. The gels were prepared in 1 X TBE (89 mM Tris-borate and 2 mM EDTA, pH 8.3) containing 1-1.5% (w/v) agarose. For PCR products from GoTaq reactions the samples were loaded directly into the wells but for all other DNA the samples were mixed with 1 x loading dye (0.25% (w/v) bromophenol blue and/or 0.25% (w/v) xylene cyanol FF in 40% (v/v) glycerol/distilled water) and loaded into the wells. To estimate size of DNA bands a DNA ladder (2-log or 1 kb, New England Biolabs, Hertfordshire) was loaded into one of the empty wells. Electrophoresis was carried out at 90 to 120 V until the desired separation was achieved. When electrophoresis was completed, gels were transferred to a tank containing 1 mg/ml ethidium bromide and left for 15 to 30 min. The DNA was detected by fluorescence of the DNA-ethidium bromide complex exposed to ultraviolet (UV) light from a transilluminator, and photographed using a Gene Flash (Syngene Bio Imaging) video camera system.

For further analysis of DNA after gel electrophoresis the area of gel containing the DNA was excised from the gel and DNA extracted using a QIAQuick Gel Extraction Kit (Qiagen, UK) as per manufacturer's instructions.

2.13.5 Gateway Cloning

To generate the pB7WG2-YC3.6 binary vector for plant transformation Gateway Cloning Technology (Invitrogen, UK) was used. The sequence of the forward and reverse *attB* PCR primers (Table 2.6) and the amplification of the *attB* PCR product were done following the manufacturer's protocol. After purification of the *attB* PCR product a 10 µl BP recombination reaction was carried out by mixing 2 µl BP Reaction Buffer, 1 µl of pDONR201 (entry) vector (150ng/µl), 5 µl *attB* PCR product and 2 µl BP Clonase II (Invitrogen). The sample was incubated overnight at 25 °C and 1 µl Proteinase K (Invitrogen) solution was added to terminate the reaction incubating the sample at 37°C for 10 min. 3 µl of the BP reaction mix was used to transform *E.coli* DH5α (see below). To ensure the entry clones had correctly assembled a region across the fusion sites and the inserted region was amplified by PCR (section 2.12.3) and sequenced (section 2.12.6).

For the LR reaction 0.6 µl of the entry clone was mixed with 0.3-0.6 µl of the destination vector (pB7WG2) and 0.3-0.6 µl Clonase Reaction Buffer (Invitrogen) to a final volume of 2.5 µl. Next, 1 µl LR Clonase II (Invitrogen) was added and the sample was incubated at 25 °C overnight. To terminate the reaction 0.5 µl Proteinase K (Invitrogen) was added and the sample incubated at 37°C for 10 min. Next, 3 µl of the LR reaction mix was used to transform *E.coli* DH5α (see 2.12.6). To ensure the entry clones had correctly assembled a region across the fusion sites and the inserted region was amplified by PCR (section 2.12.3) and sequenced (section 2.12.6).

Table 2.6: Primers used for Gateway Cloning

Gene	Forward primer 5'-sequence-3'	Reverse primer 5'-sequence-3'
attB1*-YC3.6-*attB2	GGGGACAAGTTTGTACAAAAAA GCACCCTTAATACGACTCACTATA	GGGGACCACTTTGTACAAGAAAGCTGG GTCATACGATTTAGGTGACACTATAG

2.13.6 DNA sequencing

DNA was sequenced by cycle sequencing using the di-deoxy chain termination method (Sanger et al., 1977). Each sequencing reaction had a final volume of 10 µl containing 100 ng of plasmid DNA as a template, 0.2 µM of sequencing primer and 2.5 µl Big Dye Sequencing Kit Version III

(Perkin Elmer, Massachusetts, USA). Samples were initially denatured at 94 °C for 2 min. The reaction was then cycled 25 times with denaturation (94 °C for 10 sec), annealing (50 °C for 5 sec), and elongation (60 °C for 4 min). After this cycle, the sample was held at 12 °C. The dideoxy PCR products were sent to Genome Enterprise Ltd (Norwich, UK) or Eurofins Ltd. (Germany) for sequencing. Alternatively, the DNA and primer were sent to Eurofins for the sequencing reaction and sequencing.

2.13.7 Transformation of *Escherichia coli*

Competent cells of *E. coli* DH5α were prepared as described (Inoue et al., 1990). In each transformation, 50 µl of competent cells were mixed with 2 µl ligation mix and incubated on ice for 30 min. The cells were heat shocked at 42 °C for 90 sec and chilled for 5 min on ice. The cells were mixed with 450 µl of LB medium and incubated for one hour at 37 °C. The transformation mix was plated on LB agar medium containing appropriate antibiotics and incubated at 37 °C overnight

2.13.8 Transformation of *Agrobacterium tumefaciens*

A. tumefaciens AGL1 was transformed with the pB7WG2-YC3.6 plasmid by electroporation using the protocol of McCormac et al. (1998). The transformation mix was plated on L agar medium containing spectinomycin and rifampicin and incubated at 28 °C for 2-3 days.

2.13.9 *A. tumefaciens*-mediated stable transformation of *M. truncatula*

Stable transformations of *M. truncatula* R108 and A17 with Cameleon YC3.6 using *A. tumefaciens AGI1* (pB7WG2-YC3.6) were carried out by Matthew Smoker (The Sainsbury Laboratory, Norwich). For R108 leaf tissue was used as described by Trinh et al. (1998). For A17 transgenic shoots were recovered from cotyledonary node explants as described by Zhou et al. (2004). The shoots were placed on rooting media to develop roots and then were transferred to Medicago mix soil (2.3) for seed production.

2.13.10 *Agrobacterium rhizogenes*-mediated hairy root transformation of *M. truncatula* for RNAi knockdown of *ROP9*

Seeds of *M. truncatula* A17 YC3.6 were sterilised and germinated as described in section 2.6. Under sterile conditions the tip of the radicle was removed (approximately 3 mm). Cultures of *A. rhizogenes* QUA1 pK7GWIWG2(II)-dsRED and ROP9i [(2.2) provided by Kiirika et al (2012)] were grown for 2 days at 28 ° C in 5 ml TY broth with spectinomycin (2.4) and then

sedimented by brief centrifugation and resuspended in an equal volume of fresh TY broth. A large drop of bacteria was placed in a Petri dish and the cut seedlings were dipped in the bacterial culture. Ten seedlings were transferred onto each modified FP plate (poured on a slant). The plates were placed vertically in a growth chamber (20°C/15°C, 16 h photoperiod). After one week the seedlings were transferred to fresh modified FP medium containing 25 µg/ml kanamycin and black bags were placed over the bottom of the plates. The plates were incubated for 3-4 weeks in a growth room (23 °C, 16 h photoperiod) to allow formation of hairy roots. Roots were examined using a fluorescence microscope (Leica DMR/MZFLIII) with a green filter to visualise the DsRED marker gene. Plants containing hairy roots with strong fluorescence had all roots except the largest transformed root removed and were transferred to fresh modified FP plates and were returned to the growth chamber with black bags on the plates covering the roots.

To image calcium, short sections (5-10 mm) of lateral root were excised and set up for YC3.6 fluorescence imaging as described in section 2.9, except the chambers contained only 100 µl of modified FP. Expression levels of ROP9 and two housekeeping genes EF1 and Tip41 in empty vector and ROP9 RNAi roots were quantified using qRT-PCR (2.12.13).

2.13.11 RNA Extraction and DNase treatment

For each sample, RNA was extracted from approximately 100 mg root tissue using the RNeasy Plant Mini Kit (Qiagen) according to the manufacturer's protocol. The RNA was eluted with 30 µl RNase free water. Isolated RNA was treated with Turbo DNase (Ambion, Life Technologies, UK) according to the manufacturer's protocol. The RNA was quantified with NanoDropR ND-1000 Spectrophotometer (NanoDrop Technologies) and the quality was assessed by running a sample on a 1% (w/v) agarose gel and checking the ribosomal RNA bands were of similar intensity.

2.13.12 Reverse transcription polymerase chain reaction (RT-PCR)

Complementary DNA (cDNA) was prepared from 100-500 ng of RNA using SuperScript II first strand synthesis (Life Technologies, Invitrogen) according to the manufacturer's protocol, using oligo(dT) primers (Life Technologies, Invitrogen).

Amplification of cDNA by PCR was carried out as described in section 2.12.3 using the primers listed in Table 2.7. The products were run on 1% agarose gel.

Table 2.7: Primers used in RT-PCR

Gene	Forward primer 5'-sequence-3'	Reverse primer 5'-sequence-3'
EF1	CTTTGCTTGGTGCTGTTTAGATG	ATTCCAAAGGCGGCTGCATA
MtGAP1	ATGACTCGCCTTTTTCGATCGAA	TCAAGCCCAAGCTTCTCCTCC

2.13.13 Quantitative reverse transcription polymerase chain reaction (qRT-PCR)

cDNA was prepared from RNA as described above. Quantitative RT-PCR was performed using a CFX96 Real-Time System (BIO-RAD) and using SYBR Green Master Mix (Sigma). Each 10 µl PCR reaction contained 2 µl cDNA 1:2, 5 µl SYBR Green Master Mix (Sigma), 2.6 µl MgCl$_2$ solution (Sigma) and 0.2 µl of each primer (10 µM, designed to amplify a fragment of 50-150 bp, shown in Table 2.8). An initial denaturation step of 95°C for 4 min was followed by 50 cycles of 94°C for 30 seconds, 60°C for 30 seconds, and 72°C for 30 seconds. At the end of the reaction, the samples were heated at 72°C for ten minutes. Reactions were undertaken in 96-well white microplates (Biorad, UK). The *Elongation Factor 1 (EF1)* and *TAP42-interacting* protein *(TIP41)* genes were used as internal positive controls. Results were expressed as a threshold cycle (CT) value. Normalised expression values for *MtGAP1* were calculated from the CT values using the qBASE model using two housekeeping genes (*EF1* and *TIP41)* (Hellemans et al., 2007). The qBASE model allows primer specific efficiencies to be taken into account.

Table 2.8: Primers used for qPCR

Gene	Forward primer 5'-sequence-3'	Reverse primer 5'-sequence-3'
EF1	CTTTGCTTGGTGCTGTTTAGATG	ATTCCAAAGGCGGCTGCATA
TIP41	GCTTTGCCACCTGTTGAAGT	AGCACCGCTTCCACAATAAG
MtROP9	CCTGTATTCCCCTCCCCTTC	GCCACCTTATGCTTCAAGGAG

2.14 Bioinformatics

2.14.1 Identification of *M. truncatula GAP* family

The protein sequences of the nine *Arabidopsis thaliana* RopGAPs (TAIR database) were used to search the *M. truncatula* genome (IMGAG vr 4.0) using BLAST. The top *M. truncatula* hits were then used as subject sequences to search the *A. thaliana* genome (TAIR database) to check that the *A. thaliana* RopGAPs were the top hits (reverse BLAST).

The location of introns and exons in *MtGAP1* were predicted from the genome and coding sequence (CDS) sequences using the Gene Structure Display Server (Guo et al., 2007). The protein domains in MtGAP1 were predicted using InterPro (Hunter et al., 2012).

2.14.2 Phylogenetic Tree Construction

To construct a phylogenetic tree of the RopGAP family the protein sequences of the *M. truncatula* and *A. thaliana* GAPs were entered into the "1 Click mode" tree option on the Phylogeny.fr server (Dereeper et al., 2008, Dereeper et al., 2010).

2.14.3 Root hair gene expression analysis

Using the root hair microarray data generated by Breakspear et al. (unpublished) the expression of the ROP GTPase, RopGEF and RopGAP families in wildtype and infection mutant root hairs after inoculation with *Sinorhizobium meliloti 1021* were analysed. To do this probesets were identified for the gene family members by BLAST search of the Medicago Gene Expression Atlas (MGEA) database. The geometric means of the normalised expression values for three replicates were calculated. For analysis of gene expression in wildtype root hairs the fold change in expression compared to control root hairs inoculated with *Sinorhizobium meliloti* SL44 *nodD1ABC* (unable to infect into the root) at each time point (1,3 and 5 days post inoculation) were calculated. For analysis of the infection mutant lines at 5 days post inoculation the fold changes versus wildtype root hairs inoculated with wildtype *S. meliloti* 1021 were calculated.

CHAPTER 3: DEVELOPING TOOLS FOR IMAGING CALCIUM AND REACTIVE OXYGEN SPECIES IN *MEDICAGO TRUNCATULA* ROOT HAIRS

3.1 Introduction

Fluorescent dyes and proteins can provide insights into calcium and ROS dynamics in individual cells. Of these, the Ca^{2+}-sensitive fluorescent probes are the most developed and have been used to image free Ca^{2+} in a range of situations in plants including root hair and pollen tube growth (Foreman et al., 2003, Holdaway-Clarke et al., 1997, Michard et al., 2008, Monshausen et al., 2008).

The Ca^{2+}-sensitive Oregon Green-dextran dye has been widely used for imaging NF-induced calcium responses in legume root hairs (Miwa et al., 2006a, Shaw and Long, 2003a, Walker et al., 2000). It has single excitation and emission wavelengths, is non-ratiometric and the fluorescence is proportional to the concentration of calcium ions in that cell region. Unfortunately, the fluorescence intensity also depends on the concentration of dye in a region so any fluctuations in the cell such as cytoplasmic streaming or a change in the cell volume can affect the signal. Including a non-calcium sensitive dye such as Texas Red and calculating the ratio of the fluorescence from the two dyes (pseudoratiometric) reduces the noise from cell fluctuations to improve signal quality (Shaw and Long, 2003a). Fura-2 is a Ca^{2+}-sensitive dye that allows ratiometric imaging by having excitation at two wavelengths (one calcium-dependent the other not) with emission measured at a single wavelength (Grynkiewicz et al., 1985). However, Fura-2 was found to be somewhat toxic in alfalfa root hair cells (Ehrhardt et al., 1996) so its use in legumes has been limited, although it has since been used successfully in *Sesbania rostrata* and *Medicago truncatula* (Capoen et al., 2009). To prevent the fluorescent dyes from being pumped into the vacuole the dyes are often linked to dextrans and microinjected into cells. Unfortunately, microinjection is invasive and can generate noise in calcium signals, as shown by a dose-response curve of the NF-induced calcium influx response, where even at very low concentrations (10^{-12}M) of NF the number of cells apparently inducing calcium changes never reached zero (Morieri, 2010).

The development of the ratiometric Cameleon fluorescent proteins was a major advancement in cellular calcium imaging. The most widely used are the Yellow Cameleons (such as YC2.1 and

YC3.6) consisting of Cyan Fluorescent Protein (CYP) and Yellow Fluorescent Protein (YFP) linked by the Ca^{2+}-binding domain of calmodulin and the M13 calmodulin-binding peptide from the mammalian myosin light chain kinase (Miyawaki et al., 1997, Miyawaki et al., 1999). When no Ca^{2+} is bound to the probe, excitation of the CYP domain results in an emission maximum around 480 nm. When Ca^{2+} binds, the conformation of the protein is changed so that the CYP and YFP are brought closer together and some energy is passed from CFP to YFP by Förster Resonance Energy Transfer (FRET) resulting in an enhanced emission around 540 nm from YFP and correspondingly lower emission from CFP. The ratio of YFP to CFP fluorescence is proportional to the concentration of Ca^{2+} ions in the region of interest (Miyawaki et al., 1997).

A *Medicago truncatula* stable line expressing YC2.1 was developed by Miwa et al. (2006b) and has been used in studies into symbiosis calcium signalling (Granqvist et al., 2012, Kosuta et al., 2008, Morieri et al., 2013, Sun et al., 2007). However, this reporter has a relatively small dynamic range with a maximal FRET change of 40% from zero to saturating (micromolar) calcium concentrations (Miyawaki et al., 1997). The result is that there is only a two-fold change in YFP/CFP signal across its Ca^{2+}-responsive range. Newer versions of Yellow Cameleon have been developed such as YC3.6, which has a circular version of YFP (cYFP) (Nagai et al., 2004). The dynamic range of the YC3.6 FRET signal is 84%, resulting in a six-fold change in YFP/CFP ratio across the calcium-response range, a significant improvement on YC2.1. The increased sensitivity of YC3.6 over YC2.1 revealed novel aspects of calcium signalling. For example, when YC3.6 was used to image Ca^{2+} in growing *Arabidopsis thaliana* root hair cells it became apparent that the previously described tip-calcium gradients (observed using YC2.1) are made up of oscillations that have the same period but are out of phase with the observed oscillations in growth rate (Bibikova and Gilroy, 2002, Monshausen et al., 2008). Therefore, the study of symbiosis calcium signalling could benefit from use of the YC3.6 reporter.

The tools available to image ROS in cells are much more limited. There are several fluorescent dyes such as OxyBURST Green (H_2HFF-BSA) and dihydrodichlorofluorescein (H_2DCF) derivatives that have been used to image ROS responses in a number of plant processes including root hair and pollen tube growth (Foreman et al., 2003, Liu et al., 2009, Monshausen et al., 2007). The H_2DCF derivative 5-(and-6)-chloromethyl-2',7'-dichlorodihydrofluorescein diacetate (CM-H_2DCFDA) has been used to characterise the NF-induced ROS transient in *Phaseolus vulgaris* root hairs (Cárdenas et al., 2008). Unfortunately, these dyes all share a limitation. Their change in fluorescence in response to ROS is effectively irreversible so it is not possible to directly measure declines in ROS levels (Choi et al., 2012). There are also other technical limitations;

for example the H_2DCF derivatives are susceptible to photoxidation and photobleaching from the fluorescence illumination system (Choi et al., 2012), so experiments must be carried out in a low light environment with as low fluorescence excitation intensity as possible. Also, the H_2DCF derivatives are not specific for a particular ROS species so it is impossible to infer which species is responsible for any change in dye fluorescence(Choi et al., 2012).

Some genetic GREEN FLUORESCENT PROTEIN (GFP)-based probes have been developed. The roGFPs have point mutations that make them oxidation sensitive by introducing two cysteines that can form disulphide bonds in an oxidising environment (Dooley et al., 2004, Hanson et al., 2004). This shifts the GFP excitation peak from 400 to 499 nm so the roGFPs can be used for spatio-temporal ratiometric analysis of oxidative status within cells. HyPer is another ratiometric probe but it is H_2O_2 specific. It consists of the regulatory domain of the *Escherichia coli* transcription factor OxyR (OxyR-RD) inserted into cYFP (Belousov et al., 2006, Nagai et al., 2001). When OxyR-RD binds H_2O_2, an intramolecular disulphide bond between two cysteine residues leads to a conformational change in HyPer that shifts the cYFP excitation maximum from 420 nm to 500 nm (Belousov et al., 2006, Choi et al., 2001). The disulphide bond is reduced when H_2O_2 is scavenged so the changes in HyPer fluorescence caused by ROS are fully reversible. The first report of HyPer use in plants came from Costa et al. (2010) where they used the probe and a peroxisome targeted version to image H_2O_2 in the cytoplasm and peroxisomes of *A. thaliana* and tobacco leaf cells.

However, HyPer is not without limitations. The fluorescence from HyPer is affected by pH because deprotonation of HyPer as pH rises leads to an increase in HyPer fluorescence. A pH change from 7.0 to 7.5 leads to a 3-fold increase in HyPer fluorescence, which could appear to be a 100 nM increase in H_2O_2 (Belousov et al., 2006). Therefore, the pH sensitivity of HyPer can lead to the erroneous identification of H_2O_2 increases and so it is important that when using HyPer the pH dynamics in the cell are also considered. Since NF activates an intracellular alkalisation in the tips of legume root hair cells alongside the calcium influx and ROS transient (Cárdenas et al., 2008, Ehrhardt et al., 1992, Felle et al., 1996, Felle et al., 1998, Kurkdjian, 1995), the current forms of HyPer are of limited value in this system.

This chapter describes the development of *Medicago truncatula* YC3.6-expressing stable lines and the results demonstrate that it can provide more insights into the spatial and temporal characteristics of NF-induced calcium signalling over other reporters. A method for imaging the NF-induced ROS transient in *M. truncatula* root hairs using a H_2DCF derivative (CM-H_2DCFDA) is also described. This probe was chosen because it has been previously shown to be suitable for

imaging ROS in root hair cells, including the NF-induced ROS transient in *Phaseolus vulgaris* (Cárdenas et al., 2008), and being a dye it is easy to load into plant cells and avoids any delay in studying *M. truncatula* mutant lines that would result from using a genetic probe. Importantly, it also does not suffer from the pH sensitivity that currently plagues the HyPer probe. By studying the NF-induced ROS transient in *M. truncatula* it will be possible to utilise the forward and reverse genetic tools available in this model legume to elucidate how it relates with other NF responses in root hair cells.

3.2 Results

3.2.1 Analysis of calcium responses in *Medicago truncatula* root hair cells expressing Cameleon YC3.6

The Gateway cloning technique (Chapter 2.12.5) was used to insert the YC3.6 gene (Nagai et al., 2004) into the pB7WG2 binary vector (Karimi et al., 2002) where it is under the control of the 35S promoter (Figure 3.1). *Agrobacterium tumefaciens*-mediated transformation (Chapter 2.13.9) was used to generate stable Cameleon YC3.6-expressing lines in both the wildtype Jemalong A17 and R108 ecotypes. For each ecotype 100 plants were used and shoots were recovered from two A17 and nine R108 independent calli.
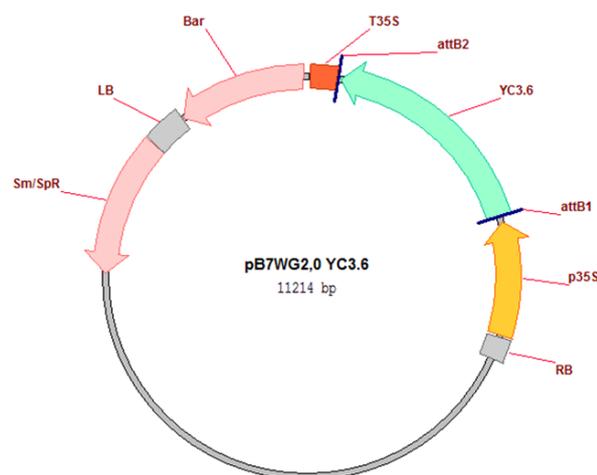
Figure 3.1: pB7WG2-YC3.6 binary vector for *A. tumefaciens*-mediated transformation.

The vector has the YC3.6 gene under control of the 35S promoter and terminator with BASTA resistance for plant selection and spectinomycin resistance for bacterial selection.

The shoots that developed roots after transfer to rooting medium were then transferred to soil (2.13.9). From these plants, seeds were produced for both A17 independent lines, and five of the nine R108 independent lines. Seedlings from the T_1 generation were germinated and grown on FP+0.1 µM AVG plates overnight (Chapter 2.7) before screening root hairs for YC3.6 expression using an inverted fluorescence microscope (Chapter 2.10), checking that the protein was present in the cytoplasm and nucleus and not in the vacuole. Transformed lines with the highest fluorescence were propagated (Table 3.1). *A. tumefaciens*-mediated transformation can result in multiple insertions of the gene of interest and this can be indicated by the segregation of YC3.6 fluorescence in the transformant lines. Neither the A17 nor R108 transformant lines showed the expected 3:1 ratio of plants expressing YC3.6 to plants not expressing YC3.6 with the T_1 generations having ratios of 1.73:1 and 4.4:1 respectively (Table 3.1). This indicates that in both cases there may be multiple copies of YC3.6 inserted into the genome. This could lead to variable YC3.6 expression levels between individuals in these plant lines, but since relative Ca^{2+} levels are calculated by the ratio of CFP/YFP fluorescence this should not greatly affect the overall signal, therefore this is not considered to be a major issue in regard to using these lines. T_1 individuals with the highest levels of YC3.6 fluorescence were selected for propagation, on the assumption that they are the most likely to be homozygous for the insertion(s).

Table 3.1: YC3.6 expression in transgenic lines of *M. truncatula*

Generation	Parental Line	Number of plants with YFP/CFP fluorescence
T_1	A17 YC3.6 3A	139/219
T_2	#1	8/9
	#2	55/55
	#4	11/11
T_1	R108 YC3.6 7A	22/27
T_2	#1	18/23
	#3	14/15

* T_1 and T_2 seedlings used for initial calcium imaging experiments.

* A17 YC3.6 3A and R108 YC3.6 7A used as parental lines for crosses.

Initial experiments were carried out using Jemalong A17 YC3.6 T_1 transformant seedlings as these lines were available first. To compare the NF-induced calcium responses from Cameleon YC3.6 to those obtained from YC2.1, seedlings of both the A17 YC3.6 and the previously established R108 YC2.1 line (Miwa et al., 2006) were germinated and grown as described above and an inverted fluorescence microscope was used for YFP/CFP fluorescence ratio acquisition at 5 second intervals (Chapter 2.10). After the start of image acquisition seedlings were treated with 10 nM NF from *Sinorhizobium meliloti* and recording was resumed. At this concentration of NF the calcium influx and calcium spiking responses were both observed when using YC2.1 or Oregon Green/Texas Red (Figure 3.2) (Miwa et al., 2006b, Morieri et al., 2013, Shaw and Long, 2003a). In the YC3.6-expressing plants, increases in cytosolic free Ca^{2+} were observed shortly after 10 NF addition, similar to the calcium influx response previously observed using other reporters (Miwa et al., 2006a, Morieri et al., 2013, Shaw and Long, 2003a) (Figure 3.2A). Ten minutes after NF addition, Ca^{2+} oscillations were observed in the YC3.6 expressing plants, similar to the nuclear calcium spiking previously observed (Shaw and Long, 2003a) (Figure 3.2A). The greater dynamic range of YC3.6 over YC2.1 is very evident here with the calcium responses having much greater amplitudes (greater changes in YFP/CFP ratio). No calcium responses were observed in root hairs of the negative control plants (water addition; 8 cells, 3 plants).
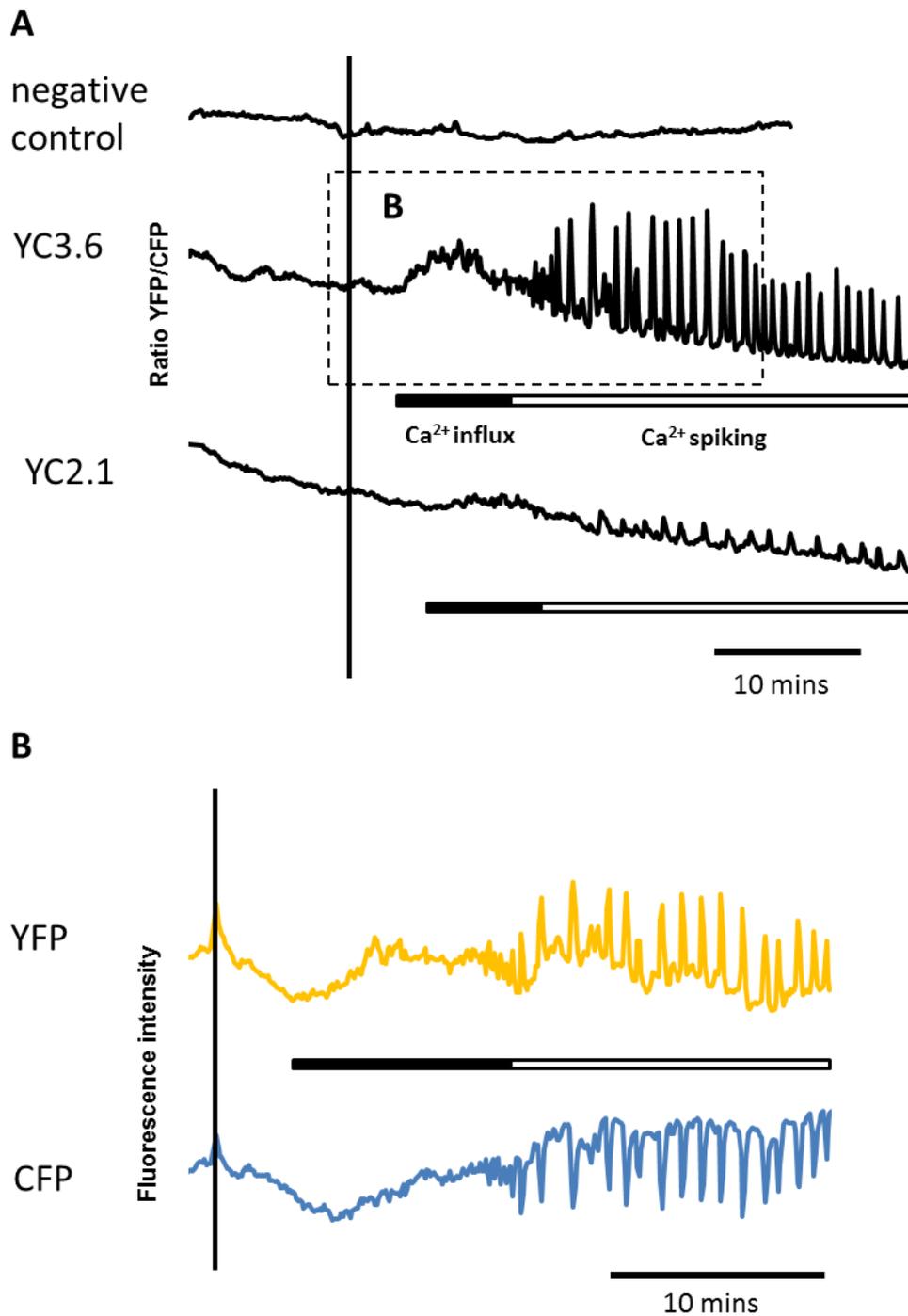
Figure 3.2: Cameleon YC3.6 versus Cameleon YC2.1.

Comparison of the NF-induced calcium responses observed in *M. truncatula* wildtype root hairs expressing Cameleon YC3.6 and YC2.1 **[A]**. The traces show data of the ratio of YFP to CFP fluorescence (arbitrary units) collected at 5 second intervals. YFP and CFP fluorescence intensities are shown for the highlighted section of the YC3.6 YFP/CFP trace **[B]**. The black vertical lines indicate 10 nM NF additions (except for the negative control where the same volume of dionised water was added).

Further analysis of calcium responses in the A17 YC3.6-expressing line was carried out using two concentrations of NF (10 nM and 0.1 nM) and data collected from three cell regions: the tip, non-tip and the whole of the root hair cell (Figure 3.3). There was no increase in cytosolic free Ca^{2+} at 0.1 nM NF (Figure 3.3B), and this is consistent with observations of the NF-induced calcium influx using YC2.1, Oregon Green/Texas Red and ion-selective electrodes (Felle et al., 1998, Felle et al., 1999b, Miwa et al., 2006b, Shaw and Long, 2003a). At 10 nM NF the increase in cytosolic free Ca^{2+} was most prominent in the tip region (Figure 3.3A), but was also visible in the non-tip region, again consistent with previous observations of the calcium influx. Since the characteristics of the increase in cytosolic free Ca^{2+} observed in the YC3.6-expressing lines are consistent with previous observations of the calcium influx, from now on it shall be referred to as the calcium influx.

The characteristics of the Ca^{2+} oscillations were also consistent with published observations of nuclear calcium spiking with the response being present at 0.1 nM NF and having a period of around 90-120 ms (Kosuta et al., 2008, Shaw and Long, 2003a, Sun et al., 2007). I shall refer to this response as calcium spiking from now on. Calcium spiking is characterised as a nuclear-localised response so it is interesting that it is also present in the tip region of the cell. Moreover, the calcium spiking signal visible in the tip region does not always reflect what is seen in the non-tip region or the overall cell, with some of the peaks absent or much reduced in the tip.

Prior to the addition of NF, the tip regions of the cells had peaks of Ca^{2+} that were not visible or are much smaller in amplitude in the non-tip and whole cell regions. The peaks were irregular and highly variable with some cells having large low frequency peaks like those at the beginning of the trace in Figure 3.3C , and others having smaller higher frequency spikes as seen towards the end of the trace. The nature of the oscillations also varied over a period of time. The smaller lower frequency spikes are similar to the tip Ca^{2+} oscillations observed in growing *A. thaliana* root hair cells (Monshausen et al., 2008).
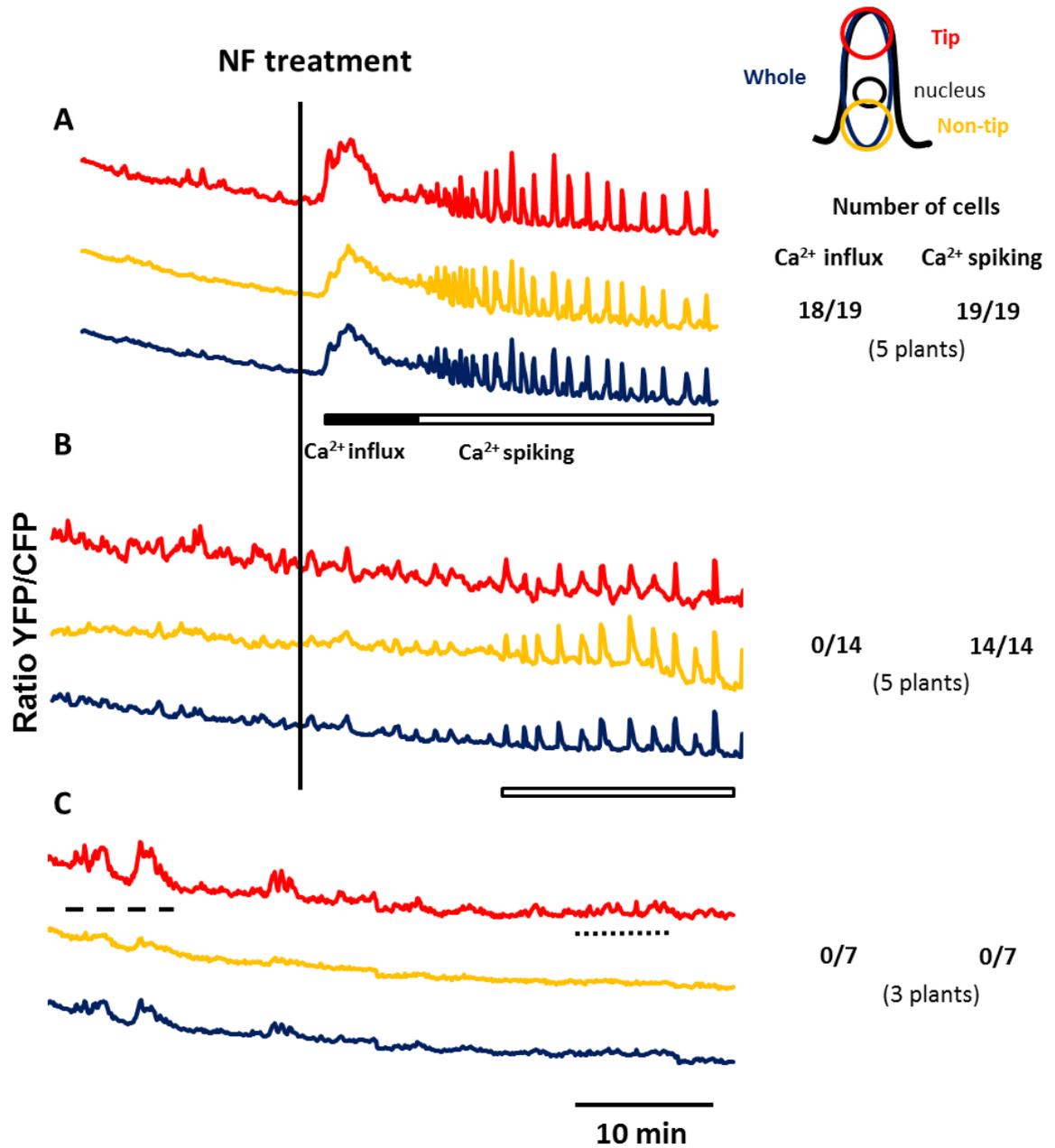
Figure 3.3: Calcium responses in *M. truncatula* A17 expressing YC3.6.

Representative traces of the ratio in YFP to CFP fluorescence (arbitrary units) collected at 5 second intervals in three cell regions (tip, non-tip and whole trunk of the cell) are shown, indicated by the areas highlighted in the images of the root hair cells on the right. The black vertical line indicates when NF (**[A]** =10 nM, **[B]** =0.1 nM) was added with incidences of calcium influx and calcium spiking indicated. In [**C**] no NF was added and the long dashed line highlights a time of larger low frequency tip oscillations and the short dashed line highlights a time of smaller higher frequency tip oscillations. The numbers indicate the number of cells with a calcium influx response/number of cells analysed from the number of plants shown in brackets.

To characterise the NF-induced calcium influx further experiments were carried out using 10 nM NF but switching from five second acquisition intervals to one second intervals (Figure 3.4). When imaging at this frequency, it was more apparent that the calcium influx starts at the tip and that the peak at the non-tip region occurred a few seconds later, consistent with the observations of Shaw and Long (2003a). It was also apparent that the calcium influx is in fact made up of several peaks of Ca^{2+} so is not just a single influx event. It should be noted that there was variation in the timing of the calcium flux after NF addition, but we could not discriminate between technical and biological reasons for these differences.
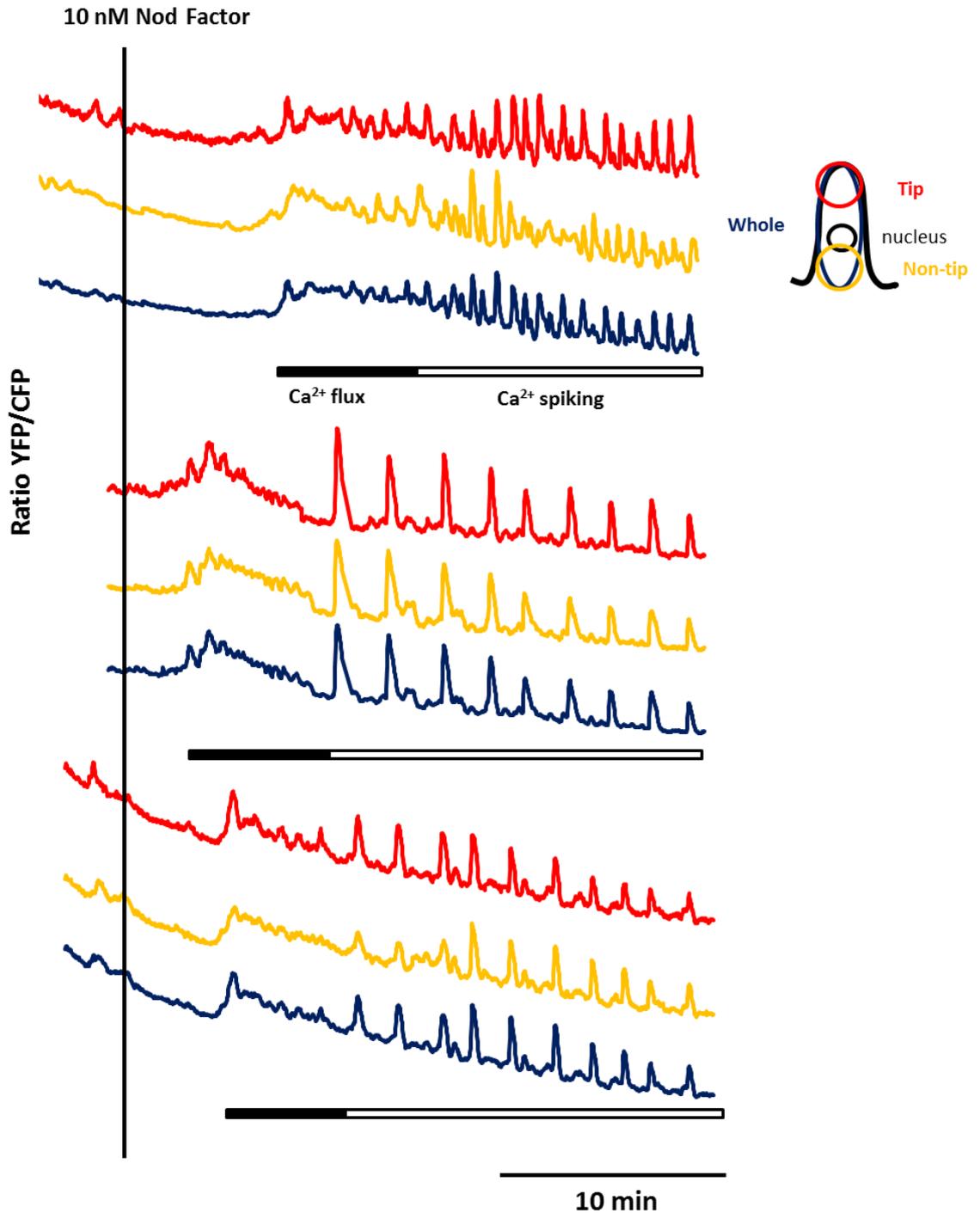
Figure 3.4: Imaging of YC3.6 at one second intervals in *M. truncatula* A17 root hair cells.

Traces of the ratio in YFP to CFP fluorescence (arbitrary units) over a period of time (minutes) for three cells from three different plants are shown. In each cell three regions were analysed (tip, non-tip and whole cell), indicated by the areas highlighted in the images of the root hair cells on the right. The black vertical line indicates when 10 nM NF was added.

3.2.2 Analysis of the NF-induced ROS transient in *M. truncatula* root hair cells using CM-H$_2$DCFDA

To analyse the NF-induced ROS transient wildtype Jemalong A17 seedling germinated and grown as above were placed on slides and incubated in FP plant growth solution containing CM-H$_2$DCFDA dye. Imaging was done at 1 second intervals with an inverted fluorescence microscope (Chapter 2.11). In 7/9 cells imaged the fluorescence intensity at the tip of the root hair cells started to increase shortly after NF addition with a peak in fluorescence intensity within 1-3 mins, consistent with the observations in *P. vulgaris* (Figure 3.4) (Cárdenas et al., 2008). After this point, fluorescence intensity started to decline, again consistent with previous observations. The oxidation of CM-H$_2$DCFDA that is responsible for the fluorescence is effectively irreversible so this decline in fluorescence intensity is probably due to a combination of fewer CM-H$_2$DCFDA molecules being oxidised and movement of already oxidised molecules away from the tip due to cytoplasmic streaming. Although this makes it impossible to comment on the spatial and temporal characteristics of the decline, the results do show that the ROS production is transient, tailing off after the peak at 1-3 mins. It should be noted that these experiments did not include a "water only" control treatment. Therefore, it is possible that the observed ROS response could be due to a "touch response" in the root hair cell caused by the addition of a solution to the media surrounding the plant. However, the absence of a ROS transient response in the NF receptor mutant *nfp* (see Chapter 5.2.2), alongside evidence from Cardenas et al. (2008) that the ROS transient is NF-specific indicate that the ROS transient responses observed here are unlikely to be an artefact caused by a touch response.
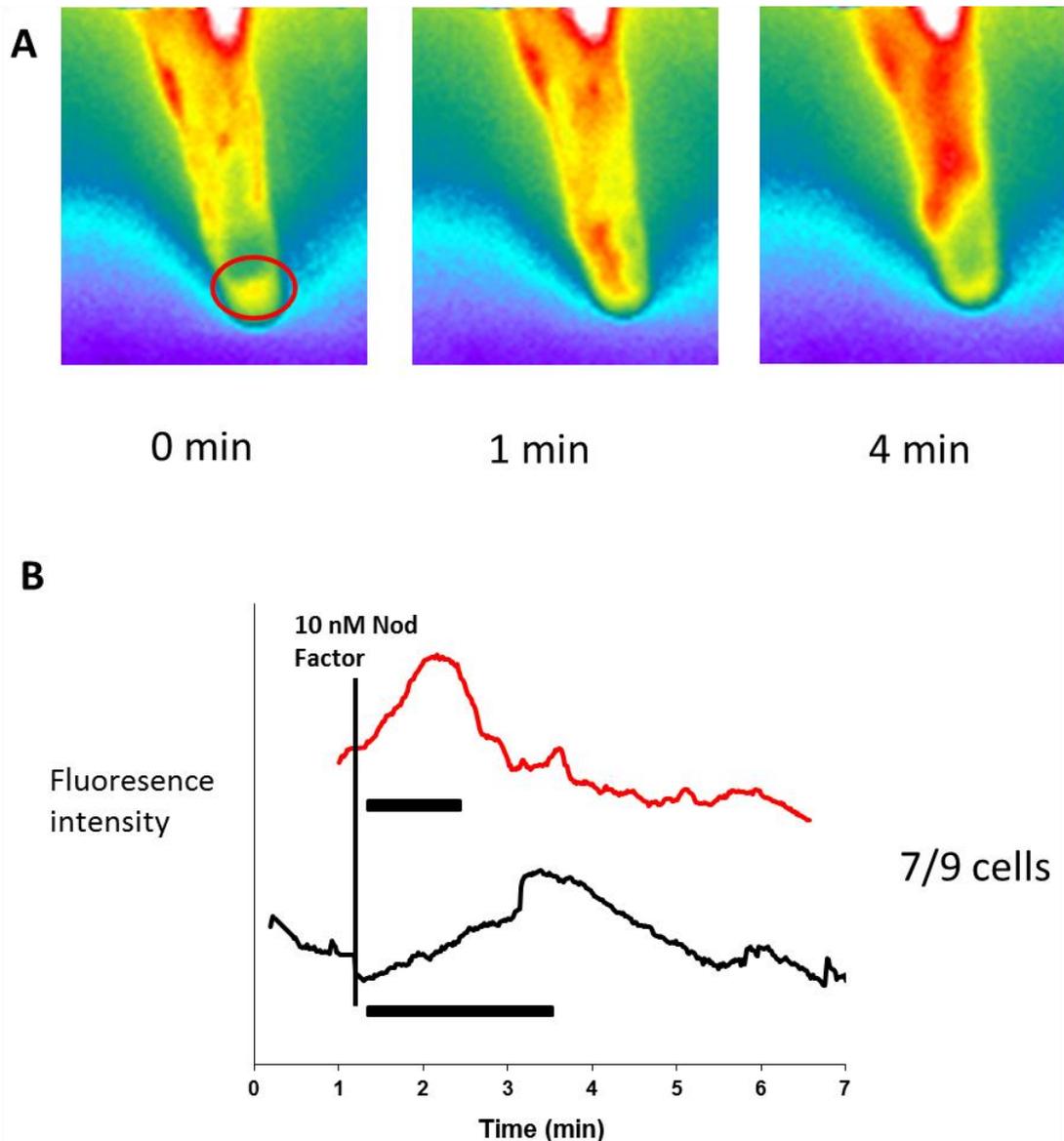
Figure 3.5: Reactive oxygen species (ROS) transient production in *M. truncatula* A17 root hairs after NF treatment.

[A] False colour images [high (white) to low (purple) fluorescence insensity] of a root hair after NF treatment (0 min), 1 min and 4 mins. The region highlighted in red corresponds to the red trace in **[B]**, where the intensity of CM-H$_2$DCFDA fluorescence is shown against time (minutes) and the addition of NF is indicated by the vertical black line. The black trace in **[B]** is from the tip region of another cell from a different plant. The black horizontal lines indicate the increase phase of ROS transient production.

3.3 Discussion

It has been known since the late 1990's that NF can induce a calcium influx at the tip of legume root hair cells (Felle et al., 1998, Felle et al., 1999b), but how it is generated and its role in nodulation is poorly understood, especially when compared to our understanding of NF-induced nuclear calcium spiking. The NF-induced ROS transient was first observed more recently (Cárdenas et al., 2008) and is even more poorly characterised. In this chapter, stable plant lines expressing YC3.6 and a protocol for imaging using CM-H_2DCFDA were established to image calcium and ROS in *M. truncatula*.

The improved FRET dynamics of YC3.6 over YC2.1 make it a better tool for spatio-temporal imaging of calcium in cells and it has provided further insights into NF-induced calcium spiking. Although NF-induced calcium spiking originates around the nucleus, it is clear from the use of YC3.6 that it is also present away from the nucleus in the tip region. It appears that the NF-induced calcium spiking observed at the tip may not always reflect what is happening at the non-tip region at the same point in time suggesting that the tip spiking is not just the result of simple diffusion of free calcium ions in the cytoplasm from the nucleus. It may be that nuclear-localised calcium spiking activates calcium spiking in the tip region. Since the nuclear membrane, the calcium store for nuclear-localised calcium spiking, is contiguous with the endoplasmic reticulum it is possible that tip-localised calcium spiking may be activated by calcium-induced calcium release along the ER starting near the nucleus. Whether the NF-induced calcium spiking observed at the tip has a function in nodulation signalling or is just an artefact of nuclear calcium spiking remains to be analysed.

The calcium influx has been previously described as a rapid increase in calcium originating at the tip and travelling along the shaft of the root hair cell (Miwa et al., 2006b, Morieri et al., 2013, Shaw and Long, 2003a). The observations in this chapter are consistent with this but also provide further information regarding the spatio-temporal characteristics. Using YC3.6 revealed that the calcium influx is made up of many individual peaks of calcium, and is not just one single calcium influx into the cytoplasm. The subsequent peaks may be the result of influxes through Ca^{2+}-sensitive Ca^{2+}-permeable channels along the plasma membrane from the site of NF activation of an initial influx of Ca^{2+}, which is presumably the Ca^{2+} current observed by Felle et al. (1998) using ion selective electrodes. It is also apparent that there is large variation in the shape of the calcium influx even when using YC3.6, which may help account for the difficulties in identifying the calcium influx with less sophisticated imaging methods (e.g. Oregon Green, YC2.1).

A limitation of the calcium and ROS imaging methods used here is that they cannot be used simultaneously so it is not possible to determine the timing of the responses relative to one another. The most accurate timing of the calcium influx come from experiments conducted using ion selective electrodes where an increase in intracellular Ca^{2+} (measured indirectly as a decrease in extracellular Ca^{2+} was initiated within seconds of NF treatment) (Felle et al., 1998, Felle et al., 1999b). There is greater variation in the timing of the initiation of the Ca^{2+} and ROS responses in the experiments in this chapter but the responses are occurring in a similar timescale after NF addition.

The *A. thaliana rhd2* mutant is defective for RBOHC-mediated ROS production and also lacks the tip-focused Ca^{2+} gradient at the root hair tip (Foreman et al., 2003). ROS treatment elevated cytoplasmic Ca^{2+} levels in the root hairs and restored cell growth suggesting that ROS may precede Ca^{2+} in root hair growth. However, the activity of RBOH proteins can be regulated both by calcium ions binding to EF-hand domains and by calcium-dependent protein kinases (CPKs), suggesting there is positive feedback between ROS and calcium (Asai et al., 2013, Dubiella et al., 2013, Keller et al., 1998, Kobayashi et al., 2007, Sagi and Fluhr, 2001, Takeda et al., 2008). It is therefore possible that positive feedback exists between the NF-induced calcium influx and ROS transient in legume root hairs with both responses being interdependent.

Using the tools for imaging Ca^{2+} and ROS in *M. truncatula* developed in this chapter it will be possible to undertake further experiments, which will hopefully enable the identification of regulators of these responses. Pharmacological approaches can be a starting point and few experiments testing compounds on the calcium influx or ROS transient have been attempted previously. Also, there are many *M. truncatula* nodulation and bacterial mutants, some of which have not been characterised for the calcium influx at all or their characterisations are tentative due to the limitations of the imaging method used. Moreover, none of these mutants have been characterised for the ROS transient. The next two chapters will present the findings from these experiments.

Chapter 4: Reactive oxygen species are required for the Nod factor-induced calcium influx

4.1 Introduction

The identification of compounds that inhibit ligand-induced responses can provide clues to the identity of proteins that may be involved. For example, NF-induced calcium spiking is inhibited by the SERCA-type Ca^{2+}-ATPase inhibitor cyclopiazonic acid (CPA) (Capoen et al., 2011, Engstrom et al., 2002). Further investigation into this family of Ca^{2+}-ATPases in *Medicago truncatula* led to the discovery that one member, MCA8, is required for calcium spiking (Capoen et al., 2011). Inhibitor approaches can be especially useful in identifying components that may not appear in forward genetic screens because they belong to multigene families or they are also required for normal growth and development.

There are several inhibitors that have been shown to block calcium spiking including U73122 (PLC inhibitor) and the Ca^{2+}-ATPase inhibitor 2,5-di-(*t*-butyl)-1,4-hydroquinone (BHQ) (Engstrom et al., 2002), but only one compound, the calcium channel inhibitor nifedipine, has been reported to inhibit the calcium influx (Felle et al., 1998). The NADPH oxidase (and other flavin-containing enzyme) inhibitor diphenyleneiodonium (DPI) is the only compound that has been reported to inhibit the NF-induced ROS transient (Cárdenas et al., 2008).

Extracellular ATP is involved in a number of signalling processes in plants including cell viability, root gravitropism, growth, inhibition of pollen germination and plant defence (Chivasa et al., 2005, Chivasa et al., 2009, Demidchik et al., 2003, Kim et al., 2006, Steinebrunner et al., 2003, Tang et al., 2003, Wu et al., 2007). In addition, extracellular ATP has been reported to inhibit calcium spiking in preliminary work by Miwa (2005). This effect was thought to be related to an ectoapyrase enzyme known as LNP, which has ATP/ADP hydrolysis activity, and was identified by its ability to bind NFs (Etzler et al., 1999, Etzler et al., 2000). Suppression of LNP reduces nodule numbers and bacterial infection (Govindarajulu et al., 2009, Roberts et al., 2013) and a *Lotus japonicus* LNP antisense line was defective for both the calcium influx and spiking responses, suggesting that LNP may regulate ATP/ADP levels during nodulation (Roberts et al., 2013).

The spatial and temporal similarities between the calcium influx and ROS transient suggest that they may be involved in a common signalling pathway. The aim of this chapter was to use inhibitors to test whether the calcium influx and ROS transient are involved in a common pathway. A secondary aim was to investigate the role of extracellular ATP on NF-induced calcium signalling. Compounds that are known to block calcium and ROS signalling in plants and other eukaryotic organisms were tested for their effects on calcium signalling and the ROS transient in *M. truncatula*.

4.2 Results

4.2.1 The NADPH oxidase inhibitor diphenyleneiodonium (DPI) inhibits the calcium influx and the ROS transient but not calcium spiking

The NADPH oxidase inhibitor DPI inhibits ROS accumulation and root hair growth in *Arabidopsis thaliana* resulting in short root hairs that resemble those of the NADPH oxidase mutant *rhd2* (Foreman et al., 2003). This suppression of root hair growth results from the lack of the tip focused calcium gradient found in root hair cells (Schiefelbein and Somerville, 1990, Wymer et al., 1997). DPI also inhibits the NF-induced ROS transient in *Phaseolus vulgaris* root hairs (Cárdenas et al., 2008). To validate this I assessed the effect of DPI on the NF-induced ROS transient in *M. truncatula.* Wild type seedlings were loaded with CM-H$_2$DCFDA (Chapter 2.11) and 50 µM DPI [dissolved in DMSO, final concentration 0.2 % (v/v)] was added 10 minutes prior to addition of 10 nM NF. None of the cells pretreated with DPI produced the ROS transient after NF addition (Figure 4.1), suggesting, not surprisingly, a role for NADPH oxidase in the ROS transient.

DPI was then tested for its ability to inhibit NF-induced calcium signalling in root hair cells. *M. truncatula* seedlings expressing Cameleon were treated with DPI at least 10 minutes prior to addition of 10 nM NF (Chapter 2.10). Pretreatment with 50 µM DPI inhibited the NF-induced calcium influx but not calcium spiking (Table 4.1, Figure 4.2). Adding 10 µM DPI did not inhibit either calcium response, suggesting that the inhibition is dose-dependent. Inhibition of the calcium influx by DPI suggests that the ROS transient may be associated with the activation of the calcium influx and this is consistent with an overlap between the temporal and spatial nature of these responses. It should be noted that a DMSO only control treatment prior to 10 nM NF addition was not carried out. However, 0.2 % DMSO treatment was carried out using A17-YC3.6 lines (Table 4.1; Figure 4.2). The treatment was not lethal to the cells during the

period of Ca^{2+} imaging (over 45 mins) and did not inhibit the calcium influx or calcium spiking (Table 4.1). Therefore, the absence of a ROS transient after DPI treatment (Fig 4.1) is not due to a loss of cell viability, but it is possible that DMSO alone could inhibit the ROS transient.
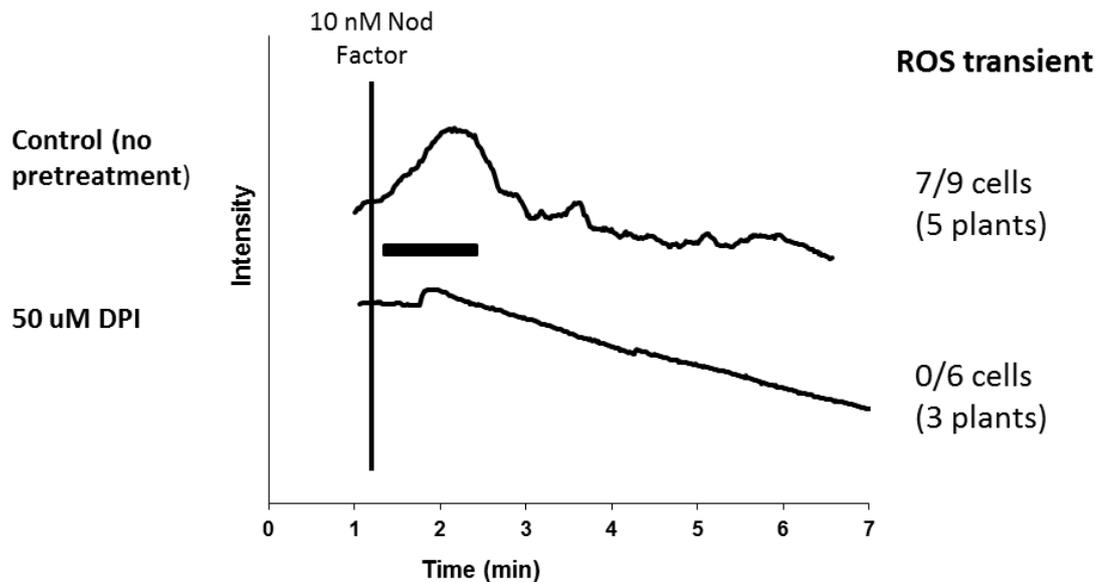
Figure 4.1: Diphenyleneiodonium (DPI) inhibits the NF-induced ROS transient in root hairs.

M. truncatula A17 seedlings were treated with CM-H$_2$DCFDA dye prior to 50 µM DPI treatment and fluorescence intensity (arbitrary units) in root hairs was recorded. The black horizontal line indicates the increase phase of ROS transient production.

Table 4.1: Summary of NF-induced calcium responses in *M. truncatula* root hair cells after inhibitor treatments.

Treatment	Target	No. of cells with		Number
		Calcium influx	Calcium spiking	of plants
Control (no pretreatment)		11/12	12/12	5
Control (0.2% DMSO)*		7/8	8/8	3
200 μM ATP		13/14	14/14	5
2 mM ATP		0/3	3/3	2
100 μM nifedipine	Ca^{2+} channel blocker	2/10	8/10	5
10 μM DPI (Diphenyleneiodonium)	Inhibitor of Flavin-containing	9/13	9/13	5
50 μM DPI	enzymes	0/10	7/10	3
50 μM LaCl₃ (Lanthanum chloride)	Ca^{2+} channel blocker	6/6	6/6	2
100 μM LaCl₃		4/12	12/12	3
500 μM suramin *	Purinoreceptor antagonist	8/11	11/11	3
40 μM CPA * (cyclopiazonic acid)	SERCA-type Ca^{2+}-ATPase antagonist	0/5	0/5	3

In all cases 10 nM NF was added. All experiments were conducted using seedlings expressing YC2.1 except for those denoted with (*), which were carried out using the YC3.6 line.
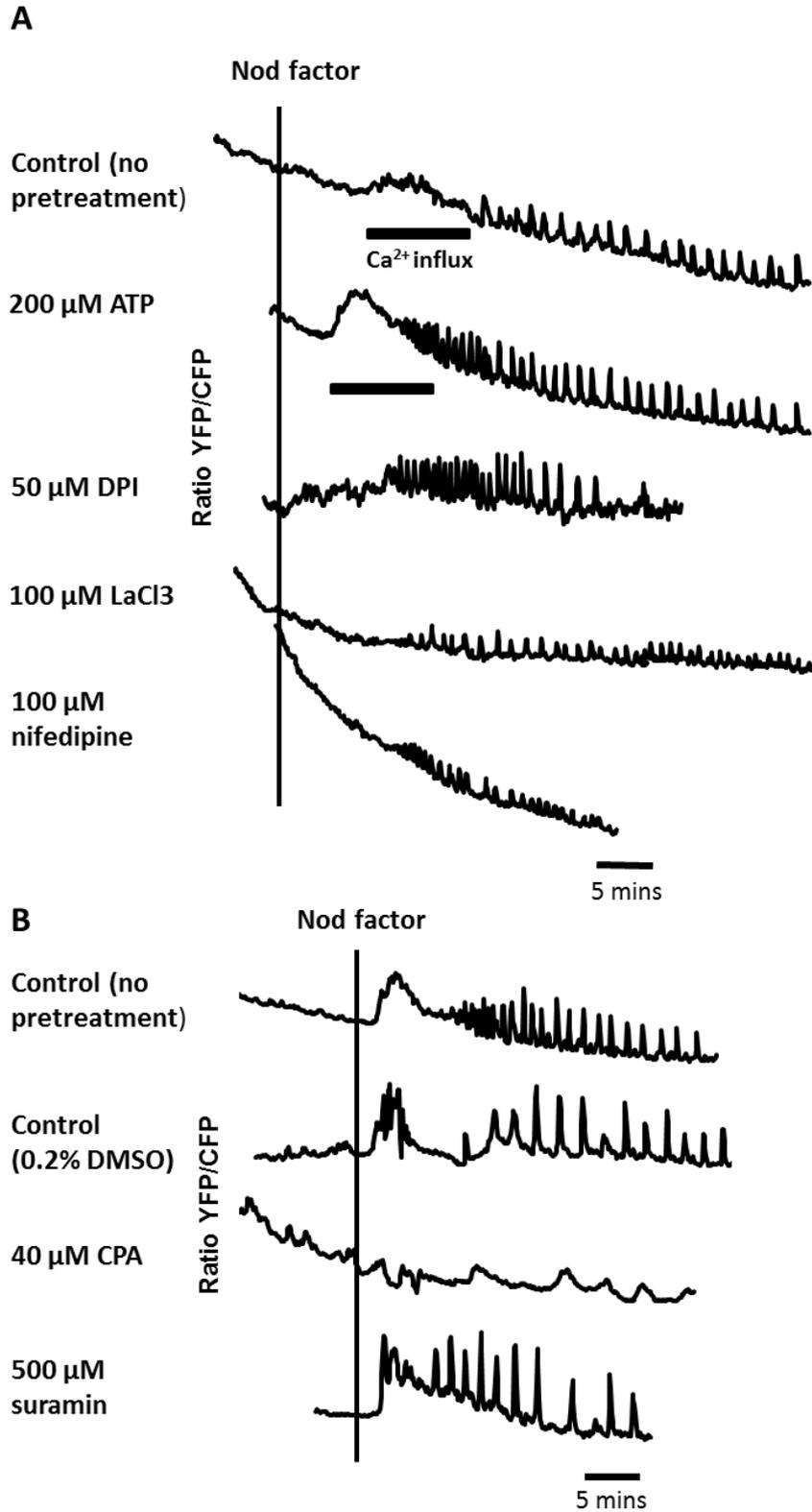
Figure 4.2: NF-induced calcium responses in *M. truncatula* root hairs after treatment with inhibitors.

Inhibitors were applied to roots of **[A]** YC2.1-expressing (R108) or **[B]** YC3.6-expressing (A17) wildtype lines. 10 nM NF was added as indicated and calcium influx responses marked by a black horizontal line. Representative traces are shown for each treatment.

4.2.2 Two Ca²⁺-channel blockers inhibit calcium influx but not spiking

The Ca^{2+} channel blockers lanthanum (La^{3+}) and nifedipine both abolish the cytosolic free Ca^{2+} gradient in *A. thaliana* root hairs leading to the cessation of root hair growth (Monshausen et al., 2008, Schiefelbein et al., 1992). Pretreatment with 100 µM (but not 50 µM) lanthanum chloride ($LaCl_3$), or 100 µM nifedipine [dissolved in DMSO, final concentration 0.1% (v/v)] resulted in a reduction in the number of cells that produced the NF-induced calcium influx, but spiking was unaffected (Table 4.1 and Figure 4.2). However, in both cases this was not a total inhibition with some cells still able to produce the calcium influx response. Pretreatment of seedlings with 40 µM CPA [dissolved in DMSO, final concentration 0.2% (v/v)] inhibited calcium spiking, as expected from previous reports (Capoen et al., 2011, Engstrom et al., 2002), but also inhibited the calcium influx. This suggests that members of the SERCA-type Ca^{2+}-ATPase family may be required for Ca^{2+} homeostasis that is necessary for an appropriate calcium influx (Table 4.1, Figure 4.2).

4.2.3 ATP treatment does not inhibit NF-induced calcium signalling

It has been previously reported that 40 µM ATP can inhibit calcium spiking (Miwa, 2005). To assess whether ATP also inhibits the calcium influx, 200 µM ATP was added to root hair cells prior to 10 nM NF treatment. However, no difference was observed in the calcium spiking or calcium influx of these cells compared to the control (NF treatment only; Table 4.1 and Figure 4.2). A higher concentration of 2 mM ATP was also assessed and although none of the cells produced a calcium influx, the cells still retained calcium spiking. However, at this high concentration cytoplasmic streaming was affected suggesting pleiotrophic effects. These findings are inconsistent with Miwa's preliminary findings so the experiment was repeated using his protocol with 40 µM ATP addition after the establishment of 1 nM NF-induced calcium spiking (Miwa, 2005). In 9/9 cells (3 plants) calcium spiking was retained after 40 µM ATP treatment. Having been unable to repeat Miwa's findings I conclude that ATP treatment does not inhibit either the calcium influx or calcium spiking.

Extracellular ATP is able to induce increases in cytosolic free Ca^{2+} and ROS in plants (Cárdenas et al., 2008, Demidchik et al., 2003, Demidchik et al., 2009, Jeter et al., 2004, Sun et al., 2012). In animals, extracellular ATP can activate purinergic receptors (Burnstock, 2007). Although no homologues of these receptors are present in plants, inhibitors of purinergic receptors including pyridoxalphosphate-6-azophenyl-2',4'-disulfonic acid (PPADS) and suramin can

inhibit ATP-induced Ca^{2+} and ROS elevations in plant cells (Jeter et al., 2004, Song et al., 2006, Sun et al., 2012). To test whether ATP may promote the NF-induced calcium influx and/or spiking, seedlings were pretreated with 500 µM suramin prior to 10 nM NF addition. Suramin treatment had no effect on the numbers of cells producing the calcium influx or calcium spiking responses (Table 4.1, Figure 4.2).

4.3 Discussion

A pharmacological approach was taken to investigate NF-induced calcium and ROS signalling. The NADPH oxidase inhibitor DPI inhibited the ROS transient, consistent with previous findings by Cardenas et al. (2008), and also inhibited the calcium influx but not calcium spiking. This suggests that NADPH oxidases may be required for the generation of the ROS transient and the calcium influx. There are seven NADPH oxidase (*RBOH*) genes in *M. truncatula* and two have already been identified as being involved in nodulation (Marino et al., 2011, Montiel et al., 2012). *MtRBOHA* is strongly upregulated in *M. truncatula* nodules and appears to be involved in nodule development (Marino et al., 2011). *Phaseolus vulgaris RBOHB* is expressed in infected root hairs and *PvRBOHB* RNAi lines had lower ROS accumulation, fewer nodules and were impaired for infection thread progression into the cortex (Marino et al., 2011, Montiel et al., 2012). *RBOH*-dependent ROS production can induce calcium influxes but RBOH proteins can also be regulated by Ca^{2+} binding to their EF-hand domains and by calcium-dependent proteins kinases (Asai et al., 2013, Dubiella et al., 2013, Foreman et al., 2003, Keller et al., 1998, Kobayashi et al., 2007, Laohavisit et al., 2012, Sagi and Fluhr, 2001, Takeda et al., 2008). NF perception could lead to the activation of RBOHs with the resulting ROS production activating a Ca^{2+} current across the plasma membrane. Positive feedback from the Ca^{2+}-permeable channel to the RBOH could then drive further ROS production and Ca^{2+} currents resulting in the ROS transient and calcium influx responses observed.

The SERCA-type Ca^{2+}-ATPase inhibitor CPA is an established inhibitor of calcium spiking and in this chapter I demonstrate that it can also inhibit the calcium influx. There are at least 10 SERCA-type Ca^{2+}-ATPases in *M. truncatula* (Capoen et al., 2011). One of these, MCA8 is required for calcium spiking to return Ca^{2+} to the nuclear periplasm (Capoen et al., 2011). The nuclear-membrane location of MCA8 means it is unlikely to be involved in generating the tip-focused calcium influx across the plasma membrane. It is unlikely that a Ca^{2+}-ATPase would be directly involved in the release of calcium across the plasma membrane, but it is possible that

Ca^{2+}-ATPases are necessary to sustain the appropriate Ca^{2+} homeostasis and this may be necessary for the calcium influx. In CPA treated cells, regulation of cytoplasmic Ca^{2+} levels would be compromised, and subsequent NF treatment may be unable to activate Ca^{2+}-permeable channels to generate the calcium influx.

ATP treatment did not inhibit either calcium influx or calcium spiking. This is inconsistent with the preliminary findings of Miwa (2005) who reported that ATP treatment inhibited calcium spiking in *M. truncatula*. Here, two experimental set-ups were used to examine the effect on calcium spiking; treatment prior to NF addition and treatment after NF-induced calcium spiking was initiated. Both produced similar results: no effect on either the calcium influx or calcium spiking. Furthermore, suramin, an animal purinergic receptor antagonist, had no effect on either calcium influx or calcium spiking. These results are puzzling when considered with the involvement of the apyrase LNP in nodulation (Govindarajulu et al., 2009, Roberts et al., 2013). Although ATP does not appear to directly modulate NF-induced calcium signalling it may still be playing a role in nodulation. In *A. thaliana* root hairs, high or very low levels of extracellular ATP inhibit root hair growth (Clark et al., 2010) and this may be relevant during rhizobial infection, but not for early signalling.

In conclusion, the results in this chapter indicate that the NF-induced ROS transient and calcium influx may both be dependent on NADPH oxidases. It would be interesting to find out whether the NADPH oxidase RBOHB, which has already been characterised as having a role in bacterial infection (Montiel et al., 2012), is required to generate the ROS transient and calcium influx. However, as a member of a multigene family this may prove difficult if there is any functional redundancy.

CHAPTER 5: ANALYSIS OF NF-INDUCED CALCIUM INFLUX AND ROS TRANSIENT RESPONSES IN NODULATION AND INFECTION MUTANTS

5.1 Introduction

There are several genes that are required for NF-induced calcium spiking but not for the NF-induced calcium influx including *DMI1, DMI2, NENA, NUP133 and NUP85* (Groth et al., 2010, Miwa et al., 2006a, Wais et al., 2000). However, the only genes found to be required for the calcium influx are *NFP* and *LNP*, which are also required for calcium spiking (Ben Amor et al., 2003, Roberts et al., 2013). These observations suggest that calcium spiking and the calcium influx are involved in separate signalling pathways downstream of NF perception. However, since *NFP* is required for all NF responses and the role of *LNP* in nodulation and bacterial infection is currently unclear, they do not provide much in the way of mechanistic information as to how the calcium influx is generated or its role in bacterial infection. The NF-induced ROS transient has not yet been studied in any nodulation or bacterial infection mutants.

The calcium influx has been implicated in bacterial infection (Morieri et al., 2013) and in *Medicago truncatula* there are several genes that have been shown to play a role in bacterial infection. Plants with mutations in *NIN*, which encodes a transcription factor that acts downstream of the Sym pathway (Marsh et al., 2007), have excessive root hair curling but produce few infection threads and do not develop nodules (Borisov et al., 2003, Marsh et al., 2007). *M. truncatula hcl* also has excessive root hair curling and does not form nodules (Catoira et al., 2001) and the gene encodes a LysM receptor-like kinase family member like the NF receptor NFP (Smit et al., 2007). The *bit1-1* allele has a mutation that blocks the function of the ERN1 transcription factor, which is required for infection thread initiation and nodule formation (Middleton et al., 2007). *(REQUIRED FOR INFECTION THREAD) RIT1* encodes a SCAR/WAVE (suppressor of cAMP receptor/WASP-family verprolin homologous protein) component involved in the regulation of the actin cytoskeleton that is required for normal infection thread, root hair and trichome development (Miyahara et al., 2010).

All these genes with roles in bacterial infection appear to play no role in activation of calcium spiking (Marsh et al., 2007, Miyahara et al., 2010, Morieri et al., 2013, Wais et al., 2000). In a study by Morieri et al. (2013), *nin-1, bit1-1* and *hcl-1* were found to retain the calcium influx response in at least some of the cells tested, but fewer cells appeared to respond than in the wildtype. However, these experiments were conducted using microinjection of a Ca^{2+}-

responsive dye and it is not clear whether the reductions in the numbers of cells that responded are biologically relevant or reflect damage or increased changes in calcium generated by this invasive technique. In preliminary studies also using microinjection, the *rit1-1* mutant was reported to be abnormal for induction of the calcium influx with only 4 of 12 cells showing this response, a significant reduction from the wildtype (Morieri, 2010). However, the *Lotus japonicus* orthologues of *RIT1* are *NAP1* and *PIR1* and *nap1/pir1* double mutants retain the calcium influx response (Morieri, 2010), so it is puzzling that the *rit1-1* mutant of *M. truncatula* appears be at least partly defective for the calcium influx.

This chapter describes the analysis of the NF-induced calcium influx in *M. truncatula* nodulation and infection mutants using YC3.6 expressing lines. Also, several nodulation mutants were characterised for the NF-induced ROS transient to provide insights as to where the response may lie in relation to the known signalling pathways.

5.2 Results

5.2.1 *ERN1* and *RIT1* are not required for the NF-induced calcium influx

To generate *M. truncatula* nodulation and bacterial infection mutant lines expressing YC3.6, the *bit1-1, rit1-1, nfp-1, dmi1-1* and *dmi1-2* mutants were cross fertilised (Chapter 2.8) with the wildtype A17-YC3.6 expressing line developed in Chapter 3. The F_2 seedlings were screened for YC3.6 fluorescence. In all the mutant populations YC3.6 fluorescence segregated and the ratios of positive/negative plants were fairly close to the expected ratio of 3:1 for segregation of a single YC3.6 gene insertion within the populations (Table 5.1). Seedlings that were positive for YC3.6 fluorescence were planted and inoculated with *Sinorhizobium meliloti* 2011 (Chapter 2.12.3) to identify plants which were defective for the symbiosis (Table 5.2). In each line the mutant phenotype was segregating within the population. The *rit1-1* YC3.6 F_2 population segregated with a ratio of 1:11 instead of the expected ratio of 1:3, but this is similar the previously observed 1:9 segregation of a *rit1-1* x wildtype A20 F2 mapping population (Richens, 2008). Plants displaying the appropriate mutant phenotype were kept for seed production. Ca^{2+} imaging experiments (Chapter 2.10) were carried out using the progeny (F_3 generation) of these plants.

Table 5.1: YC3.6 expression in F_2 generation of YC3.6 nodulation mutant lines.

Plant line	Number of plants with YC3.6 fluorescence	Ratio (YC3.6 fluorescence/no YC3.6 fluorescence)
nfp-1 YC3.6	40/55	2.7:1
bit1-1 YC3.6	46/60	3.3:1
rit1-1 YC3.6	35/50	2.3:1
dmi1-1 YC3.6	21/29	2.6:1
dmi2-1 YC3.6	40/55	2.7:1
cbs1-2 YC3.6	42/57	2.8:1

Table 5.2: Segregation of mutant phenotypes in F_2 generation of YC3.6 nodulation mutant lines.

Plant line	Mutant phenotype (21 dpi with rhizobia)	No. of plants with mutant phenotype	Ratio (mutant phenotype/wildtype)
nfp-1 YC3.6	Nod-	7/33	1:4.7
bit1-1 YC3.6	Small white nodules	8/38	1:4.7
rit1-1 YC3.6	Small white nodules	2/22	1:11
dmi1-1 YC3.6	Nod-	9/32	1:3.2
dmi2-1 YC3.6	Nod-	4/15	1:3.8
cbs1-2 YC3.6	Small white nodules *	8/32	1:4

For each mutant line, plants with YC3.6 fluorescence were planted and inoculated with *S. meliloti* 2011. After 21 days (21 dpi) plants were screened for the appropriate mutant phenotype: no nodules (nod-) or small white nodules. * Owing to the relatively weak phenotype of *cbs1-2* mutants, these plants were also genotyped by PCR for the *Tnt1* insertion in *CBS1* (2.13.3) to confirm the phenotyping results.

Consistent with previous studies, the *nfp-1* mutant lacked both the NF-induced calcium influx and calcium spiking responses (Figure 5.1) (Ben Amor et al., 2003). It retained the tip-focused calcium oscillations observed in wildtype prior to NF addition (not shown). The calcium influx was observed in 9 out of 15 cells in the *bit1-1* mutant (Figure 5.1). This was lower than in the wildtype A17 but was not a statistically significant difference (Fisher's test, two-tailed $P=$ 0.0914). The calcium influx was only observed in 3 of 6 cells in the *rit1-1* mutant, but this was not a significant difference from the wildtype ($P=$ 0.0833). There were fewer root hair cells on *rit1-1* and these were abnormal in appearance being much broader and more vacuolated than wildtype, consistent with previous observations (Miyahara et al., 2010). Together with the previous studies these results demonstrate that *ERN1* and *RIT1* are not required for the induction of the calcium influx (Morieri, 2010, Morieri et al., 2013). However, more cells will need to be analysed in order to define whether there is a significant reduction in the total number of responsive cells.
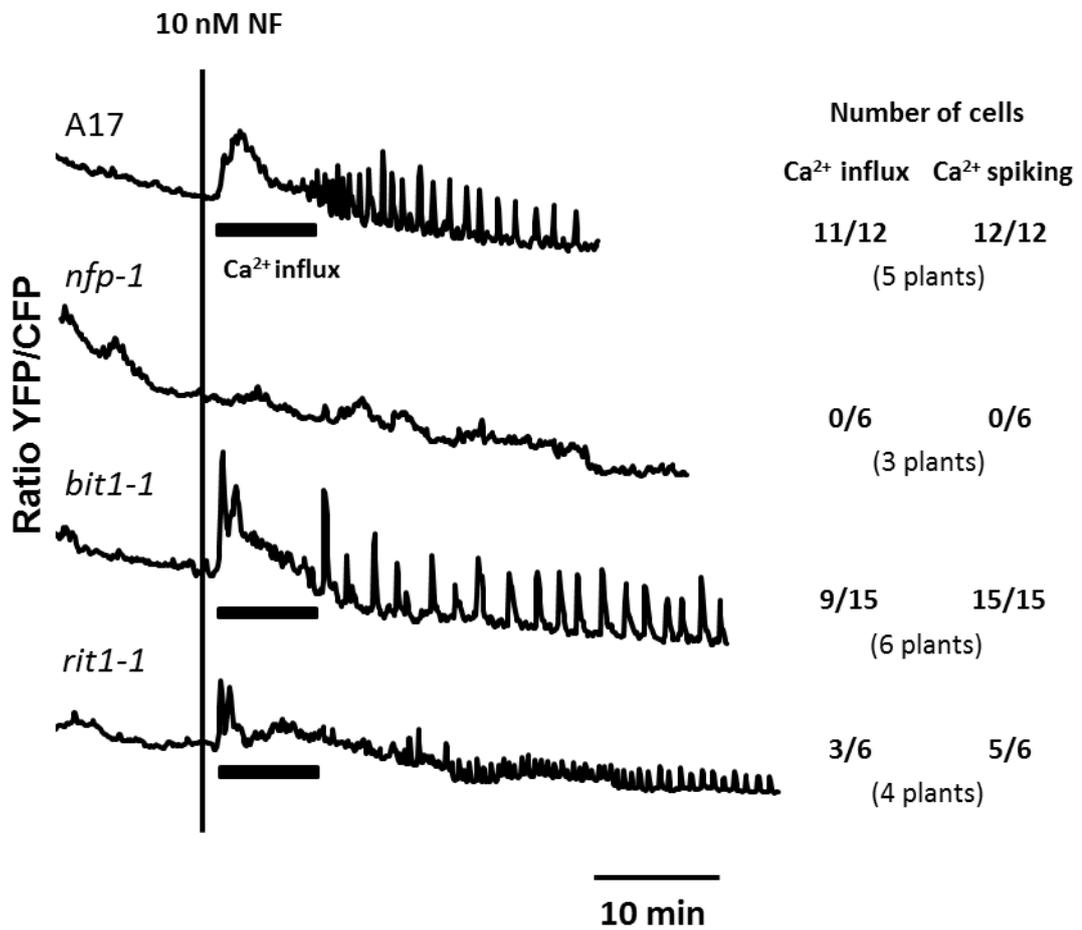
Figure 5.1: The NF-induced calcium influx is dependent on *NFP*, but not *ERN1* or *RIT1*.

Wildtype A17, *nfp, bit1-1* and *rit1-1* seedlings expressing YC3.6 were treated with 10 nM NF. Representative traces of the ratio in YFP to CFP fluorescence (arbitrary units) collected at 5 second intervals for the whole shank of the cell are shown. The black vertical line indicates when 10 nM NF was added and calcium influx responses are indicated. The numbers represent the number of cells with a calcium influx or calcium spiking response/number of cells analysed from the number of plants shown in brackets.

The *dmi1* and *dmi2* mutants both retain the calcium influx response (Miwa et al., 2006a, Shaw and Long, 2003a). However, it was reported by Shaw and Long (2003a) using microinjection of Oregon Green and Texas Red that the calcium influxes observed in these mutants appeared to be different having only a single peak that was shorter in duration than in the wildtype and the cytoplasmic calcium returned to the baseline concentration more rapidly. This suggested that *DMI1* and *DMI2* might modulate the calcium influx response. To clarify whether there might be any difference in the calcium influx responses of the *dmi1* and *dmi2* versus wildtype I collected YC3.6 fluorescence images at one second intervals from seedlings treated with 10 nM NF. The calcium influxes of the *dmi1-1* and *dmi2-1* mutants were similar to the wildtype with a large initial peak of calcium most prominent in the tip-region with a gradual decline often containing additional peaks (Figure 5.2). The decline of the calcium influx in the wildtype is generally noisier than in the *dmi1-1* and *dmi2-1* mutants (Figure 5.2), but this is likely to be due to the initiation of calcium spiking that starts around 10 minutes after NF treatment.
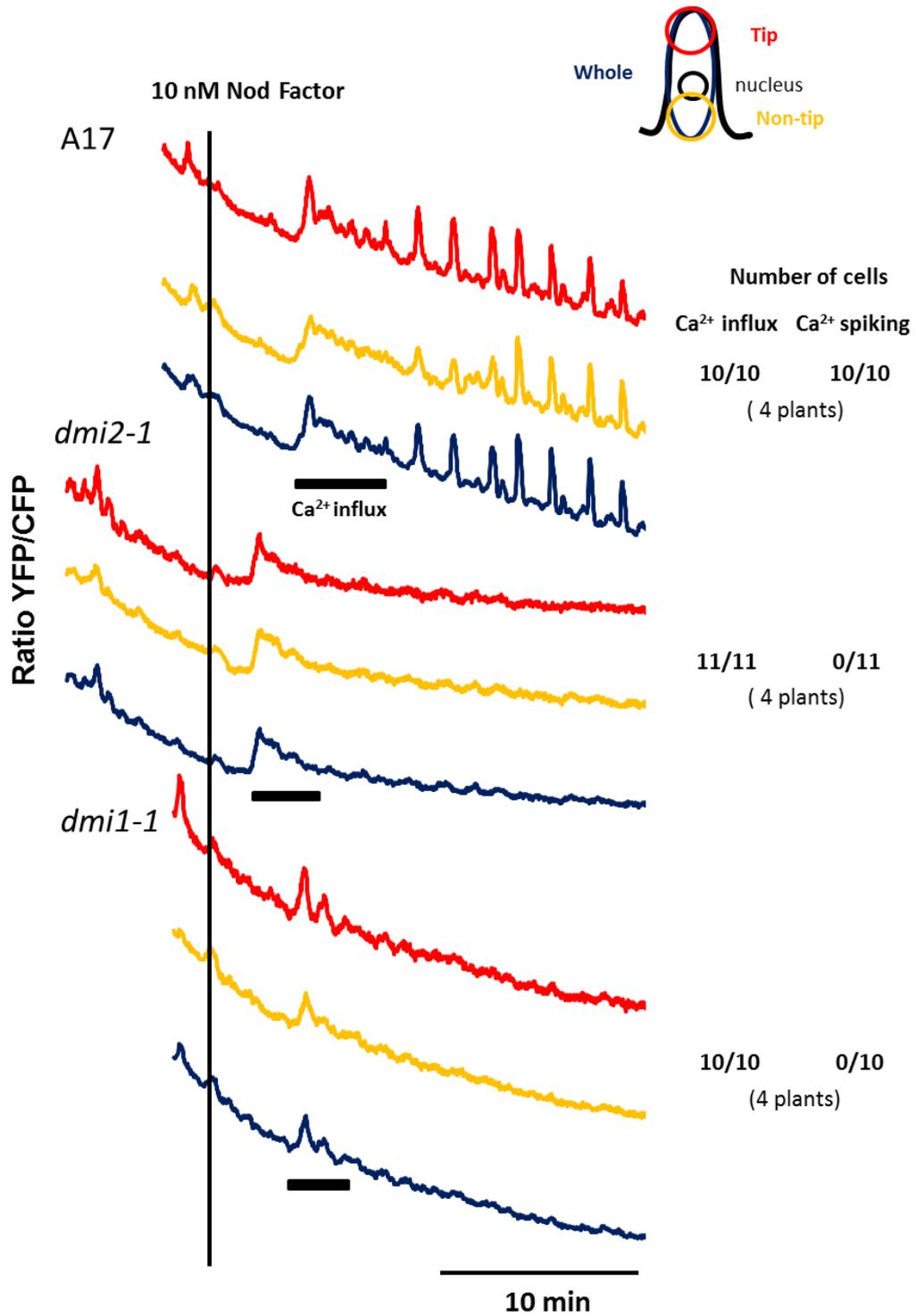
Figure 5.2: Analysis of the calcium influx in *M. truncatula* wildtype A17, *dmi1* and *dmi2* root hair cells.

Traces of the ratio in YFP to CFP fluorescence (arbitrary units) collected at one second intervals for three regions were analysed (tip, non-tip and whole cell), indicated by the areas highlighted in the images of the root hair cell at the top right. The black vertical line indicates when 10 nM NF was added. The numbers represent the number of cells with a calcium influx or calcium spiking response/number of cells analysed from the number of plants shown in brackets.

5.2.2 *NFP*, but not *DMI1* or *DMI2* is required for the NF-induced ROS transient

To investigate the ROS transient response in nodulation mutants, seedlings were treated with CM-H_2DCFDA dye prior to addition of 10 nM NF (Chapter 2.11). The ROS transient was not observed in any of the *nfp-1* cells (Figure 5.3). This suggests that the ROS transient lies downstream of the NF receptor NFP, which is also required for the NF-induced calcium influx and calcium spiking responses (Ben Amor et al., 2003). On the other hand, the ROS transient was observed in the majority of the *dmi1-1* and *dmi1-2* mutant cells (Figure 5.3), suggesting it either lies upstream of calcium spiking in the Sym pathway or may be in a parallel pathway downstream of *NFP*.
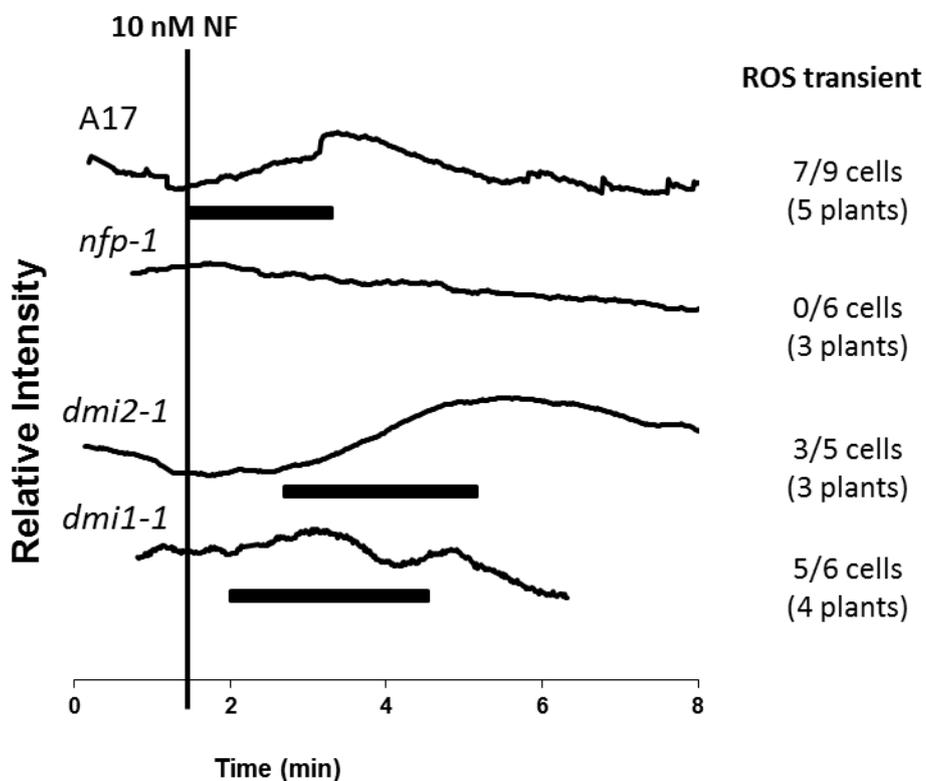
Figure 5.3: The NF-induced ROS transient is dependent on *NFP* but not *DMI1* or *DMI2.*

Wildtype A17*, nfp-1, dmi2-1* and *dmi1-1* seedlings were treated with CM-H_2DCFDA dye prior to 10 nM NF addition and fluorescence intensity (arbitrary units) in root hairs recorded with representative traces of tips of root hairs shown. Black lines indicate ROS transient production.

5.2.3 *CBS1* is not required for NF-induced calcium responses or the ROS transient

M. truncatula plants with mutations in *CBS1* are defective for bacterial infection producing many infection foci that fail to progress to infection threads (Guan, D., Sinharoy, S., personal communications). *CBS1* encodes a cystathionine beta-synthase (CBS) domain-containing protein (Sinharoy S., personal communication). In *A. thaliana* the CBS domain-containing proteins CBSX1 and CBSX2 can interact with and directly regulate thioredoxins, thereby regulating H_2O_2 levels (Yoo et al., 2011). This suggests that CBS1 may be involved in regulation of ROS levels during nodulation. The infection threads of the *cbs1-2* mutant appear to accumulate higher levels of ROS than wildtype (Liu, C., personal communication). I therefore analysed the *cbs1-2* mutant for NF-induced calcium signalling and the ROS transient.

To image calcium, root hairs were microinjected with Oregon Green and Texas Red prior to addition of 10 nM NF (Chapter 2.9). Fluorescence was measure at five second intervals. The *cbs1-2* mutant retained the calcium influx and calcium spiking responses with all five cells tested with 10 nM NF (Figure 5.4). Therefore, *cbs1* is not required for either the NF-induced calcium influx or calcium spiking. Since CBS1 may have a role in the regulation of ROS I thought it was possible that it may act as a negative regulator of the calcium influx and ROS responses so the experiments were repeated using a lower concentration of NF to test for increased sensitivity. By this point the F_3 progeny of a cross of the *cbs1-2* mutant with R108-YC3.6 (Chapter 2.8; Tables 5.1 and 5.2) was available so these experiments were carried out using this line (Chapter 2.10). After 0.1 nM NF addition none of the seven cells in the *cbs1-2*-YC3.6 line produced the calcium influx but they retained calcium spiking (Figure 5.4). This is similar to the wildtype R108 so the *cbs1-2* mutant does not appear to be more sensitive for induction of the calcium influx.
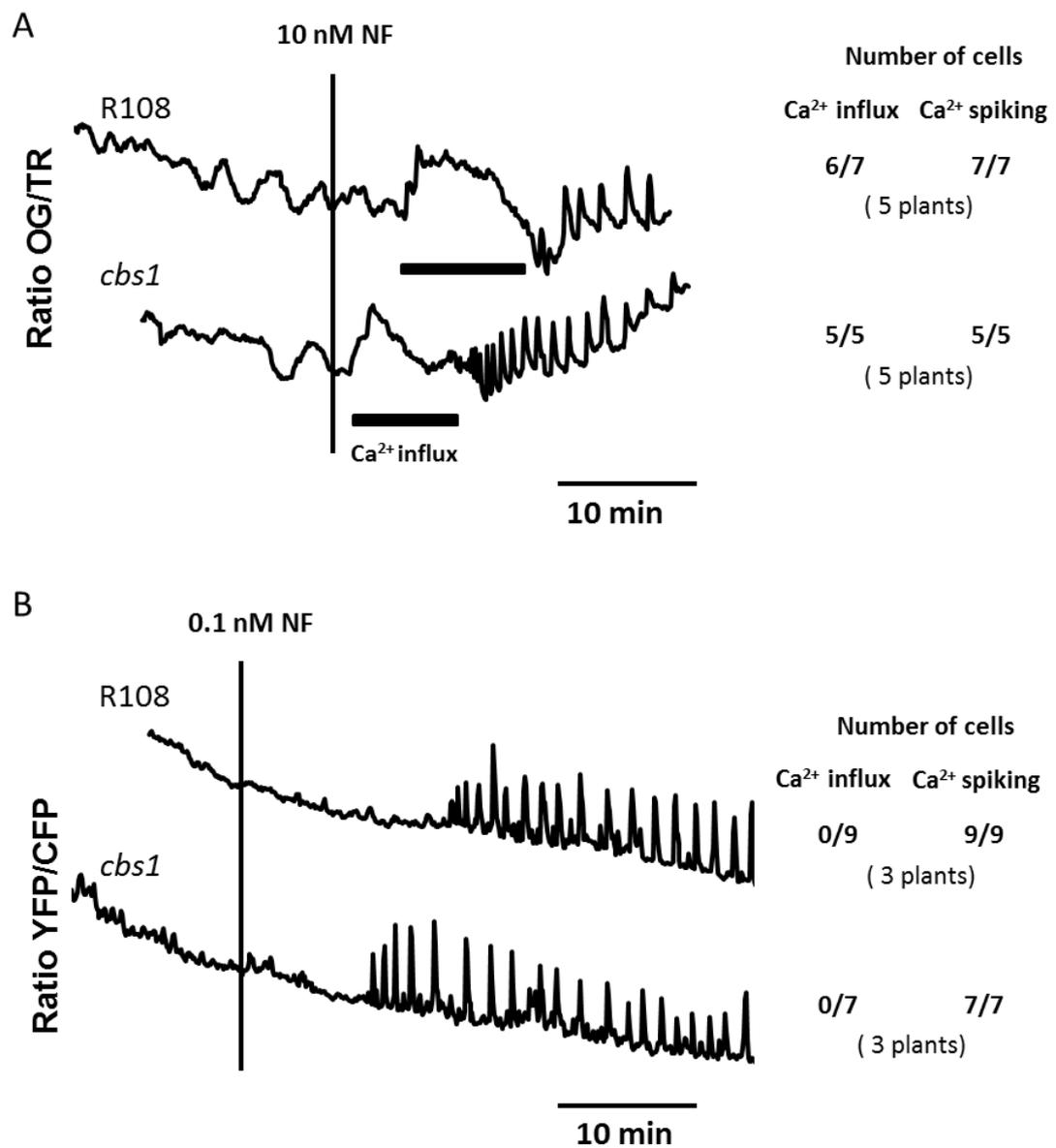
Figure 5.4: *CBS1* is not required for NF-induced calcium responses.

Wildtype R108 and *cbs1* root hairs were microinjected with Oregon Green and Texas Red fluorescent dyes and treated with 10 nM NF **[A]**. Wildtype R108 and *cbs1* root hairs expressing YC3.6 were treated with 0.1 nM NF **[B]**. Representative traces of Oregon Green/Texas Red **[A]** or YFP/CFP **[B]** fluorescence collected at five second intervals for the whole shank of the cells are shown.

To analyse the ROS transient in *cbs1-2,* seedlings were treated with CM-H$_2$DCFDA dye prior to addition of 10 nM or 0.1 nM NF. After 10 nM NF addition, both wildtype R108 and *cbs1-2* mutant root hairs produced the ROS transient (Figure 5.5). At 0.1 nM NF the ROS transient response was absent from both wildtype R108 and *cbs1-2* root hairs (Figure 5.3). These results suggest that CBS1 is not required for the NF-induced ROS transient, and that it also does not appear to be a negative regulator of the response. The results also demonstrate that in the wildtype the ROS transient is only activated by higher concentrations of NF; it was not activated at 0.1 nM NF, a concentration that can reliably induce nuclear calcium spiking (Miwa et al., 2006a, Morieri et al., 2013, Shaw and Long, 2003a).
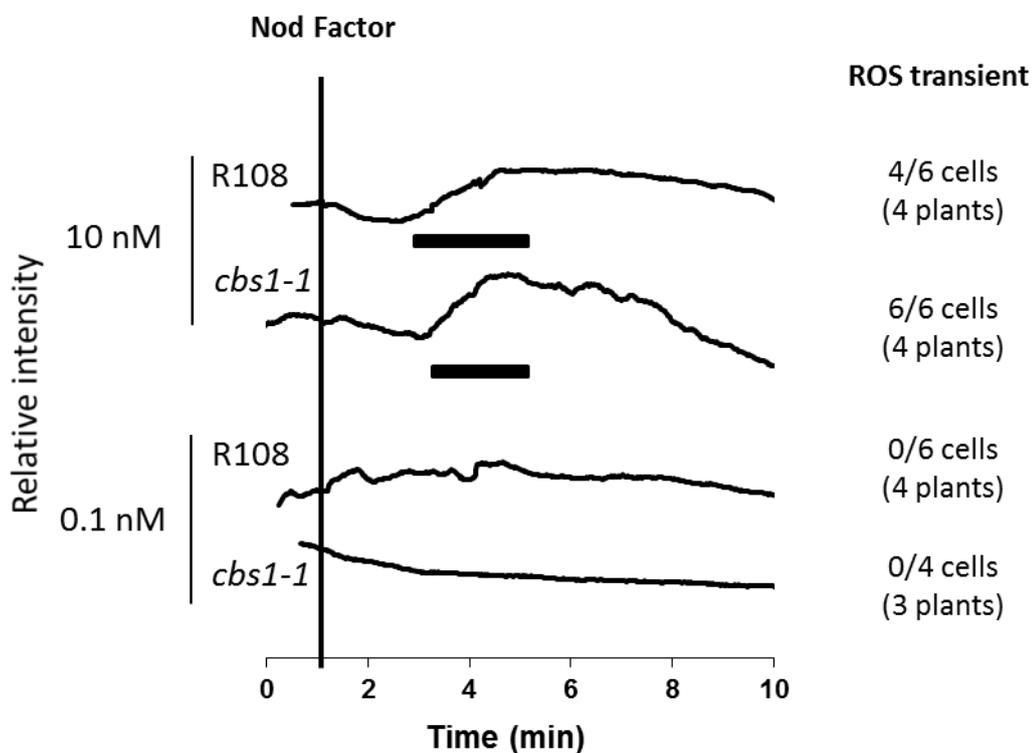
Figure 5.5: *CBS1* is not required for the NF-induced ROS transient.

Seedlings were treated with CM-H$_2$DCFDA prior to 10 nM or 0.1 nM NF treatment and fluorescence intensity (arbitrary units) recorded. Representative traces of tips of root hairs are shown. Black lines indicate ROS transient production.

5.2.4 A sulphated mycorrhizal lipochitooligosaccharide (MycA) can induce a tip-focused calcium influx

AM fungi produce lipochitooligosaccharides (LCOs) that are similar in structure to rhizobial NFs and can activate nuclear calcium spiking (Czaja et al., 2012, Genre et al., 2013, Maillet et al., 2011). The calcium influx has a higher stringency for NF structure than calcium spiking. Single modifications such as the loss of the *NodL* acetylation resulted in 100-fold lower activity for activation of the calcium influx in *M. truncatula* while calcium spiking was unaffected (Morieri et al., 2013). I analysed the ability of a sulphated Myc-LCO [S-Myc-LCO; LCO-IV(C16:0,S)] and a non-sulphated Myc-LCO [NS-Myc-LCO; LCO-IV(C18:1D9Z)] produced by *Rhizophagus irregularis* (Maillet et al., 2011) to activate a tip-focused calcium influx in A17-YC3.6-expressing plants using fluorescence acquisition intervals of 5 seconds.

Addition of 10 nM S-Myc-LCO to *M. truncatula* seedlings can activate nuclear calcium spiking (Sun, J., personal communication). NS-Myc-LCO can also activate nuclear calcium spiking but at a higher concentration of 100 nM (Sun, J., personal communication). For reliable activation of the NF-induced calcium influx, approximately 100-fold higher concentrations of NF are required than those needed to activate calcium spiking (Miwa et al., 2006a, Morieri et al., 2013). Therefore, to test whether S-Myc-LCO and NS-Myc-LCO could activate the calcium influx the seedlings were treated with 1 µM S-Myc-LCO or 10 µM NS-Myc-LCO. Addition of 1 µM S-Myc-LCO produced tip-focused calcium influx responses in most cells (Figure 5.6). The shape and timing of the calcium influxes were very similar to those observed after addition of 10 nM NF with a rapid influx consisting of several peaks followed by a slower decline (Figure 5.6). However, treatment with NS-Myc-LCO did not induce the calcium influx in any of the cells observed (Figure 5.6). This is consistent with previous observations that non-sulphated LCOs are able to activate calcium spiking but not the calcium influx (Shaw and Long, 2003a).
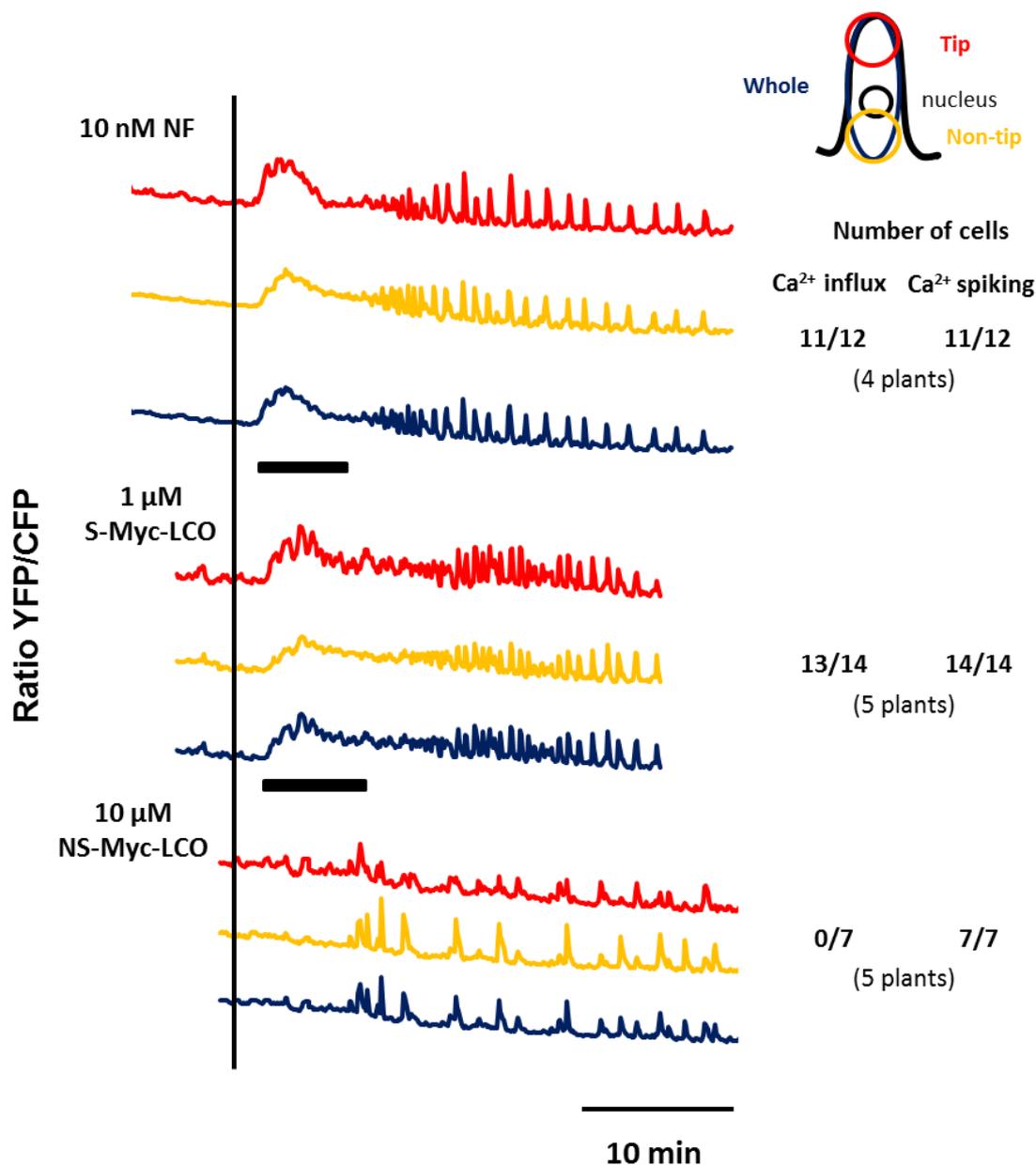
Figure 5.6: Sulphated Myc-LCO can induce a tip-focused calcium influx.

M. truncatula A17 expressing YC3.6 seedlings were treated with 10 nM NF, 1 µM MycA or 10 µM MycB at the time indicated by the vertical line. Traces of the ratio in YFP to CFP fluorescence (arbitrary units) collected at five second intervals for three regions were analysed (tip, non-tip and whole cell), indicated by the areas highlighted in the images of the root hair cell at the top right. The numbers represent the number of cells with a calcium influx or calcium spiking response/number of cells analysed from the number of plants shown in brackets.

5.3 Discussion

This chapter describes the use of some *M. truncatula* nodulation and bacterial infection mutants to further characterise the NF-induced calcium influx and ROS transient responses. Consistent with previous studies, I found that the NF-induced calcium influx is dependent on the NF receptor *NFP* but not the Sym pathway components *DMI1* and *DMI2,* which are required for nuclear calcium spiking (Ben Amor et al., 2003, Miwa et al., 2006a, Shaw and Long, 2003a).

Like the NF-induced calcium influx, the ROS transient is dependent on *NFP* but does not require *DMI1* or *DMI2.* This suggests that the ROS transient may either lie upstream of calcium spiking in the Sym pathway or may belong to a parallel pathway downstream of *NFP*. The first possibility seems unlikely because the ROS transient was activated by 10 nM NF but not 0.1 nM treatment, demonstrating that it requires higher concentrations of NF than calcium spiking, which can be reliably activated at picomolar concentrations of NF (Morieri et al., 2013). The NF-induced calcium influx and the ROS transient require similarly high (nanomolar) concentrations of NF for activation (Miwa et al., 2006a, Morieri et al., 2013, Shaw and Long, 2003a), so it is possible that they belong to the same parallel pathway downstream of *NFP*.

The infection genes *ERN1* and *RIT1* are not required for NF-induced calcium responses. This is perhaps not surprising because *ERN1* encodes a transcription factor and *RIT1* encodes a SCAR/WAVE component involved in regulation of the actin cytoskeleton (Middleton et al., 2007, Miyahara et al., 2010), so they would be more likely to act downstream of the calcium influx.

CBS1 is not required for NF-induced calcium influx, calcium spiking or the ROS transient. After the NF-induced ROS transient increase in root hair cells there is a decline of ROS in legume roots (Lohar et al., 2007, Shaw and Long, 2003b) and it may be that *CBS1* is involved in this response to down-regulate defence responses during infection.

The sulphated Myc-LCO activated a tip-focused calcium influx in root hairs but the non-sulphated Myc-LCO did not. The structure of S-Myc-LCO is very similar to *S. meliloti* NF [NodSm-IV (C16:2, S, Ac)], so it is not surprising that it can activate a calcium influx. However, S-Myc-LCO does not appear to be as active as NF because a calcium influx has not been observed at 10 nM S-Myc-LCO concentrations (Sun, J. personal communication), whereas 10 nM NF can activate a calcium influx in most cells (Miwa et al., 2006a, Morieri et al., 2013, Shaw and Long, 2003a).

Interestingly, S-Myc-LCO [LCO-IV(C16:0,S)] lacks the O-acetylation on the terminal non-reducing sugar of *S. meliloti* NF. NF produced by *S. meloliti nodL* mutant bacteria [LCO IV(C16:2, S)] is also missing this acetylation, and has 100 fold lower activity for the calcium influx, requiring a concentration of 1 mM to induce it in the majority of *M. truncatula* cells (Morieri et al., 2013). This is the same as the concentration of S-Myc-LCO used in this chapter to activate a calcium influx, providing further evidence for the importance of the O-acetylation for induction of calcium influx.

Whether the activation of the calcium influx by S-Myc-LCO is biologically relevant for colonisation of AM fungi remains to be seen, however, because the site of contact and infection by fungi is generally non-root hair (atrichoblast) epidermal cells. As yet there are no reports of whether atrichoblasts produce a calcium influx in response to NF or Myc-LCO treatment. With the exception of root hair curling, which does not occur during mycorrhization, the infection processes of rhizobia and mycorrhizal fungi are very similar with invaginations of the plant cell membranes guiding the microbes to the cortex (Parniske, 2008a). It is therefore possible that the calcium influx could be a signal during both processes.

The NF-induced calcium influx and ROS transient have several characteristics in common. Both originate at the tip of root hair cells and are activated within 1-2 minutes of NF addition (Chapter 3) (Cárdenas et al., 2008, Felle et al., 1998, Miwa et al., 2006a, Shaw and Long, 2003a, Walker et al., 2000). The NADPH oxidase inhibitor DPI inhibits both the NF-induced calcium influx and the ROS transient but not calcium spiking (Chapter 4) (Cárdenas et al., 2008). The calcium influx and ROS transient are activated by similar concentrations of NF (1-10 nM) (Cárdenas et al., 2008, Miwa et al., 2006a, Morieri et al., 2013, Shaw and Long, 2003a) and require the NF receptor *NFP*, but not *DMI1* and *DMI2* (this chapter) (Ben Amor et al., 2003, Miwa et al., 2006a, Shaw and Long, 2003a). Taken together these shared spatial, temporal, pharmacological and genetic characteristics indicate that the NF-induced calcium influx and ROS transient may be involved in a shared pathway downstream of *NFP*, parallel to calcium spiking. This possibility is explored further in the next chapter using a reverse genetics approach to investigate the involvement of ROP signalling in the regulation of calcium and ROS production during bacterial infection.

CHAPTER 6: A RopGAP IS INVOLVED IN BACTERIAL INFECTION

6.1 Introduction

In many legumes, infection by rhizobia during the establishment of symbiosis occurs through root hair cells and requires changes in the normal polar growth of the root hairs. The curling of root hairs entraps rhizobia within infection pockets (Chapter 1 Figure 1.1), from which infection threads develop to guide the dividing rhizobia through the root hair cell into the root cortex. NF treatment induces growth of *Medicago truncatula* root hairs (Oldroyd et al., 2001b) and spot inoculation of NF to root hairs is sufficient to induce root hair curling (Esseling et al., 2003), suggesting that local activation of NF signalling is able to alter the axis of polar growth during bacterial infection.

Developmental polar growth of root hairs is regulated by members of the ROP GTPase family, which are monomeric G proteins that regulate vesicle trafficking and cytoskeletal changes to enable polarised cell expansion (Kost, 2008). The ROP GTPases are regulated by the RopGEFs, which activate ROP signalling activity by exchanging ROP-bound GDP for GTP (Figure 1.5). In contrast RopGAPs assist the intrinsic GTPase activity of the ROPs to convert GTP to GDP to thus return the ROP to an inactive state (Kost, 2008). In addition, RhoGDIs can regulate the ROPs by binding to ROP-GDP bound forms and removing them from the plasma membrane, which has been suggested to be necessary for recycling the ROPs back to the growing root hair tip (Carol et al., 2005, Klahre et al., 2006).

In root hairs and pollen tubes, ROP GTPases localise to the growing apex (Kost et al., 1999, Li et al., 1999, Molendijk et al., 2001). The activities of RopGEFs, RopGAPs and RhoGDIs are thought to maintain a zone of active ROP GTPases at the tip, thus maintaining polar growth (Craddock et al., 2012, Kost, 2008). Any disturbance of this regulation can lead to alterations in cell growth. Overexpression of ROPs or ROPGEFs can lead to broader localisation and loss of polar growth in root hairs and pollen tubes (Gu et al., 2006, Jones et al., 2002, Kost et al., 1999, Li et al., 1999, Molendijk et al., 2001, Zhang and McCormick, 2007). Overexpression of *RopGAPs* reduces pollen tube growth and an RNAi double knockdown of *AtGAP1* and *AtGAP3* led to an increase in pollen tube length (Fu et al., 2001, Hwang et al., 2010, Klahre and Kost, 2006).

Several ROP GTPases have already been implicated in rhizobial infection in legumes. Three *M. truncatula ROPs* were upregulated in roots and root hairs upon inoculation with *Sinorhizobium*

meliloti (Liu et al., 2010). RNAi knockdown of *MtROP9* inhibited a NF-induced ROS response and fewer nodules were formed (Kiirika et al., 2012). LjROP6 interacts with the NF receptor LjNFR5 (Ke et al., 2012) and RNAi knockdown of *LjROP6* led to a defect in infection thread progression and fewer nodules (Ke et al., 2012).

It is possible that NF may activate root hair curling and infection thread formation via the existing regulators of polar growth. To investigate this possibility a reverse genetics approach was used to identify candidates of the *ROP*, *RopGEF* and *RopGAP* families that might be involved in bacterial infection. To do this, gene expression in *M. truncatula* root hairs during infection with *S. meliloti* was analysed using microarray data generated by Breakspear et al. (unpublished). From this analysis a *RopGAP* gene, *MtGAP1* emerged as a promising candidate and *Tnt1* insertion mutant lines were characterised for bacterial infection and nodulation. In addition, the NF-induced calcium signalling responses of *MtROP9* RNAi knockdown lines were also examined.

6.2 Results

6.2.1 Expression of *M. truncatula ROP*s, *RopGAP*s and *RopGEF*s in root hairs during bacterial infection

Seven *ROP* and ten *RopGEF* genes have been identified in *M. truncatula* (Liu et al., 2010, Riely et al., 2011) (Table 6.1). To identify the *M. truncatula RopGAP* genes, the protein sequences of the nine *Arabidopsis thaliana* RopGAPs in the TAIR database were used to search the *M. truncatula* genome (IMGAG vr 4.0) using BLAST, followed by reverse BLAST of the top hits against the *A. thaliana* genome (TAIR) (Chapter 2.14.1). This process identified 12 *MtRopGAP* family members (Table 6.2).

Table 6.1: *M. truncatula* ROP and RopGEF families

IMGAG number	Gene name (if applicable)	Genbank Accession	MGEA probeset(s)
Medtr8g075240	*MtROP6*	AF498359	Mtr.40463.1.S1_at Mtr.51873.1.S1_s_at
Medtr5g022600	*MtROP9*	AF498358	Mtr.43489.1.S1_at
Medtr4g073250		AF498357	Mtr.47026.1.S1_at
Medtr4g088055		EU178798	Mtr.41157.1.S1_at
Medtr2g090875		EU164777	Mtr.50278.1.S1_s_at Mtr.50278.1.S1_at
Medtr6g087980		DQ836313	Mtr.15539.1.S1_s_at Mtr.35940.1.S1_at
Medtr3g078260		EU625287	Mtr.5759.1.S1_at
Medtr4g075640	*RopGEF1*	JF340147	Mtr.34189.1.S1_at Mtr.31727.1.S1_at
Medtr8g030850	*RopGEF2*	JF340143	Mtr.38441.1.S1_at Mtr.10136.1.S1_at
Medtr7g077690	*RopGEF3*	JF340144.1	Mtr.26010.1.S1_at Mtr.39957.1.S1_s_at
Medtr3g069590	*RopGEF5*	JF340145.1	Mtr.13888.1.S1_at
Medtr5g081410	*RopGEF6*	JF340142.1	Mtr.13731.1.S1_at Mtr.7515.1.S1_at
Medtr7g065220	*RopGEF7a*	JF340146	
Medtr4g019770	*RopGEF7b*	JF340151	Mtr.45538.1.S1_at
Medtr6g087700	*RopGEF8*	JF340148	Mtr.15948.1.S1_at
Medtr2g101830	*RopGEF12*	JF340149.1	Mtr.6541.1.S1_at
Medtr5g025960	*RopGEF14*	JF340150.1	Mtr.10377.1.S1_s_at Mtr.10377.1.S1_at

Table 6.2: *M. truncatula* RopGAP family

	Gene	MGEA probeset(s)
	Medtr8g026680 (*MtGAP1*)	Mtr.9886.1.S1_at Mtr.37069.1.S1_at
	Medtr1g089500	Mtr.6812.1.S1_at Mtr.1434.1.S1_at
		Mtr.4727.1.S1_at
CRIB domain	Medtr2g086580	Mtr.41759.1.S1_at
+GAP domain	Medtr4g052850	
	Medtr5g064420	
	Medtr7g081615	
	Medtr7g104900	Mtr.757.1.S1_s_at Mtr.35205.1.S1_at
	Medtr7g107560	Mtr.39712.1.S1_at
Pleckstrin	Medtr3g100580	
Homology	Medtr5g065960	
domain +GAP	Medtr5g089490	Mtr.9907.1.S1_at
GAP domain only	Medtr4g029530	Mtr.41371.1.S1_s_at Mtr.39180.1.S1_at

Breakspear et al. (unpublished) carried out microarray experiments to analyse gene expression in *M. truncatula* root hairs during infection with *S. meliloti* 1021, using both wildtype and mutant plant lines. I analysed the expression of the *ROPs*, *RopGAPs* and *RopGEFs* in wildtype A17 root hairs after identifying MtGEA (*Medicago truncatula* Gene Expression Atlas) probesets (Benedito et al., 2008, He et al., 2009) for each gene where possible (Tables 6.1 and 6.2; Chapter 2.14.3). There were no significant changes in expression of the seven *MtROP* genes present on the chip in wildtype A17 root hairs at one, three, or five days after inoculation with *S. meliloti* 1021 relative to the control root hairs [inoculated with *S. meliloti* SL44 *(nodΔD1ABC)*, a strain unable to produce NFs] (Figure 6.1A).

I also analysed the expression of the *ROPs*, *RopGAPs* and *ROPGEFs* in root hairs of three mutant lines. The hypernodulation mutant *skl-1* forms many more infection threads than wildtype (Penmetsa and Cook, 1997). Infection-related genes are more highly upregulated in the mRNA extracted from *skl-1* root hairs than wildtype, which is likely to be due to the increased numbers of infected root hairs within the *skl-1* root hair samples (Breakspear A., personal communication). The *nin-1* and *bit1-1* mutants are defective for the transcription

factors NIN and ERN1, respectively, which are both required for bacterial infection and nodule formation (Marsh et al., 2007, Middleton et al., 2007). There were no significant differences in expression of the *ROPs* in *skl-1, nin-1* or *bit1-1* compared to wildtype root hairs at five days (Figure 6.1B).
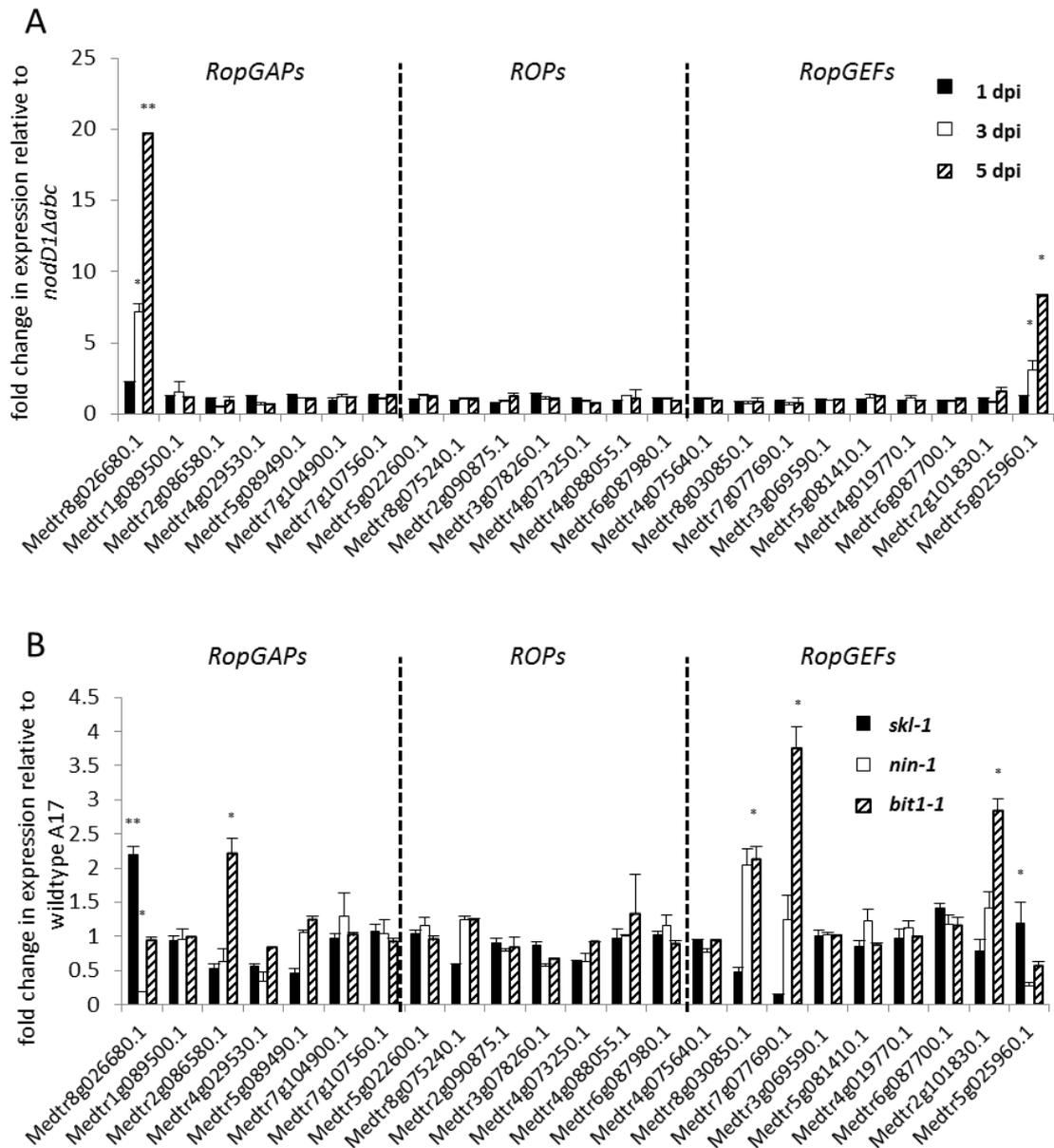
Figure 6.1: Expression of *ROP*, *RopGAP* and *RopGEF* families in *M. truncatula* root hairs.

[A] Wildtype A17 root hairs at 1, 3 and 5 days after inoculation with *S. meliloti* 1021 (WT). Fold changes of the geometric mean expression values ± SEM relative to control root hairs inoculated with *S. meliloti* SL44 *nodΔD1abc*, which is unable to produce NFs. **[B]** *skl, nin* and *ern* mutant root hairs 5 days after inoculation with *S. meliloti* 1021. Fold changes of the geometric mean expression values ± SEM relative to wildtype A17 inoculated with *S. meliloti* 1021. Student's *t* tests were performed comparing each condition to the appropriate control (*$P < 0.05$; **$P < 0.01$). Root hair expression data were generated by A. Breakspear (n=3).

Probesets were found for seven RopGAPs and nine RopGEFs. One *RopGAP* (*MtGAP1*/Medtr8g026680) and one *RopGEF* (*RopGEF14*/Medtr5g025960) were significantly up-regulated in wildtype root hairs at three and five days after inoculation with *S. meliloti* 1021 (Figure 6.1A). Also, both were upregulated in the hypernodulatoin mutant *skl-1* and downregulated in *nin-1,* but there was no change in expression in *bit1-1* compared with the wildtype (Figure 6.1B). These data suggest that *MtGAP1* and *RopGEF14* may be involved in bacterial infection, regulated directly or indirectly by NIN.

One *RopGAP* (Medtr2g089500), and two RopGEFs *RopGEF3* and *RopGEF12* showed no change in root hair expression following inoculation of wildtype but were upregulated in the *bit1-1* infection mutant (Figure 6.1). This suggests that they may be negatively regulated, either directly or indirectly by ERN1.

6.2.2 The *M. truncatula RopGAP* family

The expression profile of *MtGAP1* made it a good candidate for further investigation of a possible role in bacterial infection. *A. thaliana* is reported to have ten RopGAPs but I could only find evidence for nine in the literature and in the TAIR database (Hwang et al., 2008, Schaefer et al., 2011a, Schaefer et al., 2011b, Wu et al., 2000). The members segregate into three subfamilies, with all three having a conserved GAP catalytic domain, which is responsible for aiding the intrinsic GTPase activity of the ROP GTPases (Schaefer et al., 2011a, Schaefer et al., 2011b, Wu et al., 2000). Members of two of the subfamilies have an additional domain, either a Cdc42/Rac INTERACTIVE BINDING (CRIB; ROP-binding) domain or a Pleckstrin Homology domain (suggesting they may be regulated by phosphoinositides) (Bos et al., 2007, Hwang et al., 2008, Schaefer et al., 2011a, Schaefer et al., 2011b, Wu et al., 2000). A phylogenetic tree of the *A. thaliana* and *M. truncatula* RopGAP protein sequences was drawn using the Phylogeny.fr Server (Chapter 2.14.2). The MtRopGAPs segregate out into the same three subfamilies as the *A. thaliana* RopGAPs (Figure 6.2, Table 6.2).
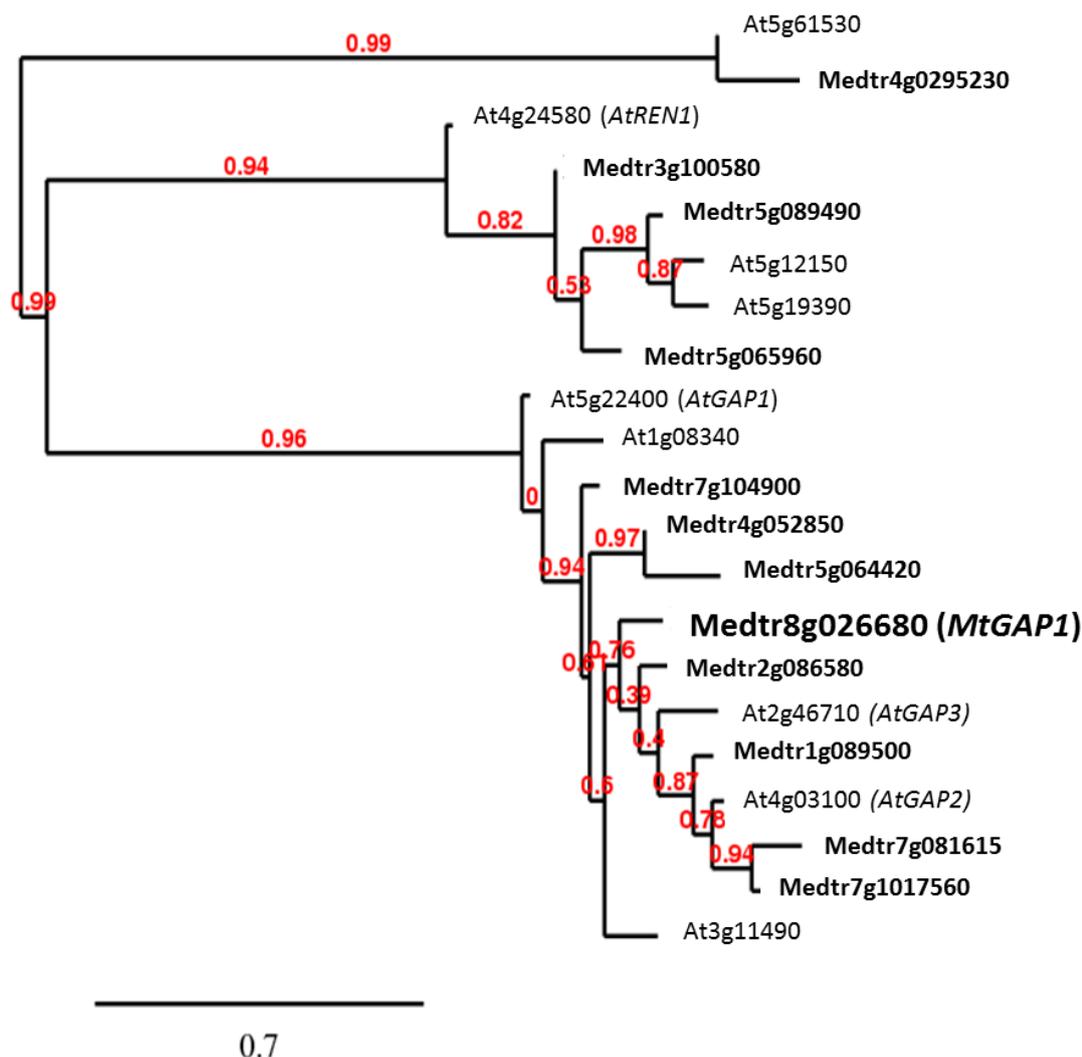
Figure 6.2: Phylogenetic analysis of *M. truncatula* and *Arabidopsis thaliana* RopGAP families.

The tree was constructed based on protein sequences using the Phylogeny.fr server. The scale bar represents a phylogenetic distance of 0.7 (arbitrary units). Red numbers refer to bootstrap values for each branch.

MtGAP1 (Medtr8g0266800) belongs to the CRIB-domain subfamily along with AtGAP1, AtGAP2 and AtGAP3 (Figure 6.2) (Schaefer et al., 2011a, Schaefer et al., 2011b, Wu et al., 2000). For this reason I have called it MtGAP1 and shall refer to it by this name from now on. I acquired T_1 generation seeds of two *Tnt1* transposon insertion lines with insertions in *MtGAP1* from the Samuel Roberts Noble Foundation (R108 ecotype background) (Tadege et al., 2008). These seeds were segregating populations so the plants were genotyped for the *GAP1 Tnt1* insertions using PCR to amplify a region of the *MtGAP1* gene that included the sites of the insertions (Chapter 2.13.3). Individuals that were homozygous or heterozygous for a *Tnt1* insertion in

MtGAP1 were kept to produce seed. The first experiments were done using the progeny of the homozygous T_1 individuals (T_2) and later experiments using the T_3 generation.

For both lines the *Tnt1* insertions are within the final exon of the coding sequence (Figure 6.3A). The *Tnt1* transposon is around 5 kb long (Grandbastien et al., 1989) so insertions into exons would be expected to generate null mutants. To check this was the case, expression of the full length *MtGAP1* mRNA in root tissue from the *Tnt1* lines was examined using reverse transcription (RT)-PCR (Chapter 2.13.12). The *gap1-1* mutant did not express the *GAP1* mRNA and thus appears to be a null allele (Figure 6.3B). However, surprisingly the *gap1-2* mutant retained some expression, although the expression was weaker than the wildtype R108, suggesting that the *Tnt1* insertion may be spliced out of the *gap1-2* allele, at least some of the time.
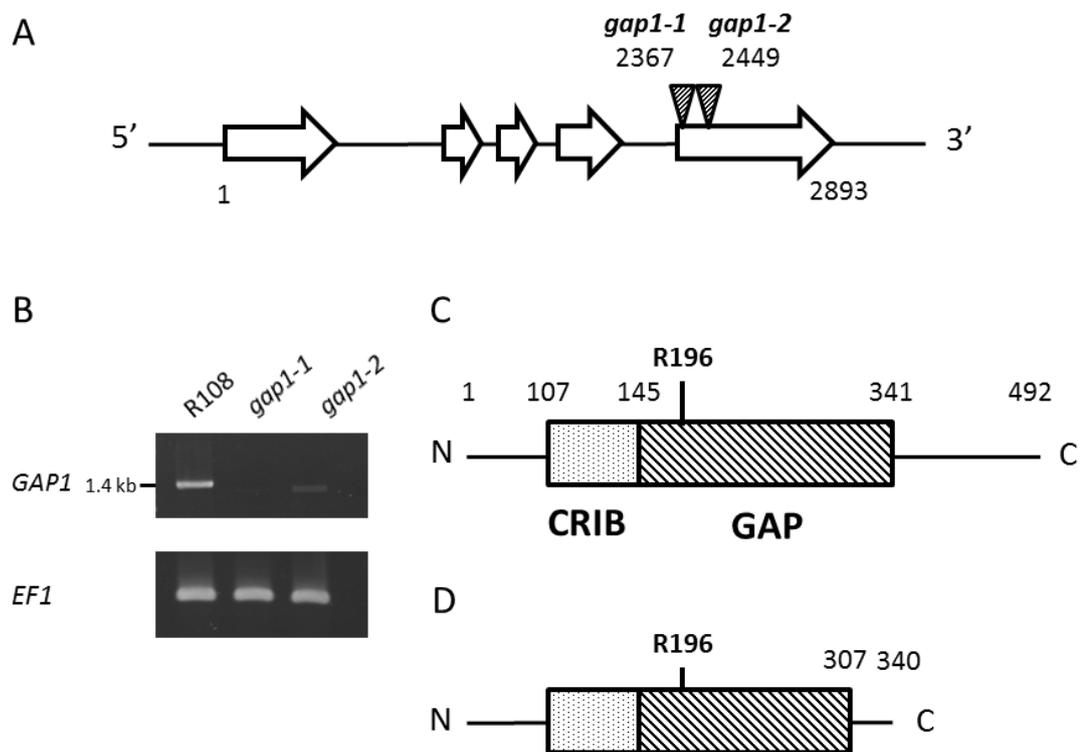
Figure 6.3: *M. truncatula gap1 Tnt1* insertion alleles.

[A] The structure of the *GAP1* gene with exons marked with arrows. The positions of the *Tnt1* insertions in *gap1-1* and *gap1-2* alleles are marked with triangles with numbers referring to the nucleotide position from the start of the coding sequence. **[B]** RT-PCR of full length *GAP1* mRNA and *EF1* (housekeeping gene) in wildtype R108 and the *gap1* mutant alleles. **[C-D]** The predicted protein structures of the **[C]** wildtype and **[D]** *gap1-2* GAP1. The CRIB and GAP protein domains and the conserved arginine 196 residue are highlighted. The numbers refer to the amino acid position from the N-terminus.

The mRNA for *GAP1* was slightly smaller in *gap1-2* compared to wildtype (Figure 6.3B). On closer inspection this band was found to be made up of three individual bands (data not shown). The most abundant band was amplified by PCR and sequenced (Chapter 2.13.6). This band had a 165 bp deletion from positions 921-1086, resulting in a frame shift and an early stop codon. If this mRNA was translated the resulting protein would be truncated, missing the final 34 amino acids of the GAP domain and the C-terminus (Figure 6.3C). However, this protein would still have the arginine residue at position 196 (equivalent to Arg-159 in AtRopGAP2), which is highly conserved within plant and animal GAP proteins and is important for catalytic activity, slotting into the ROP protein to stabilise the transition state of GTP hydrolysis (Bos et al., 2007, Schaefer et al., 2011a, Schaefer et al., 2011b). Therefore, it is possible that the protein expressed in the *gap1-2* allele is at least partially functional and so the *gap1-2 Tnt1* insertion line may be a weak allele.

6.2.3 *gap1* mutants produce fewer infection threads after inoculation with *Sinorhizobium meliloti*

To investigate whether *MtGAP1* is involved in bacterial infection wildtype R108 and *gap1* seedlings were grown on BNM agar containing 0.1 µM AVG and inoculated with a *lacZ*-expressing strain of *S. meliloti* 2011 (Chapter 2.12.4; *S. meliloti* 2011 was used because inoculation of *S. meliloti* 1021 onto wildtype R108 only resulted in low levels of bacterial infection and nodule formation that was difficult to quantify). After six days the roots were stained with X-Gal to visualise the bacteria. The blue-stained bacteria made it possible to identify infection events on the root and these were separated into three categories: infection foci, infection threads in the root hairs and ramifying infection threads in the root cortex.

The *gap1* mutants had less than half the number of total infection events compared to the wildtype R108 (Figure 6.4A). Both *gap1* mutants had fewer infection events at each stage (infection foci, infection threads in the epidermis and ramifying infection threads), suggesting *MtGAP1* may be involved early in infection thread development perhaps in root hair curling and/or infection thread initiation. The infection threads in the *gap1* mutants were abnormal in appearance. Instead of the tight curls that formed in the wildtype to entrap the rhizobia (Figure 6.4B), the *gap1-1* mutant infection threads seemed to have formed from root hairs that had bent over onto the root surface (Figure 6.4C) or in some cases the infection thread seemed to have initiated from the tip of the root hair with no curl at all (Figure 6.4D). Also, the

infection threads were often thicker compared to the wildtype and sometimes branched within the root hair. Many of the infection threads on *gap1-2* also looked very similar to those on *gap1-1* (Figure 6.4E) but some also looked like the wildtype (Figure 6.4F). The lack of curling in *gap1* infection threads suggests that *MtGAP1* may be involved in normal root hair curling.
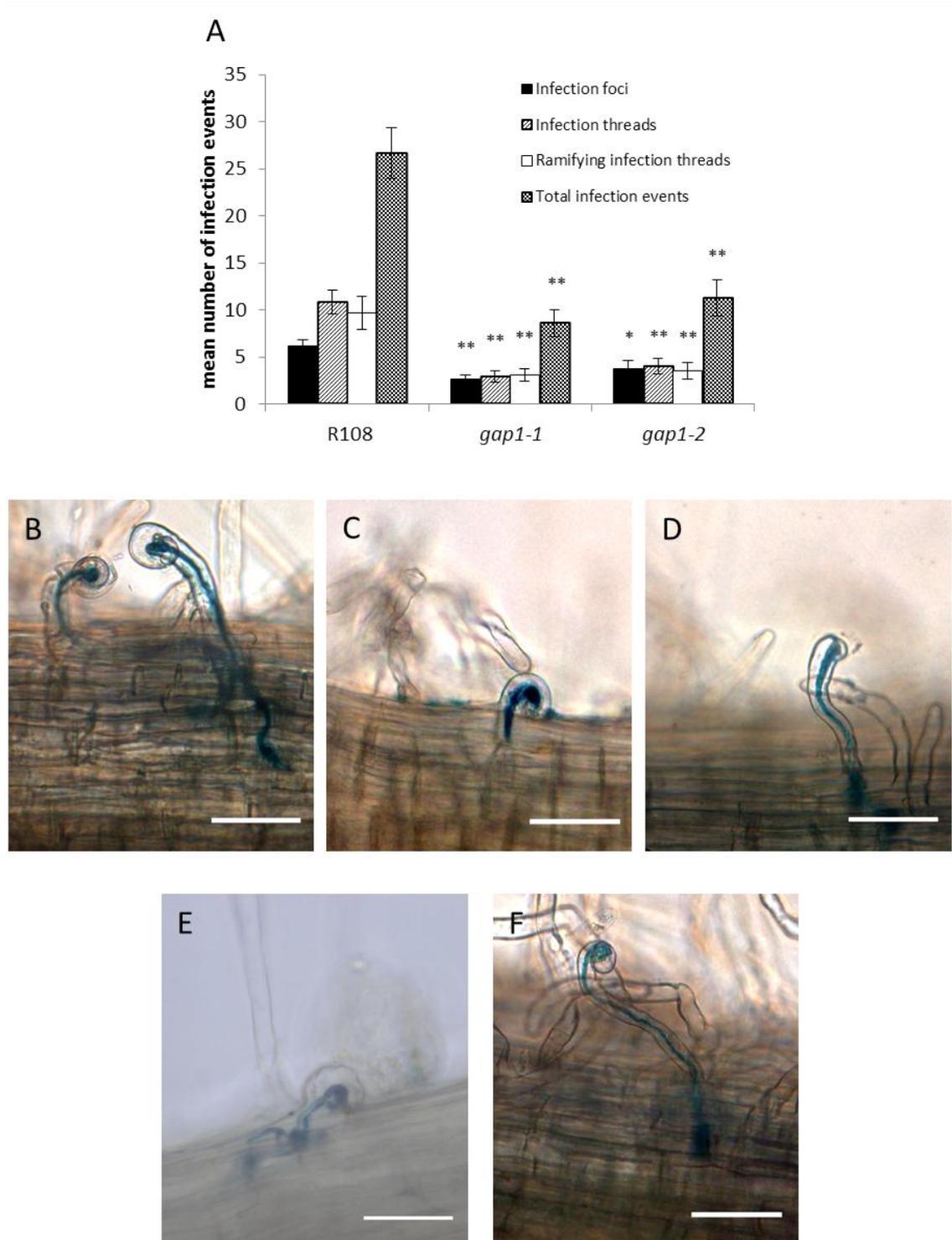
Figure 6.4: *gap1* mutants produce fewer infection events after inoculation with *S. meliloti*.

Seedlings were inoculated with a *S. meliloti* 2011 strain expressing *lacZ*. After 6 days roots were stained using X-Gal and infection events were quantified in three groups: infection foci, infection threads in root hairs and ramifying infection threads in the cortex **[A]**. Y- axis: mean ± SEM of two independent trials sampling a total of n ≥ 18 plants. Student t-tests were done comparing each mutant to the wildtype (*$P < 0.05$; **$P < 0.01$). Representative images of infection threads **[B-F]**: R108 **[B]**, *gap1-1* **[C-D]**, *gap1-2* **[E-F]**. Scale bars: 50 µm.

To find out whether nodule formation is affected in the *gap1* mutants, plants were grown in low nutrient conditions (terragreen-sand mix) and inoculated with *S. meliloti* 2011 (Chapter 2.12.3) to count the number of nodules formed. At all four timepoints (7, 10, 14 and 21 days post inoculation) the *gap1-1* plants had significantly fewer nodules than the wildtype (Figure 6.5). However, the *gap1-2* plants had similar numbers of nodules to the wildtype at all four timepoints. The infection thread and nodule phenotypes support the earlier prediction that *gap1-2* is a weaker allele. By 21 days both *gap1* mutants and the wildtype had mature pink nodules. The pink colour is due to the presence of leghaemoglobin and indicates that the nodules were infected and fixing nitrogen so mutations in *gap1* do not appear to affect nodule function.
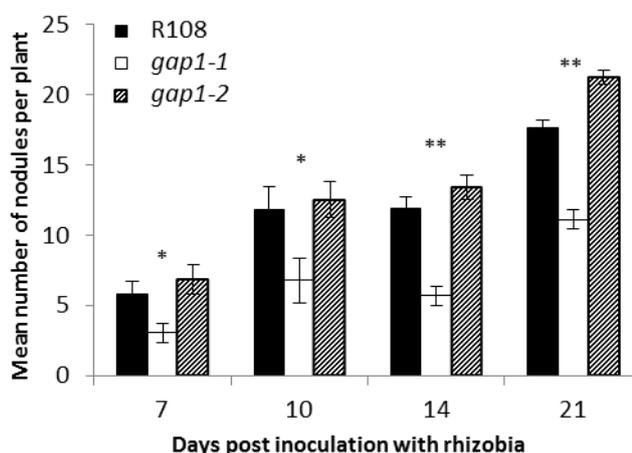
Figure 6.5: Nodule formation in *gap1* mutants.

Wildtype R108 and *gap1* mutant plants were inoculated with *S. meliloti* 2011. Mean nodule number ± SEM at 7, 10, 14, or 21 days post inoculation (n ≥ 14 for each timepoint, two independent trials). Student t-tests were performed comparing each mutant to the wildtype ($*P < 0.05$; $**P < 0.01$).

6.2.4 NF-induced root hair deformation is retained in the *gap1* mutants

NF treatment can induce root hair deformation in legumes, where the root hairs swell, change growth axis and sometimes branch (Kurkdjian, 1995). To analyse this response in the *gap1* mutants, seedlings were placed in Fahraeus slides and treated with 10 nM NF (Chapter 2.12.2). Twenty-four hours later the seedlings were scored as either positive or negative for root hair

deformation. Both *gap1* mutants retained NF-induced root hair deformation (Figure 6.6). It appears that the response may have been more pronounced in the *gap1* mutants but it is not possible to quantify. Nevertheless, *GAP1* is not required for NF-induced root hair deformation. This suggests that the lack of root hair curling during infection in the *gap1* mutants is not due to an inability to detect NFs and activate cell expansion.
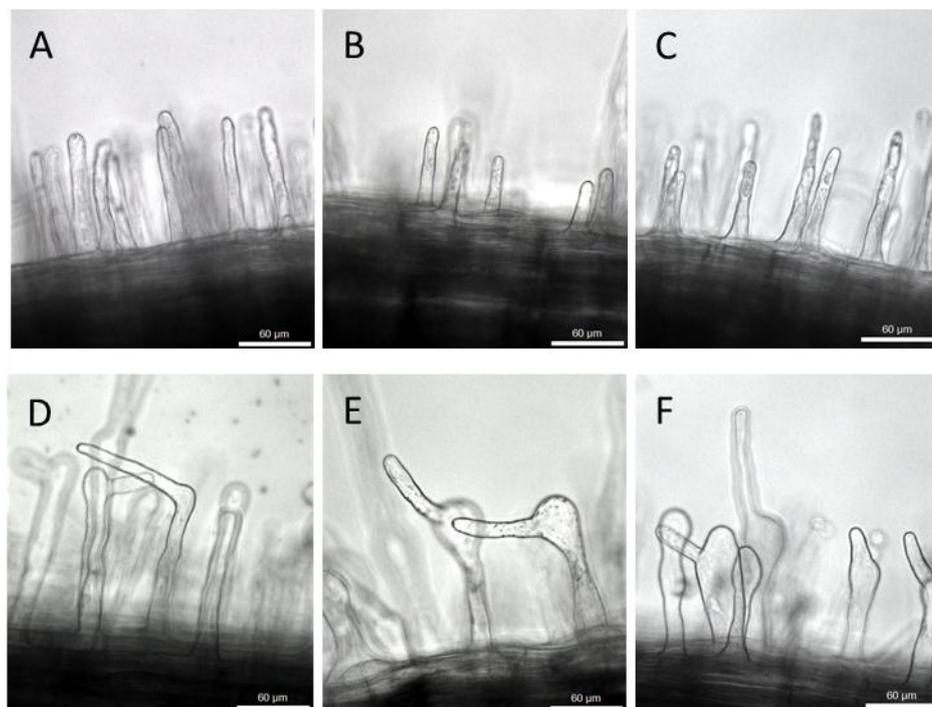
Figure 6.6: *MtGAP1* is not required for NF-induced root hair deformation.

Root hair responses in wildtype R108 and *gap1* mutants 24 hours after NF addition. Untreated root hairs **[A-C]** and 10 nM NF treated root hairs **[D-F]**. **[A and D]** wildtype R108, **[B and E]** *gap1-1* and **[C and F]** *gap2-1*. Number of plants ≥ 5 in one trial. Scale bars: 60 μm.

6.2.5 *gap1* mutants have longer root hairs

To check whether the bacterial infection phenotypes of the *gap1* mutants could be due to a defect in developmental growth of the root or root hairs, seeds were germinated and grown on BNM agar for 72 hours (Chapter 2.12.1). There was no difference in the root length of the *gap1* mutants and wildtype (Figure 6.7F). To assess root hair length, hairs were measured at the point along the root where the root hairs first become fully vacuolated, indicating they are mature. The *gap1* mutant root hairs were significantly longer than wildtype with *gap1-1* root

hairs longer than *gap1-2* (Figure 6.7E). This suggests that *MtGAP1* may be a negative regulator of root hair growth.
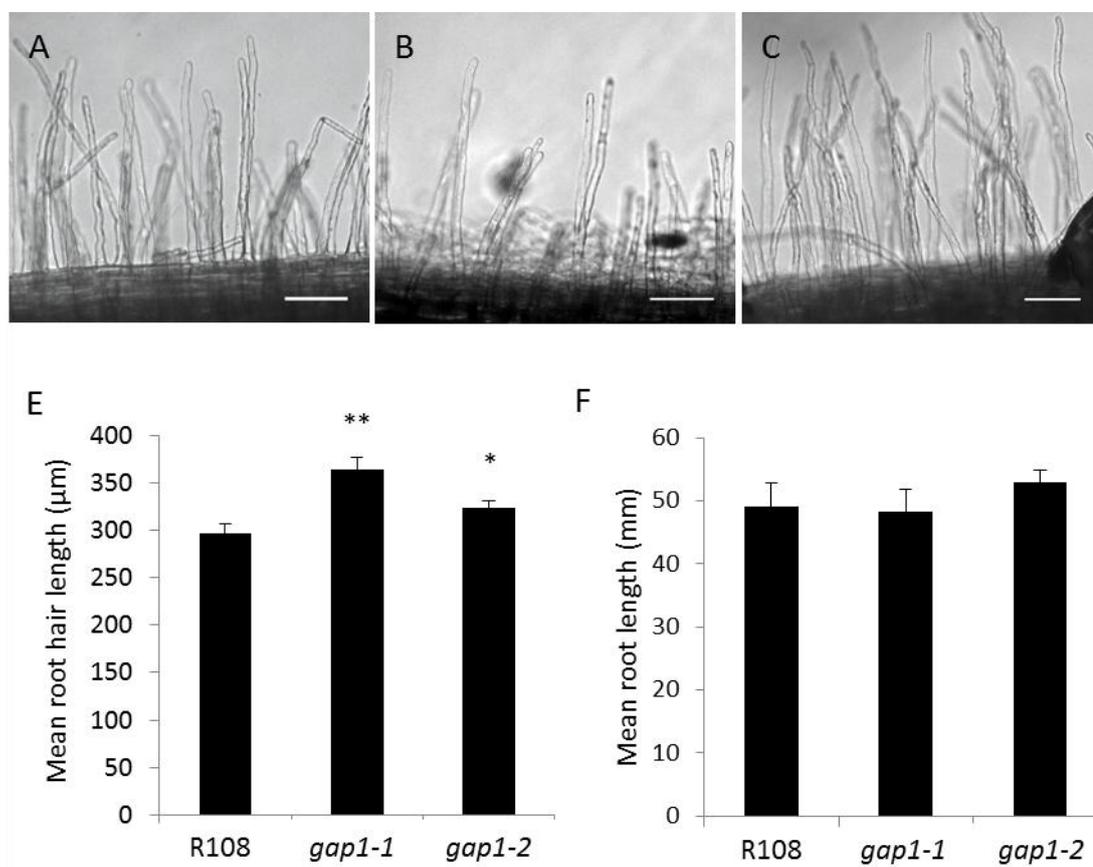
Figure 6.7: *MtGAP1* is a negative regulator of developmental root hair growth.

After 72 hours on BNM agar plates mature root hairs of R108 **[A]**, *gap1-1* **[B]** and *gap1-2* **[C]** root hairs were measured from microscope images (n ≥ 20 from at least 3 plants, ImageJ). Y-axis: mean ± SEM of one trial **[E]**. The seedling root lengths **[F]** were measured from photographs using ImageJ (n ≥ 7). Student t-tests were performed comparing each mutant to the wildtype (*$P < 0.05$; **$P < 0.01$). Scale bars: 100 µm.

6.2.6 The *gap1-1* mutant is hypersensitive for the NF-induced calcium influx

Having found that *MtGAP1* is involved in bacterial infection I wanted to find out whether it is involved in the generation of the NF-induced calcium influx. No *gap-1-1* mutant line expressing YC3.6 was available, so seedlings of the *gap1-1* allele were microinjected with the Oregon Green and Texas Red dyes for pseudo-ratiometric imaging of cytosolic free Ca^{2+} (Chapter 2.10). After 10 nM NF addition the majority of the *gap1-1* root hairs produced a calcium influx, which was similar to that in the wildtype R108 (Figure 6.8A and B). Given that the GAPs are generally considered to be negative regulators of ROP GTPase signalling and the *gap1* mutants had

longer root hairs I considered the possibility that *gap1-1* could be more sensitive to NF for activation of the calcium influx due to a loss of negative regulation. Seedlings were treated with a lower concentration of NF. Addition of 0.1 nM NF induced a calcium influx in five of ten *gap1-1* cells, but not in the wildtype. This suggests that *GAP1* may be a negative regulator of the calcium influx (Figure 6.8C and D).
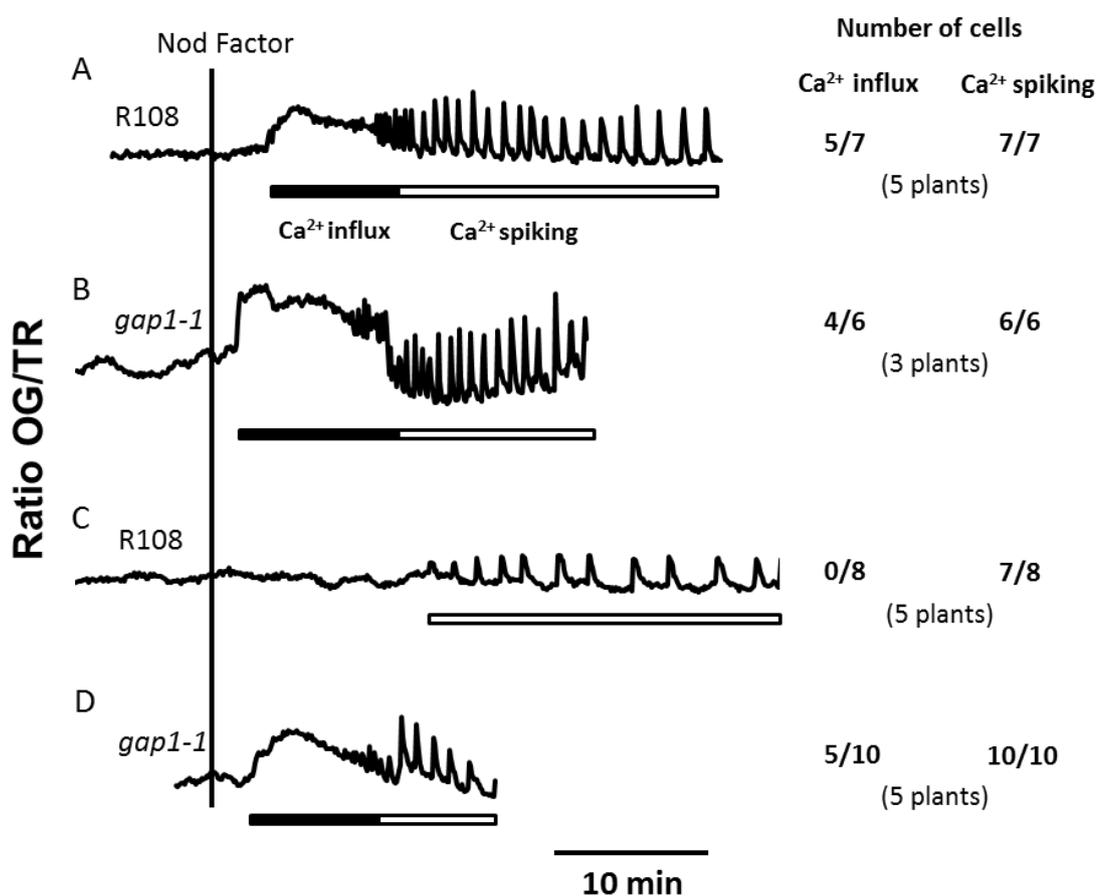
Figure 6.8: The *gap1-1* mutant is hypersensitive for the calcium influx.

Wildtype R108 **[A** and **C]** and *gap1-1* **[B** and **D]** root hairs were microinjected with Oregon Green and Texas Red fluorescent dyes and treated with 10 nM **[A-B]** or 0.1 nM **[C-D]** NF. Representative traces of changes in Oregon Green/Texas Red fluorescence against time (min) for the whole shaft of the cell are shown.

6.2.7 *MtROP9* appears to be involved in NF-induced calcium signalling

If *MtGAP1* is a negative regulator of ROP signalling and NF-induced calcium influx, then it is possible that the ROP GTPases that are involved in bacterial infection may also be required for activation of the calcium influx. To test this idea *Agrobacterium rhizogenes* was used to generate transformed roots of *M. truncatula* A17-YC3.6 expressing a *MtROP9* RNAi construct made by Kiirika et al. (2012) (Chapter 2.13.10). The construct has been previously shown to silence *MtROP9* but not other closely-related ROP GTPase family members (Kiirika et al., 2012). Small sections of transformed lateral roots were cut off and used for calcium imaging with YC3.6. The root hairs in the *ROP9* RNAi knockdown lines were wider and more highly vacuolated than the vector control plants but otherwise appeared to be healthy. In the *ROP9* RNAi knockdown lines the percentage of cells with the NF-induced calcium influx was significantly reduced compared to the vector control (Fisher's Test; Figure 6.9). There was also a smaller, but statistically significant reduction in the percentage of cells with NF-induced calcium spiking. *MtROP9* expression was efficiently knocked down in roots of the *MtROP9* RNAi knockdown lines with average normalized expression of 0.08 relative to the vector control roots (1.0). These data suggest that *MtROP9* may be involved in NF-induced calcium signalling.

A
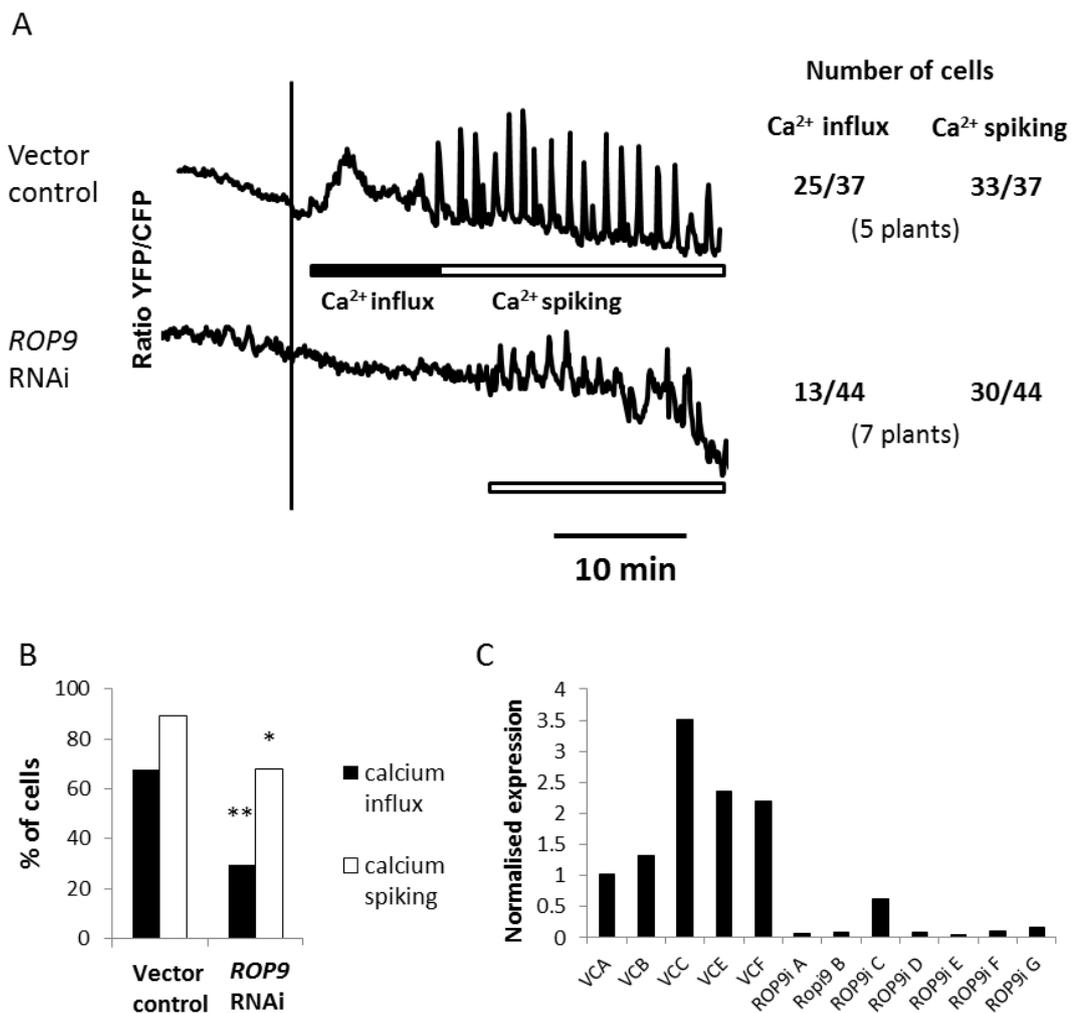
Figure 6.9: *ROP9* is involved in the activation of the calcium influx.

Calcium responses in YC3.6-expressing *ROP9* RNAi lines after 10 nM NF addition. Representative traces of changes in YFP/CFP fluorescence against time (min) for the whole shaft of the cell are shown, with the horizontal line indicating 10 nM NF addition **[A]**. Individual root hairs were scored as positive or negative for the calcium influx and calcium spiking and the percentages of cells producing responses shown **[B].** The Fisher's statistical test was carried out for each response using the number of positive and negative cells (*P = 0.011 and **P = 0.0004). Normalised expression of *ROP9* in vector control and *ROP9* RNAi lines (individual plants) **[C]**.

6.3 Discussion

Using a reverse genetics approach I found that a *M. truncatula RopGAP* is involved in bacterial infection. *MtGAP1* was upregulated in root hairs during bacterial infection and *gap1* mutants had fewer, and abnormal-looking infection events compared to the wildtype. *MtGAP1* also appears to be a negative regulator of the NF-induced calcium influx as *gap1-1* mutants were hypersensitive for calcium influx induction.

The *gap1-1* allele generates a null mutant with no detectable expression of the *MtGAP1* mRNA. However, the *gap1-2* mutant retained some *MtGAP1* expression, although below wildtype levels. The frame shift deletion in the *GAP1-2* mRNA would result in a truncated protein that lacks the end of the GAP domain and the C-terminus. It is possible that this truncated protein could still be at least partially functional because it retains the arginine residue at position 196, which is crucial for the activity of other GAP proteins and is highly conserved amongst both animal and plant RopGAPs (Schaefer et al., 2011a, Schaefer et al., 2011b). This could account for the discrepancies between the *gap1-1* and *gap1-2* phenotypes. Both alleles had a similar reduction in infection events after inoculation with *S. meliloti* but only *gap1-1* had a reduction in nodule numbers. The C-terminus of MtGAP1 is not a recognised protein domain but could have a regulatory role, so the *gap1-2* allele may encode a functional but less tightly regulated protein. Perhaps tight regulation of MtGAP1 activity is required during bacterial infection but not so important during nodule formation. Another possibility is that the observed reduction in nodule numbers in *gap1-1* is due to the presence of a background mutation because *Tnt1* insertion lines have an average of 25 insertions (Tadege et al., 2008). Complementation of the *gap1-1* mutant with *MtGAP1* would clarify whether it has a role in nodule formation as well as bacterial infection.

What role is *MtGAP1* playing in bacterial infection? RopGAPs are generally considered to be negative regulators of ROP signalling. RNAi double knockdowns of *AtGAP1* and *AtGAP3* increased pollen tube length (Hwang 2010). The *gap1* mutants had longer root hairs than wildtype, suggesting *MtGAP1* may play a similar role to *AtGAP1* and *AtGAP3* (Hwang et al., 2010) as a negative regulator of polar cell growth. Using computer modelling, van Batenberg et al. (1986) predicted that rhizobia could induce root hair curling by attaching to the growing tip area and re-directing tip growth. Spot inoculation of NF can induce root hair curling even in the absence of rhizobia (Esseling et al., 2003). Presumably, during bacterial infection, locally high concentrations of NF on the root hair surface can induce a change in the axis of cell expansion resulting in root hair curling. If GAP1 is a negative regulator of ROP signalling then it

is possible that in a *gap1* mutant, a lower concentration of NF can lead to a sufficiently high enough level of ROP signalling activation to change the growth axis. However, instead of a locally high concentration of NF activating a change in growth axis, the lower NF concentration may be present in many locations over the root surface so there would be cell expansion in multiple directions, effectively preventing root hair curling. By negatively regulating ROP signalling MtGAP1 may maintain a threshold for the realignment of polar growth during infection.

The subcellular localisation of the RopGAPs suggests that they may act to limit the area in which ROPs are active. ROP GTPases are associated with the apex of tip growing cells (Kost et al., 1999, Li et al., 1999, Molendijk et al., 2001), whereas in tobacco pollen tubes, NtRhoGAP1 (of the CRIB domain subfamily) localises to the plasma membrane at the flanks of the tip but not at the apex itself (Klahre and Kost, 2006). It maybe that during root hair curling and/or infection thread formation, MtGAP1 flanks the area of active ROP GTPases to maintain the zone of polarised cell expansion. However, REN1, an *A. thaliana* RopGAP belonging to the Pleckstrin-Homology domain subfamily is localised to the tip of pollen tubes where it appears to function as a global inhibitor of ROP signalling (Hwang et al., 2008). The subcellular localisation of MtGAP1 during bacterial infection may provide some insights into its function.

During bacterial infection the axis of polar growth needs to change, but still must be tightly regulated to enable root hair curling and infection thread formation. It is therefore not surprising that a *RopGEF* gene is also upregulated during infection with a similar expression pattern to that of *MtGAP1*. It is possible that *MtGAP1* and *RopGEF14* are upregulated to mediate the shifts in polar growth axis during root hair curling and/or infection thread formation.

The involvement of *MtGAP1* in bacterial infection implicates members of the ROP GTPase family and two members have already been found to be involved in bacterial infection (Ke et al., 2012, Kiirika et al., 2012). However, in the root hair microarray data no ROP GTPases were upregulated during rhizobial infection in root hairs. This is puzzling because three ROPs (including MtROP6 and MtROP9) have been found to be upregulated in root hairs after inoculation with rhizobia using promoter:GUS fusions (Liu et al., 2010). Different controls were used in these experiments. The microarray experiments here used root hairs inoculated with *S. meliloti* SL44 *(nodΔD1ABC)*, which does not produce NF so cannot infect the plant; in contrast Liu et al. (2010) used uninoculated root hairs. Using *S. meliloti* SL44 *(nodΔD1ABC)* could induce plant genes due to the presence of other bacterial signals such as exopolysaccharides (Jones et

al., 2008), which are also required for bacterial infection, or conserved bacterial PAMPs, which can activate defence responses in the plant (Monaghan and Zipfel, 2012). Therefore, it seems that the ROPs are not upregulated in response to NF during bacterial infection but may instead be upregulated by other bacterial signals.

MtROP9 RNAi lines produce fewer nodules and lack a NF-induced ROS response (Kiirika et al., 2012). I was able to use the ROP9 RNAi construct made by Kiirika et al. (2012) to knock down *MtROP9* expression in wildtype YC3.6 expressing plants. There was a significant reduction in the percentage of cells that produced the NF-induced calcium influx, suggesting that *MtROP9* may be involved in generating this response and this warrants further investigation. In future it would be interesting to find out whether *MtROP6* is also involved in NF-induced calcium influx and whether *MtGAP1* can directly bind to either or both of these ROP GTPases. Interestingly, there was also a slight but significant reduction in the calcium spiking responses in the *MtROP9* RNAi lines, suggesting that *MtROP9* may also play a role in early nodulation signalling.

CHAPTER 7: GENERAL DISCUSSION

7.1 *MtGAP1*: a novel gene involved in bacterial infection

Infection of legumes by rhizobia through root hairs requires alterations in polar growth; root hair curling is necessary to entrap the rhizobia within infection pockets and the formation of infection threads to guide the rhizobia to the developing nodule (Figure 1.1). Polar growth of root hairs and pollen tubes is regulated by ROP GTPases and recently two legume ROP GTPases with roles in bacterial infection have been identified (Ke et al., 2012, Kiirika et al., 2012). In this thesis I found MtGAP1, a member of the family of ROP-GTPase-Activating Proteins (RopGAPs), is involved in rhizobial infection (Chapter 6).

MtGAP1 has a different role in bacterial infection than previously identified genes such as *NIN, ERN1* and *LYK3.* Compared to wildtype, *gap1* mutants form fewer infection threads and many of these appear to form from root hairs that have not properly curled. This is different to the excessive root hair curling found in *nin* and *lyk3 (hcl)* mutants (Borisov et al., 2003, Catoira et al., 2001, Marsh et al., 2007). The infection threads that do form in *gap1* mutants are able to progress into the cortex and infect developing nodules so that mature (pink) nodules form on the mutants on a similar timescale to the wildtype. This suggests that the *MtGAP1* is involved in the early stages of infection in root hair curling and the initiation of infection threads. However *MtGAP1* may be less important for infection thread progression and is not required for nodule formation and function. This is different from *NIN*, *ERN1* and *LYK3*, which are all required for bacterial infection but are also required for development of mature nodules (Borisov et al., 2003, Catoira et al., 2001, Marsh et al., 2007).

7.2 The NF-induced calcium influx and ROS transient could belong to a common signalling pathway in bacterial infection

The RopGAPs assist the intrinsic GTPase activity of the ROPs to hydrolyse GTP to GDP (Kost, 2008). ROP GTPases can activate a number of downstream responses including Ca^{2+} influxes, ROS production, F-actin assembly, and polar exocytosis (Craddock et al., 2012). In growing root hairs and pollen tubes ROPs regulate the tip-focused NADPH oxidase-dependent ROS and Ca^{2+} gradients that are required for polar growth (Figure 1.5) (Carol et al., 2005, Foreman et al.,

2003, Herrmann and Felle, 1995, Jones et al., 1995, Jones et al., 2007). The Ca^{2+} influxes and ROS production are both dependent on each other and linked by positive feedback (Asai et al., 2013, Dubiella et al., 2013, Foreman et al., 2003, Keller et al., 1998, Kobayashi et al., 2007, Sagi and Fluhr, 2001, Takeda et al., 2008). During nodulation, NFs induce a calcium influx and ROS transient at the tip of root hair cells (Cárdenas et al., 2008, Felle et al., 1998, Miwa et al., 2006a, Shaw and Long, 2003a, Walker et al., 2000) and I investigated whether it is possible that these responses could be generated using similar mechanisms to the developmental tip Ca^{2+} and ROS gradients.

There is evidence to suggest that the NF-induced calcium influx and ROS transient may lie in a common pathway. The responses are temporally co-incident and are activated by similar concentrations of NF (Figure 7.1) (Chapter 3 and 5) (Cárdenas et al., 2008, Miwa et al., 2006a, Morieri et al., 2013, Shaw and Long, 2003a). They both depend on the NF receptor *NFP* but are independent of the Sym pathway components *DMI1* and *DMI2* (Chapter 5) (Ben Amor et al., 2003, Miwa et al., 2006a). Furthermore, both responses are inhibited by the NADPH oxidase inhibitor DPI (Chapter 4) (Cárdenas et al., 2008). This suggests that, like the Ca^{2+} and ROS gradients in polar root hair growth, the NF-induced calcium influx and ROS transient are both dependent on NADPH oxidases. The calcium influx has been implicated in bacterial infection (Morieri et al., 2013) and as two ROPs and a NADPH oxidase have recently been found to be involved in bacterial infection (Ke et al., 2012, Kiirika et al., 2012, Montiel et al., 2012), it seems possible that NF-activation of ROP signalling may be responsible for the activation of the calcium influx and ROS transient. This hypothesis is supported by the observations in this thesis that *gap1* mutants appeared to be hypersensitive for the NF-induced calcium influx, and that there was a reduction in calcium influx responses in *ROP9* RNAi knockdown lines (Chapter 6).
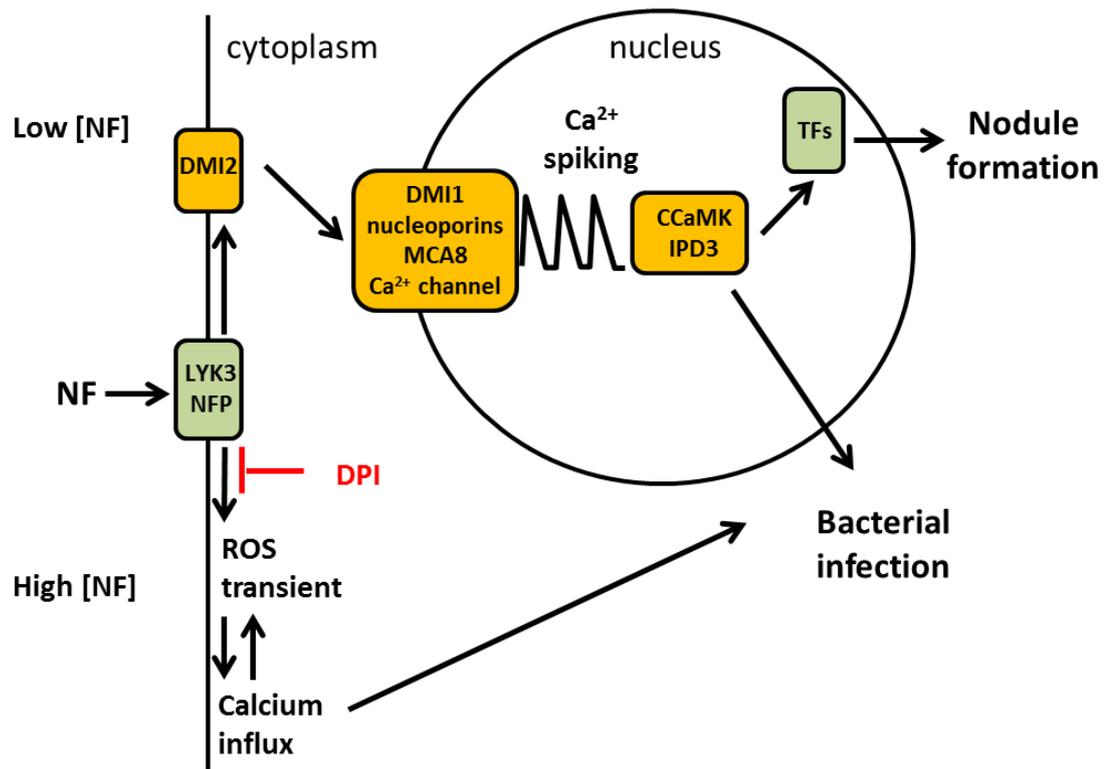
Figure 7.1 NF-induced calcium and ROS signalling

NF is perceived at the plant cell surface by the NF receptors NFP and LYK3. Low concentrations of NF are sufficient to activate the Sym pathway (yellow), leading to the production of nuclear-localised calcium spiking and the activation of CCaMK and IPD3, leading to changes in gene expression required for nodule formation and bacterial infection. At higher NF concentrations, a parallel signalling pathway downstream of the NF receptor NFP but independent of calcium spiking is proposed. Its activation leads to ROS transient production and a calcium influx at the tip of root hair cells. Both the ROS transient and calcium are inhibited by the NADPH oxidase inhibitor DPI.

From the findings of this thesis it is possible to up-date the model of calcium influx activation proposed in Chapter 1 (Figure 1.6). In the model, NF perception leads to the activation of ROP GTPases by direct binding to NF receptors (Figure 7.2). The ROPs, which are regulated by MtGAP1 and MtRopGEF14, activate the NF-induced ROS transient and calcium influx, root hair curling and infection thread formation. However, this model is over-simplistic because it does not take into account the various stages of bacterial infection where different polar growth processes take place.
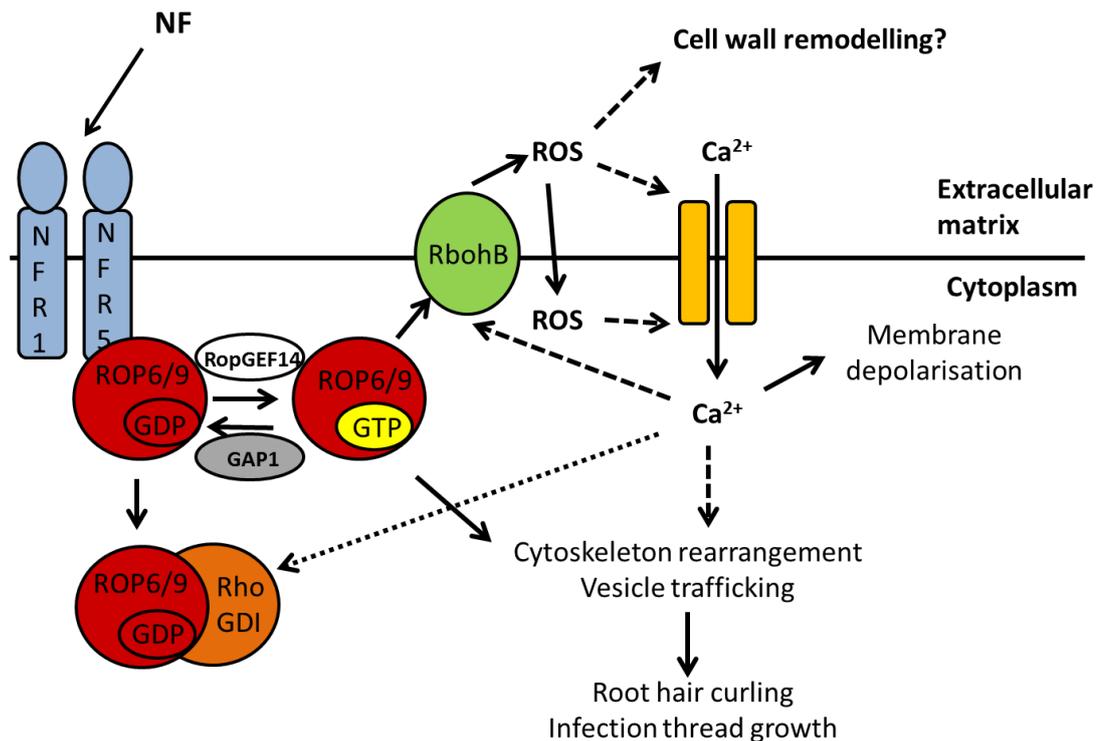
Figure 7.2: ROP signalling during bacterial infection

ROP6/ROP9 signalling is activated by NF binding to NF receptors. ROP6/ROP9 activate RBOHB, producing a ROS transient. This promotes cell wall remodelling and the activation of a calcium influx. ROS as H_2O_2 can enter the cell through plasma membrane aquaporins. Ca^{2+} and ROP GTPases regulate cytoskeletal rearrangement and vesicle trafficking to generate root-hair curling around attached rhizobia and to regulate infection thread formation. There may also be crosstalk with the Sym pathway via ROP6 induction of *NIN* and *ENOD40* gene expression. Cycling of ROP GTPases between GDP- and GTP- bound states by RopGEF14 and GAP1 and sequestering in the cytoplasm by Ca^{2+}-regulated RhoGDIs ensure ROP activity can be appropriately localised to drive new membrane formation in the appropriate location and direction.

7.3 ROP signalling during root hair curling

To generate a root hair curl around the attached rhizobia, the axis of root hair polar growth needs to shift from its position at the tip of the root hair cell during normal development. Before root hair curling begins root hair elongation stops and the tip swells (Sieberer et al., 2005), suggesting that the axis of polar growth is eliminated, leading to some isotropic cell expansion (swelling) before polar growth is re-established in a new position. Spot inoculation of NF is sufficient to generate root hair curling (Esseling et al., 2003) and LjROP6 can interact directly with the NF receptor NFR5 (Ke et al., 2012), suggesting that localised activation of NF signalling may shift the zone of active ROPs from their normal location at the tips of growing root hair cells (Kost, 2008) towards the site of NF perception (Figure 7.3). In their new position the ROPs would continue to regulate the actin cytoskeleton and vesicle trafficking to drive cell expansion as they do during normal root hair growth (Kost, 2008). To shift and maintain the small zone of active ROPs required for polar growth, RopGEFs and RopGAPs would also need to be present to regulate ROP activity. *MtGAP1* was upregulated during bacterial infection and *gap1* mutants lacked normal root hair curling (Chapter 6). *MtRopGEF14* was also upregulated during bacterial infection and therefore may also be involved in root hair curling alongside *MtGAP1*.

Does NF activate a unique set of ROP signalling machinery to normal root hair growth or does it utilise the same components? The phenotype of *the gap1* mutants suggests that there could be convergence early on. Alongside the defect in rhizobial infection the *gap1* mutants had longer root hairs than wildtype (Chapter 6), so MtGAP1 also appears to be involved in developmental root hair growth and may simply shift its location during root hair curling. Could this also be the case for MtRopGEF14? Further investigation of *MtRopGEF14* and *MtROPGEF2*, which regulates normal root hair elongation but is not upregulated during rhizobial infection (Riely et al., 2011), would be an interesting area for future study.

In pollen tube growth there appears to be two distinct roles for RopGAPs. The CRIB-domain containing RhoGAP1 is localised to the flanks of the tip but not the tip itself and this is thought to limit the zone of active ROPs to tip (Klahre and Kost, 2006). However, the Pleckstrin Homology (PH)-domain containing GAP, REN1, is localised to the tip of the cell and in this location acts as a global inhibitor of ROPs (Hwang et al., 2008). Following this example it is possible that there are other RopGAPs with different roles in root hair curling.
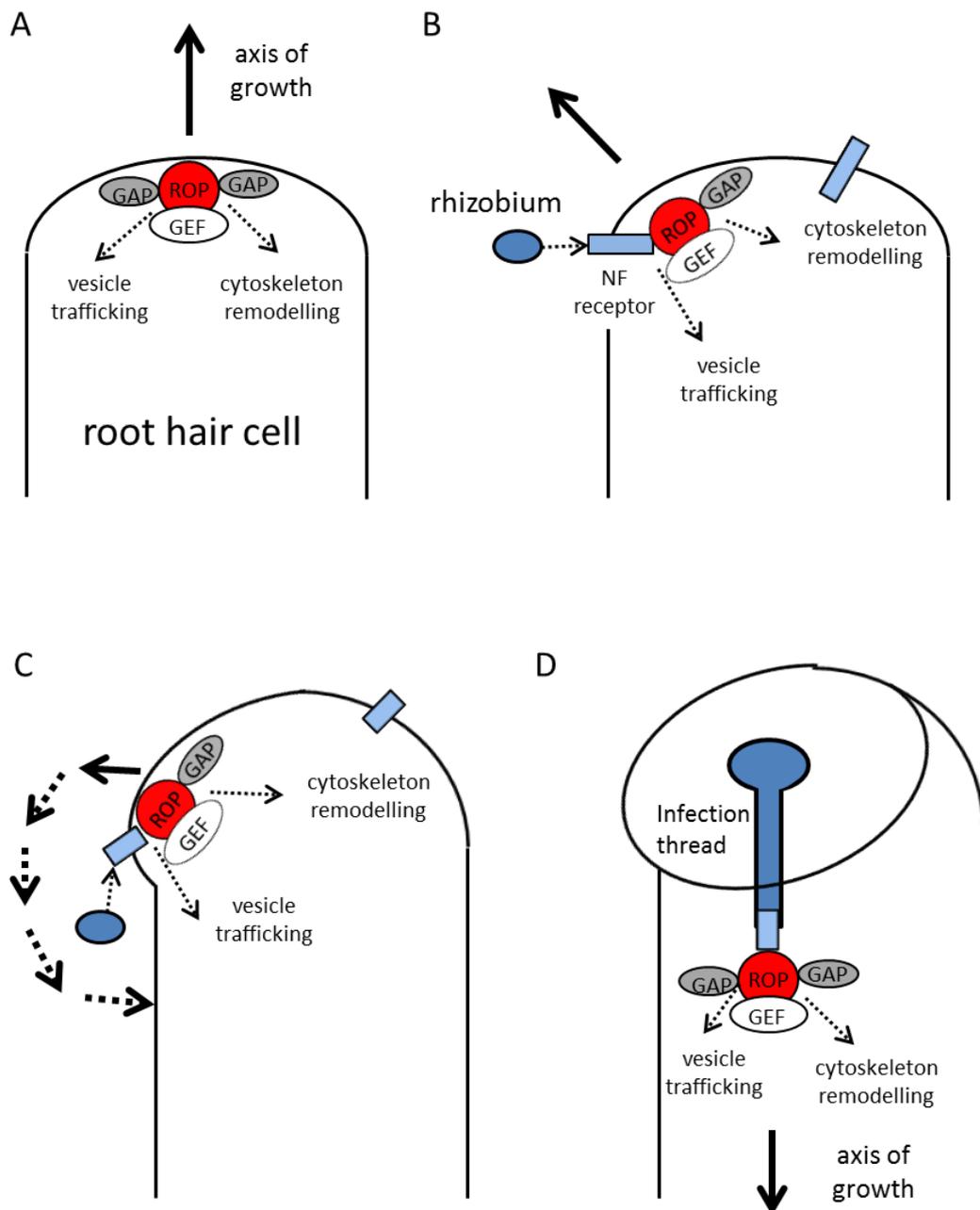
Figure 7.3: Model of polar growth during root hair curling and infection thread formation.

[A] A growing root hair cell has a region of active ROP GTPases and their regulators (RopGEFs and RopGAPs, including GAP1) at the tip of the cell driving cell expansion by regulating vesicle trafficking and the cytoskeleton. **[B]** NF perception: when rhizobia are nearby, NF perception in a localised region of the cell shifts the location of ROP6/9, RopGEF14 and GAP1 towards the site of NF perception, shifting the axis of cell expansion. **[C]** Root hair curling: NF-promoted cell expansion in root hairs continues to entrap the rhizobia in an infection pocket (infection focus). **[D]** Infection thread formation: The NF concentration in the infection focus rises until it reaches a threshold that activates the ROS transient and calcium influx. This leads to a switch in ROP GTPase signalling from cell expansion to promote cell ingrowth, which produces an infection thread.

Which ROPs are involved in root hair curling? Three *ROPs* are upregulated in root hairs during rhizobial infection including *ROP6* and *ROP9* (Ke et al., 2012, Liu et al., 2010), although this upregulation appears to be independent of NFs (Chapter 6). RNAi knockdowns of *ROP6* and *ROP9* both resulted in the formation of fewer nodules but the bacterial infection phenotypes reported appear to be subtly different (Ke et al., 2012, Kiirika et al., 2012). *Lotus japonicus ROP6* RNAi lines had large numbers of infection threads in the epidermis but few in the cortex (Ke et al., 2012), suggesting that there is a defect in infection thread progression from the epidermis into the cortex. *M. truncatula ROP9* RNAi lines were delayed for bacterial infection and root hair development appeared to be abnormal with basal and/or tip swelling (Kiirika et al., 2012). Also, the *ROP9* RNAi lines were impaired for root growth. On the basis of these results, it appears that ROP9 is a better candidate for a ROP GTPase involved in normal root hair growth and is recruited for root hair curling during rhizobial infection. However, it is also possible that ROP6 may be involved in root hair curling instead of, or alongside ROP9. Identification and characterisation of stable mutants for these genes would be very useful in determining their roles in bacterial infection.

7.4 ROP signalling during infection thread formation

Infection thread formation requires a different kind of polar growth from root hair elongation. During root hair elongation ROP GTPases accumulate at the tip to drive deposition of new membrane and cell wall outwards, but during infection thread formation new membrane and cell wall are deposited to produce an ingrowth (Figure 7.3D).

Infection thread formation has similarities with the formation of ingrowths in leaf pavement cells. Leaf pavement cells fit together like a jigsaw due to the formation of outgrowths (lobes) and ingrowths (indentations). In *A. thaliana*, two ROP GTPases, ROP2 and ROP6 act antagonistically to promote the formation of outgrowths and ingrowths (Fu et al., 2005). AtROP2 promotes outgrowth formation via interaction with RIC4, which mediates changes in the actin cytoskeleton. AtROP6 promotes the formation of ingrowths by interacting with RIC1, which promotes microtubule rearrangement (Fu et al., 2005). Infection thread formation could be similar to formation of pavement cell lobes, but with the result of a tube instead of a leaf indentation. Interestingly, the closest *Lotus japonicus* homologue of *AtROP6* is *LjROP6* (Ke et al., 2012), so it is possible that during bacterial infection LjROP6 mediates ingrowth of the membrane to generate infection threads (Figure 7.3D).

If ROP6 does indeed mediate cell ingrowth during infection thread formation in a similar way to leaf indentation in *A. thaliana,* it seems unlikely that it also mediates cell expansion during root hair curling, supporting the idea that other ROPs (*e.g.* ROP9) could be involved in root hair curling with LjROP6 recruited later. However, it is also possible that the same ROPs are involved throughout bacterial infection but they are differentially regulated or modified during root hair curling and infection thread formation so that they interact with different ROP effectors (RICs, RIPs etc.) for cell expansion or ingrowth, respectively. ROP effectors include SCAR/WAVE components, which regulate actin polymerization (Hussey et al., 2006). AtPIR121 interacts with AtROP2 (Basu et al., 2004) and AtSCAR2 interacts specifically with the active form of AtROP7 (Uhrig et al., 2007). The legume SCAR/WAVE mutants *rit1-1, nap1* and *pir1* all have short root hairs and trichomes and after inoculation with rhizobia develop swollen infection threads that abort in root hairs (Miyahara et al., 2010, Yokota et al., 2009). It is possible that during bacterial infection ROP6/ROP9 interact directly with MtRIT1/LjNAP1 to regulate actin polymerisation.

The flotillins FLOT2 and FLOT4 and the remorin SymREM1 are required for bacterial infection (Haney and Long, 2010, Lefebvre et al., 2010) and may interact with ROP GTPases. Flotillins are associated with lipid rafts and are required for the activation of the Rho-GTPases Rac1 and cdc42 in animal cells (Langhorst et al., 2008). SymREM1 can interact with the NF receptors NFP and LYK3 (Lefebvre et al., 2010). Since LjROP6 interacts with NFR5 (homologous to NFP) (Ke et al., 2012), it is possible that ROP6 and SymREM1 may belong to the same complex during bacterial infection.

Like root hair curling, the zone of active ROPs during infection thread formation would be expected to be regulated by the activities of RopGAPs and RopGEFs. The root hair microarray data suggests that *MtGAP1* and *MtRopGEF14*, which were the only members up-regulated during bacterial infection, are the most likely candidates (Chapter 6). However, it is possible that other RopGAPs and RopGEFs are involved. If MtGAP1 and MtRopGEF14 are involved in both root hair curling and infection thread formation they may need to be able to bind multiple ROP GTPases. *A. thaliana* RopGAP2 binds with higher affinity to AtROP1, ROP7 and ROP9 than ROP2, ROP3 and ROP4 (Schaefer et al., 2011a). Likewise, MtRopGEF2 binds preferentially to MtROP5, ROP6, ROP9 and ROP11 (Riely et al., 2011), suggesting that although there is some specificity, it is possible for individual RopGAPs and RopGEFs to have high affinity binding with several ROPs.

7.5 The role of the NF-induced calcium influx and ROS transient in bacterial infection

Although there are several similarities between the NF-induced calcium influx and ROS transient compared with developmental tip Ca^{2+} and ROS gradients in root hairs, there is one crucial difference. The NF-induced calcium influx and ROS transient responses appear to be transient events in root hair cells, whereas the tip Ca^{2+} and ROS gradients are maintained throughout polar growth (Foreman et al., 2003, Herrmann and Felle, 1995, Jones et al., 1995, Monshausen et al., 2007, Monshausen et al., 2008). Therefore, it is more likely that, instead of being involved directly in promoting membrane and cell wall deposition during infection, the NF-induced calcium influx and ROS transient may have a signalling or co-ordinating role at a specific stage of bacterial infection.

Both the calcium influx and ROS transient require higher concentrations of NFs to be activated than other NF-responses including nuclear calcium spiking and root hair deformation (Chapter 5) (Catoira et al., 2000, Miwa et al., 2006a, Morieri et al., 2013, Shaw and Long, 2003a). This suggests the calcium influx and ROS transient are activated later than other NF-responses once a threshold concentration of NF has been reached. A NF lacking the *NodL*-determined acetyl group, equivalent to that made by the *S. meliloti nodL* mutant is 100 fold less active at inducing the calcium influx than wildtype NF (Morieri et al., 2013). *S. meliloti nodL* mutants are delayed for infection into legumes, forming enlarged infection foci but few infection threads (Ardourel et al., 1994), suggesting that the calcium influx may be required for infection thread initiation.

The NF-induced calcium influx and ROS transient could act as signals for the transition from root hair curling to infection thread growth (Figure 7.3). During root hair curling the local NF concentration on the plant cell surface closest to the rhizobia would gradually increase as the rhizobia become trapped within the infection foci and continue to divide. The increasing concentration of NF could lead to increasing levels of ROP9 and/or ROP6 signalling. Presumably, at some point NF may reach a threshold level required for activation of the calcium influx and ROS transient, which could lead to the recruitment of the machinery required for infection thread initiation and growth. The *gap1* mutants appeared to be hypersensitive for induction of the calcium influx and infection threads formed in root hairs that had not properly curled to form enclosed infection pockets (Chapter 6). This suggests that negative regulation of ROP signalling by MtGAP1 may help to ensure that the calcium influx is

only activated after root hair curling when the population of rhizobia trapped with the infection pocket is sufficiently large to support infection thread development.

In *A. thaliana* leaf pavement cells, a calcium-dependent protein kinase CPK3 phosphorylates RhoGDI1, promoting its binding to ROP GTPases (Wu et al., 2013). RhoGDIs bind to GDP-bound ROPs and sequester them in the cytosol. In growing root hair cells RhoGDI1 is required for the correct localisation of ROP2 (Carol et al., 2005), demonstrating that RhoGDIs can regulate the subcellular location of ROPs. In *M. truncatula,* the calcium-dependent protein kinase CDPK1 is involved in normal root and root hair development and is also required for efficient rhizobial and mycorrhizal colonisation (Ivashuta et al., 2005). *CDPK1* RNAi roots had short abnormal-looking root hairs (swollen tips, growth redirection and branching), which lacked the tip ROS gradient observed in wildtype and had an altered actin cytoskeleton (Ivashuta et al., 2005). When inoculated with *S. meliloti* infection threads on *CDPK1 RNAi* roots were defective for progression into the cortex and few nodules were formed.   It is possible that during bacterial infection the calcium influx could lead to CPK-dependent phosphorylation of RhoGDIs leading to the removal of ROPs from the curling root hair tip and the accumulation of ROPs at the site of infection thread initiation.

If root hair curling uses the same mechanisms as normal polar growth, then localised gradients of Ca^{2+} and ROS should be present, but instead of being tip-focused these gradients would be shifted to the new growth axis. It would be technically challenging to observe Ca^{2+} and ROS dynamics during bacterial infection of root hair cells but recent studies examining nuclear calcium spiking during bacterial infection (Sieberer et al., 2012) suggest that it might be possible.

7.5 Hormones and bacterial infection

The plant hormones ethylene and auxin both promote normal root hair elongation (Muday et al., 2012, Pitts et al., 1998, Strader et al., 2010, Tanimoto et al., 1995). It is thought that ethylene promotes root hair elongation by modulating auxin signalling (Muday et al., 2012). Auxin can activate ROP signalling (Lin et al., 2012, Tao et al., 2002, Xu et al., 2010) with feedback via ROP regulation of auxin transporters (Chen et al., 2012b). What roles do these hormones play in bacterial infection?

Auxin promotes nodule formation (de Billy et al., 2001, Takanashi et al., 2011), but its role in bacterial infection has been little studied. In the symbiosis between *Casuarina glauca* and the Nitrogen-fixing actinomycete *Frankia*, expression of the *AUX1* auxin-influx transporter is associated with infected plant cells (Peret et al., 2007), so it is possible that auxin may promote bacterial infection during the legume-rhizobia symbiosis. Ethylene is an inhibitor of bacterial infection and nodule formation and *skl* (orthologue of *A. thaliana EIN2*) mutants produce many more infection threads and nodules than the wildtype (Oldroyd et al., 2001b, Penmetsa et al., 2008). Ethylene inhibits both NF-induced calcium spiking and the calcium influx (Morieri et al., 2013, Oldroyd et al., 2001b), suggesting that ethylene inhibition of nodulation and bacterial infection is mediated via inhibition of NF-signalling. NF promotion of root hair elongation is independent of ethylene (Oldroyd et al., 2001b), suggesting NF uses a parallel pathway to activate ROP signalling, which may or may not involve auxin.

7.6 Is there crosstalk between ROP signalling and the common symbiosis (Sym) pathway?

To establish a successful symbiosis, nodule formation and bacterial infection need to be co-ordinated. Much of this co-ordination is achieved by the Sym pathway, which upregulates many genes involved in nodule formation and/or bacterial infection (Oldroyd et al., 2011). This includes the transcription factors *NIN* and *ERN1*, which are required for both processes (Marsh et al., 2007, Middleton et al., 2007). Both *MtGAP1* and *MtRopGEF14* were downregulated root hairs of the *nin* mutant relative to wildtype (Chapter 6) suggesting they may be regulated directly or indirectly by NIN. Therefore, the Sym pathway may modulate ROP signalling to promote root hair curling and infection thread formation.

It appears that the Sym pathway may be differentially activated during bacterial infection. Genre et al. (2012) found that the frequency of nuclear calcium spiking in individual cells changes during bacterial infection. Outer cortical cells have low frequency calcium spiking prior to contact with bacteria. This then switches to a higher frequency when the infection thread containing the bacteria reaches the cell and continues to grow through it. This suggests that high frequency calcium spiking may be associated with the progression of infection threads. It is possible that this shift in frequency of calcium spiking leads to the altered regulation of ROP signalling to promote infection thread progression through the cortical cell.

ROP signalling may also be able to modulate the Sym pathway. *Lotus japonicus ROP6* RNAi lines had decreased *NIN* and *ENOD11* expression (Ke et al., 2012). This could be a consequence of the lines having reduced bacterial infection and nodule formation rather than ROP6 regulation of the Sym pathway. However, in this work I found that *ROP9* RNAi lines had a small, but statistically significant reduction in NF-induced calcium spiking alongside the much larger reduction in the calcium influx (Chapter 6). This suggests that alongside a role in bacterial infection *ROP9* could be involved in feedback regulation of calcium spiking. Therefore it is possible that ROP signalling may provide the Sym pathway with feedback regarding the progress of bacterial infection.

7.7 Conclusions and future work

NF can induce two separate calcium responses in legume root hairs. Nuclear calcium spiking is central to the Sym pathway, which is required for the activation of genes required for nodule formation and bacterial infection. The tip-focused calcium influx is less-well studied but it has been proposed to be involved in infection thread initiation during bacterial infection (Morieri et al., 2013). NF also induces a ROS transient in the tip of root hair cells. In this thesis I studied the NF-induced calcium influx and ROS transient responses in *M. truncatula*. I found that, along with being spatially and temporally co-incident (Chapter 3), the responses require similar concentrations of NF to be activated (Chapter 5), are both inhibited by the NADPH oxidase inhibitor DPI (Chapter 4) and are both dependent on the NF receptor NFP but independent of the Sym pathway components DMI1 and DMI2. These shared characteristics suggest that the NF-induced calcium influx and ROS transient are part of a common signalling pathway during bacterial infection.

I found a ROP-activating protein *MtGAP1* is upregulated in root hairs during bacterial infection and is involved in normal root hair curling and infection thread development (Chapter 6). Two pieces of evidence directly link ROP signalling with the NF-induced calcium influx: *gap1* mutants were hypersensitive for induction of the calcium influx, and there was a reduction in the number of calcium influx responses in *ROP9* RNAi knockdown lines (Chapter 6). Drawing parallels between developmental root hair elongation and bacterial infection, I propose that local perception of NF on the root hair surface shifts the intracellular localisation of ROPs and their regulators to change the axis of cell expansion for root hair curling. Once the rhizobia are entrapped within an infection focus, the rising NF concentration triggers the ROS transient and

calcium influx, which signal for the recruitment of ROPs to the site of infection thread initiation.

There are several experiments that are already planned for the continuation of this project. Complementation of *gap1* mutants with MtGAP1 will confirm whether the observed phenotypes are due to mutations in *MtGAP1* instead of other background mutations present in the *Tnt1* insertions lines. This will be especially useful because although the infection thread phenotype is consistent between the two *gap1* alleles, only *gap1-1* has a reduction in nodule number. Calcium imaging using a *gap1-1*-YC3.6 stable line will be carried out to confirm the observed hypersensitivity for NF-induced calcium influx in *gap1-1* by constructing a dose response curve for this mutant over a range of NF concentrations. The *gap1-1* line will also be tested for the NF-induced ROS transient.

In the longer term there are many directions that further investigations could take. Acquiring stable mutant lines for *ROP6, ROP9, RopGEF14* and *RBOHB* would be a useful starting point for further studies on these genes as RNAi knockdown lines still retain some expression and the expression of other closely-related genes can also be affected. It is possible to construct dominant negative and constitutively active versions of ROP GTPases (Jones et al., 2002, Li et al., 1998, Li et al., 1999), which could also be used to provide insights into their roles in symbiosis. Apart from the NFR5-ROP6 interaction, all the other interactions between proteins proposed in Figure 7.2 are theoretical, based on ROP signalling in other systems. Finding out which ROPs can interact with which RopGAPs and RopGEFs would demonstrate whether the model is valid and could also potentially identify other candidates in these families worthy of investigation. RhoGDIs are another family of ROP regulators, so investigating this family in the context of rhizobial infection could also be informative.

It would also be interesting to identify the Ca^{2+}-permeable channels involved in generating the NF-induced calcium influx. Members of the annexin, CNGC (cyclic nucleotide gates channels) and GLR (glutamate-like receptors) families are implicated in mediating Ca^{2+} influxes in plants (Finka et al., 2012, Ma et al., 2010, Michard et al., 2011, Swarbreck et al., 2013, Wang et al., 2013). Of these, the annexins are the most promising candidates for mediating the ROS-induced Ca^{2+} influxes observed during polar root hair growth. Several plant annexins have been shown to mediate calcium influxes *in vitro* (Hofmann et al., 2000, Laohavisit et al., 2009, Laohavisit et al., 2010). *Arabidopsis thaliana ann1* mutants lack ROS-induced Ca^{2+} conductance required for root hair cell growth and ANN1 reconstitutes ROS-induced Ca^{2+} conductance in lipid bilayers (Laohavisit et al., 2012). Three *Medicago truncatula* annexins *MtAnn1*, *MtAnn2*

and *MtAnn3* are upregulated in roots during symbiosis (de Carvalho-Niebel et al., 2002, Gong et al., 2012, Niebel et al., 1998). It is possible that they or other annexin family members may mediate the NF-induced calcium influx.

Drawing on parallels with developmental root hair elongation, the results presented in this thesis provide a link between the NF-induced calcium influx and ROS transient responses and ROP signalling during rhizobial infection in legumes. Future investigations will provide further insights into rhizobial infection and may also prove useful for understanding ROP signalling in other contexts including polar growth of root hairs and defence signalling.

REFERENCES

Ane, J. M., Kiss, G. B., Riely, B. K., Penmetsa, R. V., Oldroyd, G. E. D., Ayax, C., Levy, J., Debelle, F., Baek, J. M., Kalo, P., Rosenberg, C., Roe, B. A., Long, S. R., Denarie, J. & Cook, D. R. (2004). *Medicago truncatula DMI1* required for bacterial and fungal symbioses in legumes. *Science,* **303,** 1364-1367.

Apel, K. & Hirt, H. (2004). Reactive oxygen species: metabolism, oxidative stress, and signal transduction. *Annual Review of Plant Biology,* **55,** 373-99.

Ardourel, M., Demont, N., Debelle, F. D., Maillet, F., Debilly, F., Prome, J. C., Denarie, J. & Truchet, G. (1994). *Rhizobium meliloti* lipooligosaccharide nodulation factors - different structural requirements for bacterial entry into target root hair-cells and induction of plant symbiotic developmental responses. *Plant Cell,* **6,** 1357-1374.

Asai, S., Ichikawa, T., Nomura, H., Kobayashi, M., Kamiyoshihara, Y., Mori, H., Kadota, Y., Zipfel, C., Jones, J. D. G. & Yoshioka, H. (2013). The variable domain of a plant calcium-dependent protein kinase (CDPK) confers subcellular localization and substrate recognition for NADPH Oxidase. *Journal of Biological Chemistry,* **288,** 14332-14340.

Basu, D., El-Assal, S. E. D., Le, J., Mallery, E. L. & Szymanski, D. B. (2004). Interchangeable functions of Arabidopsis PIROGI and the human WAVE complex subunit SRA1 during leaf epidermal development. *Development,* **131,** 4345-4355.

Belousov, V. V., Fradkov, A. F., Lukyanov, K. A., Staroverov, D. B., Shakhbazov, K. S., Terskikh, A. V. & Lukyanov, S. (2006). Genetically encoded fluorescent indicator for intracellular hydrogen peroxide. *Nature Methods,* **3,** 281-286.

Ben Amor, B., Shaw, S. L., Oldroyd, G. E. D., Maillet, F., Penmetsa, R. V., Cook, D., Long, S. R., Denarie, J. & Gough, C. (2003). The *NFP* locus of *Medicago truncatula* controls an early step of Nod factor signal transduction upstream of a rapid calcium flux and root hair deformation. *Plant Journal,* **34,** 495-506.

Benedito, V. A., Torres-Jerez, I., Murray, J. D., Andriankaja, A., Allen, S., Kakar, K., Wandrey, M., Verdier, J., Zuber, H., Ott, T., Moreau, S., Niebel, A., Frickey, T., Weiller, G., He, J., Dai, X. B., Zhao, P. X., Tang, Y. H. & Udvardi, M. K. (2008). A gene expression atlas of the model legume *Medicago truncatula*. *Plant Journal,* **55,** 504-513.

Berken, A. & Wittinghofer, A. (2008). Structure and function of Rho-type molecular switches in plants. *Plant Physiology and Biochemistry,* **46,** 380-93.

Bibikova, T. & Gilroy, S. (2002). Root hair development. *Journal of Plant Growth Regulation,* **21,** 383-415.

Bibikova, T. N., Jacob, T., Dahse, I. & Gilroy, S. (1998). Localized changes in apoplastic and cytoplasmic pH are associated with root hair development in *Arabidopsis thaliana*. *Development,* **125,** 2925-2934.

Bienert, G. P., Moller, A. L. B., Kristiansen, K. A., Schulz, A., Moller, I. M., Schjoerring, J. K. & Jahn, T. P. (2007). Specific aquaporins facilitate the diffusion of hydrogen peroxide across membranes. *Journal of Biological Chemistry,* **282,** 1183-1192.

Blanco, F. A., Meschini, E. P., Zanetti, M. E. & Aguilar, O. M. (2009). A small GTPase of the Rab family is required for root hair formation and preinfection stages of the common bean-*Rhizobium* symbiotic association. *Plant Cell,* **21,** 2797-810.

Borisov, A. Y., Madsen, L. H., Tsyganov, V. E., Umehara, Y., Voroshilova, V. A., Batagov, A. O., Sandal, N., Mortensen, A., Schauser, L., Ellis, N., Tikhonovich, I. A. &

Stougaard, J. (2003). The *sym35* gene required for root nodule development in pea is an ortholog of *nin* from *Lotus japonicus*. *Plant Physiology,* **131,** 1009-1017.

Bos, J. L., Rehmann, H. & Wittinghofer, A. (2007). GEFs and GAPs: Critical elements in the control of small G proteins. *Cell,* **129,** 865-877.

Burnstock, G. (2007). Purine and pyrimidine receptors. *Cellular and Molecular Life Sciences,* **64,** 1471-1483.

Capoen, W., Den Herder, J., Sun, J. H., Verplancke, C., De Keyser, A., De Rycke, R., Goormachtig, S., Oldroyd, G. & Holsters, M. (2009). Calcium spiking patterns and the role of the Calcium/Calmodulin-Dependent Kinase CCaMK in lateral root base nodulation of *Sesbania rostrata*. *Plant Cell,* **21,** 1526-1540.

Capoen, W., Sun, J., Wysham, D., Otegui, M. S., Venkateshwaran, M., Hirsch, S., Miwa, H., Downie, J. A., Morris, R. J., Ane, J. M. & Oldroyd, G. E. D. (2011). Nuclear membranes control symbiotic calcium signaling of legumes. *Proceedings of the National Academy of Sciences of the United States of America,* **108,** 14348-14353.

Cárdenas, L., Vidali, L., Domnguez, J., Prez, H., Sánchez, F., Hepler, P. K. & Quinto, C. (1998). Rearrangement of actin microfilaments in plant root hairs responding to *Rhizobium etli* nodulation signals. *Plant Physiology,* **116,** 871-877.

Cárdenas, L., Martinez, A., Sánchez, F. & Quinto, C. (2008). Fast, transient and specific intracellular ROS changes in living root hair cells responding to Nod factors (NFs). *Plant Journal,* **56,** 802-813.

Carol, R. J., Takeda, S., Linstead, P., Durrant, M. C., Kakesova, H., Derbyshire, P., Drea, S., Zarsky, V. & Dolan, L. (2005). A RhoGDP dissociation inhibitor spatially regulates growth in root hair cells. *Nature,* **438,** 1013-1016.

Catoira, R., Galera, C., de Billy, F., Penmetsa, R. V., Journet, E. P., Maillet, F., Rosenberg, C., Cook, D., Gough, C. & Denarie, J. (2000). Four genes of *Medicago truncatula* controlling components of a nod factor transduction pathway. *Plant Cell,* **12,** 1647-66.

Catoira, R., Timmers, A. C. J., Maillet, F., Galera, C., Penmetsa, R. V., Cook, D., Denarie, J. & Gough, C. (2001). The *HCL* gene of *Medicago truncatula* controls *Rhizobium*-induced root hair curling. *Development,* **128,** 1507-1518.

Charpentier, M., Bredemeier, R., Wanner, G., Takeda, N., Schleiff, E. & Parniske, M. (2008). *Lotus japonicus* CASTOR and POLLUX are ion channels essential for perinuclear calcium spiking in legume root endosymbiosis. *Plant Cell,* **20,** 3467-3479.

Charpentier, M., Vaz Martins, T., Granqvist, E., Oldroyd, G. & Morris, R. (2013). The role of DMI1 in establishing Ca^{2+} oscillations in legume symbioses. *Plant Signaling and Behavior,* **8**.

Charron, D., Pingret, J. L., Chabaud, M., Journet, E. P. & Barker, D. G. (2004). Pharmacological evidence that multiple phospholipid signaling pathways link rhizobium nodulation factor perception in *Medicago truncatula* root hairs to intracellular responses, including Ca^{2+} spiking and specific ENOD gene expression. *Plant Physiology,* **136,** 3582-3593.

Chen, T., Zhu, H., Ke, D., Cai, K., Wang, C., Gou, H., Hong, Z. & Zhang, Z. (2012a). A MAP kinase kinase interacts with SymRK and regulates nodule organogenesis in *Lotus japonicus*. *Plant Cell,* **24,** 823-38.

Chen, X., Naramoto, S., Robert, S., Tejos, R., Lofke, C., Lin, D. S., Yang, Z. B. & Friml, J. (2012b). ABP1 and ROP6 GTPase Signaling Regulate Clathrin-Mediated Endocytosis in Arabidopsis Roots. *Current Biology,* **22,** 1326-1332.

Chivasa, S., Ndimba, B. K., Simon, W. J., Lindsey, K. & Slabas, A. R. (2005). Extracellular ATP functions as an endogenous external metabolite regulating plant cell viability. *Plant Cell,* **17,** 3019-3034.

Chivasa, S., Tome, D. F., Murphy, A. M., Hamilton, J. M., Lindsey, K. & Carr, J. P. (2009). Extracellular ATP: a modulator of cell death and pathogen defense in plants. *Plant Signal Behav,* **4,** 1078-1080.

Choi, H. J., Kim, S. J., Mukhopadhyay, P., Cho, S., Woo, J. R., Storz, G. & Ryu, S. E. (2001). Structural basis of the redox switch in the OxyR transcription factor. *Cell,* **105,** 103-113.

Choi, J., Tanaka, K., Cao, Y. R., Qi, Y., Qiu, J., Liang, Y., Lee, S. Y. & Stacey, G. (2014). Identification of a Plant Receptor for Extracellular ATP. *Science,* **343,** 290-294.

Choi, W. G., Swanson, S. J. & Gilroy, S. (2012). High-resolution imaging of Ca^{2+}, redox status, ROS and pH using GFP biosensors. *Plant Journal,* **70,** 118-128.

Clark, G., Wu, M., Wat, N., Onyirimba, J., Pham, T., Herz, N., Ogoti, J., Gomez, D., Canales, A. A., Aranda, G., Blizard, M., Nyberg, T., Terry, A., Torres, J., Wu, J. A. & Roux, S. J. (2010). Both the stimulation and inhibition of root hair growth induced by extracellular nucleotides in Arabidopsis are mediated by nitric oxide and reactive oxygen species. *Plant Molecular Biology,* **74,** 423-435.

Cook, D., Dreyer, D., Bonnet, D., Howell, M., Nony, E. & Vandenbosch, K. (1995). Transient induction of a peroxidase gene in *Medicago truncatula* precedes infection by *Rhizobium melliloti*. *Plant Cell,* **7,** 43-55.

Cosgrove, D. J. (1999). Enzymes and other agents that enhance cell wall extensibility. *Annual Review of Plant Physiology and Plant Molecular Biology,* **50,** 391-417.

Costa, A., Drago, I., Behera, S., Zottini, M., Pizzo, P., Schroeder, J. I., Pozzan, T. & Lo Schiavo, F. (2010). H_2O_2 in plant peroxisomes: an *in vivo* analysis uncovers a Ca^{2+}-dependent scavenging system. *Plant Journal,* **62,** 760-772.

Craddock, C., Lavagi, I. & Yang, Z. (2012). New insights into Rho signaling from plant ROP/Rac GTPases. *Trends in Cell Biology,* **22,** 492-501.

Czaja, L. F., Hogekamp, C., Lamm, P., Maillet, F., Martinez, E. A., Samain, E., Denarie, J., Kuster, H. & Hohnjec, N. (2012). Transcriptional responses toward diffusible signals from symbiotic microbes reveal MtNFP- and MtDMI3-dependent reprogramming of host gene expression by arbuscular mycorrhizal fungal lipochitooligosaccharides. *Plant Physiology,* **159,** 1671-1685.

de Billy, F., Grosjean, C., May, S., Bennett, M. & Cullimore, J. V. (2001). Expression studies on AUX1-like genes in *Medicago truncatula* suggest that auxin is required at two steps in early nodule development. *Molecular Plant-Microbe Interactions,* **14,** 267-277.

de Carvalho-Niebel, F., Timmers, A. C. J., Chabaud, M., Defaux-Petras, A. & Barker, D. G. (2002). The Nod factor-elicited annexin MtAnn1 is preferentially localised at the nuclear periphery in symbiotically activated root tissues of *Medicago truncatula*. *Plant Journal,* **32,** 343-352.

De Koninck, P. & Schulman, H. (1998). Sensitivity of CaM kinase II to the frequency of Ca^{2+} oscillations. *Science,* **279,** 227-230.

Demidchik, V., Nichols, C., Oliynyk, M., Dark, A., Glover, B. J. & Davies, J. M. (2003). Is ATP a signaling agent in plants? *Plant Physiology,* **133,** 456-461.

Demidchik, V., Shang, Z. L., Shin, R., Thompson, E., Rubio, L., Laohavisit, A., Mortimer, J. C., Chivasa, S., Slabas, A. R., Glover, B. J., Schachtman, D. P., Shabala, S.

N. & Davies, J. M. (2009). Plant extracellular ATP signalling by plasma membrane NADPH oxidase and Ca^{2+} channels. *Plant Journal,* **58,** 903-913.

Demidchik, V., Shang, Z. L., Shin, R., Colaco, R., Laohavisit, A., Shabala, S. & Davies, J. M. (2011). Receptor-like activity evoked by extracellular ADP in Arabidopsis root epidermal plasma membrane. *Plant Physiology,* **156,** 1375-1385.

den Hartog, M., Musgrave, A. & Munnik, T. (2001). Nod factor-induced phosphatidic acid and diacylglycerol pyrophosphate formation: a role for phospholipase C and D in root hair deformation. *Plant Journal,* **25,** 55-65.

den Hartog, M., Verhoef, N. & Munnik, T. (2003). Nod factor and elicitors activate different phospholipid signaling pathways in suspension-cultured alfalfa cells. *Plant Physiology,* **132,** 311-317.

Denarie, J., Debelle, F. & Prome, J. C. (1996). *Rhizobium* lipo-chitooligosaccharide nodulation factors: signaling molecules mediating recognition and morphogenesis. *Annual Review of Biochemistry,* **65,** 503-535.

Dereeper, A., Guignon, V., Blanc, G., Audic, S., Buffet, S., Chevenet, F., Dufayard, J. F., Guindon, S., Lefort, V., Lescot, M., Claverie, J. M. & Gascuel, O. (2008). Phylogeny.fr: robust phylogenetic analysis for the non-specialist. *Nucleic Acids Research,* **36,** W465-W469.

Dereeper, A., Audic, S., Claverie, J. M. & Blanc, G. (2010). BLAST-EXPLORER helps you building datasets for phylogenetic analysis. *Bmc Evolutionary Biology,* **10**.

Dodd, A. N., Kudla, J. & Sanders, D. 2010. The language of calcium signaling. *In:* Merchant, S., Briggs, W. R. & Ort, D. (eds.) *Annual Review of Plant Biology, Vol 61.* Palo Alto: Annual Reviews.

Dooley, C. T., Dore, T. M., Hanson, G. T., Jackson, W. C., Remington, S. J. & Tsien, R. Y. (2004). Imaging dynamic redox changes in mammalian cells with green fluorescent protein indicators. *Journal of Biological Chemistry,* **279,** 22284-22293.

Duan, Q. H., Kita, D., Li, C., Cheung, A. Y. & Wu, H. M. (2010). FERONIA receptor-like kinase regulates RHO GTPase signaling of root hair development. *Proceedings of the National Academy of Sciences of the United States of America,* **107,** 17821-17826.

Dubiella, U., Seybold, H., Durian, G., Komander, E., Lassig, R., Witte, C. P., Schulze, W. X. & Romeis, T. (2013). Calcium-dependent protein kinase/NADPH oxidase activation circuit is required for rapid defense signal propagation. *Proceedings of the National Academy of Sciences of the United States of America,* **110,** 8744-8749.

Dynowski, M., Schaaf, G., Loque, D., Moran, O. & Ludewig, U. (2008). Plant plasma membrane water channels conduct the signalling molecule H2O2. *Biochem J,* **414,** 53-61.

Edwards, A., Heckmann, A. B., Yousafzai, F., Duc, G. & Downie, J. A. (2007). Structural implications of mutations in the pea *SYM8* symbiosis gene, the *DMI1* ortholog, encoding a predicted ion channel. *Molecular Plant-Microbe Interactions,* **20,** 1183-1191.

Ehrhardt, D. W., Atkinson, E. M. & Long, S. R. (1992). Depolarization of alfalfa root hair membrane potential by *Rhizobium meliloti* Nod factors. *Science,* **256,** 998-1000.

Ehrhardt, D. W., Wais, R. & Long, S. R. (1996). Calcium spiking in plant root hairs responding to *Rhizobium* nodulation signals. *Cell,* **85,** 673-681.

Endre, G., Kereszt, A., Kevei, Z., Mihacea, S., Kalo, P. & Kiss, G. B. (2002). A receptor kinase gene regulating symbiotic nodule development. *Nature,* **417,** 962-966.

Engstrom, E. M., Ehrhardt, D. W., Mitra, R. M. & Long, S. R. (2002). Pharmacological analysis of nod factor-induced calcium spiking in *Medicago truncatula*. Evidence for the requirement of type IIA calcium pumps and phosphoinositide signaling. *Plant Physiology,* **128,** 1390-1401.

Esseling, J. J., Lhuissier, F. G. P. & Emons, A. M. C. (2003). Nod factor-induced root hair curling: continuous polar growth towards the point of nod factor application. *Plant Physiology,* **132,** 1982-1988.

Etzler, M. E., Kalsi, G., Ewing, N. N., Roberts, N. J., Day, R. B. & Murphy, J. B. (1999). A Nod factor binding lectin with apyrase activity from legume roots. *Proceedings of the National Academy of Sciences of the United States of America,* **96,** 5856-5861.

Etzler, M. E., Roberts, N. J., Wu, B., Kalsi, G., Hoye, E. & Murphy, J. B. (2000). LNP: A Nod factor-binding protein from legume roots is involved in the initiation of the rhizobium-legume symbiosis. *Glycobiology,* **10,** 1077-1077.

Fahraeus, G. (1957). The infection of clover root hairs by nodule bacteria studied by a simple glass slide technique. *J Gen Microbiol,* **16,** 374-81.

Feijo, J. A., Sainhas, J., Holdaway-Clarke, T., Cordeiro, M. S., Kunkel, J. G. & Hepler, P. K. (2001). Cellular oscillations and the regulation of growth: the pollen tube paradigm. *Bioessays,* **23,** 86-94.

Felle, H. H., Kondorosi, E., Kondorosi, A. & Schultze, M. (1996). Rapid alkalinization in alfalfa root hairs in response to rhizobial lipochitooligosaccharide signals. *Plant Journal,* **10,** 295-301.

Felle, H. H., Kondorosi, E., Kondorosi, A. & Schultze, M. (1998). The role of ion fluxes in Nod factor signalling in *Medicago sativa*. *Plant Journal,* **13,** 455-463.

Felle, H. H., Kondorosi, E., Kondorosi, A. & Schultze, M. (1999a). Nod factors modulate the concentration of cytosolic free calcium differently in growing and non-growing root hairs of *Medicago sativa L*. *Planta,* **209,** 207-212.

Felle, H. H., Kondorosi, E., Kondorosi, A. & Schultze, M. (1999b). Elevation of the cytosolic free [Ca^{2+}] is indispensable for the transduction of the nod factor signal in alfalfa. *Plant Physiology,* **121,** 273-279.

Felle, H. H., Kondorosi, E., Kondorosi, A. & Schultze, M. (2000). How alfalfa root hairs discriminate between Nod factors and oligochitin elicitors. *Plant Physiology,* **124,** 1373-1380.

Finka, A., Cuendet, A. F. H., Maathuis, F. J. M., Saidi, Y. & Goloubinoff, P. (2012). Plasma membrane cyclic nucleotide gated calcium channels control land plant thermal sensing and acquired thermotolerance. *Plant Cell,* **24,** 3333-3348.

Foreman, J., Demidchik, V., Bothwell, J. H. F., Mylona, P., Miedema, H., Torres, M. A., Linstead, P., Costa, S., Brownlee, C., Jones, J. D. G., Davies, J. M. & Dolan, L. (2003). Reactive oxygen species produced by NADPH oxidase regulate plant cell growth. *Nature,* **422,** 442-446.

Fournier, J., Timmers, A. C. J., Sieberer, B. J., Jauneau, A., Chabaud, M. & Barker, D. G. (2008). Mechanism of infection thread elongation in root hairs of *Medicago truncatula* and dynamic interplay with associated rhizobial colonization. *Plant Physiology,* **148,** 1985-1995.

Fu, Y., Wu, G. & Yang, Z. B. (2001). Rop GTPase-dependent dynamics of tip-localized F-actin controls tip growth in pollen tubes. *Journal of Cell Biology,* **152,** 1019-1032.

Fu, Y., Gu, Y., Zheng, Z. L., Wasteneys, G. & Yang, Z. B. (2005). Arabidopsis interdigitating cell growth requires two antagonistic pathways with opposing action on cell morphogenesis. *Cell,* **120,** 687-700.

Genre, A., Chabaud, M., Balzergue, C., Puech-Pages, V., Novero, M., Rey, T., Fournier, J., Rochange, S., Becard, G., Bonfante, P. & Barker, D. G. (2013). Short-chain chitin oligomers from arbuscular mycorrhizal fungi trigger nuclear Ca^{2+} spiking in *Medicago truncatula* roots and their production is enhanced by strigolactone. *New Phytologist,* **198,** 190-202.

Gleason, C., Chaudhuri, S., Yang, T. B., Munoz, A., Poovaiah, B. W. & Oldroyd, G. E. D. (2006). Nodulation independent of rhizobia induced by a calcium-activated kinase lacking autoinhibition. *Nature,* **441,** 1149-1152.

Gobbato, E., Marsh, J. F., Vernie, T., Wang, E., Maillet, F., Kim, J., Miller, J. B., Sun, J., Bano, S. A., Ratet, P., Mysore, K. S., Denarie, J., Schultze, M. & Oldroyd, G. E. D. (2012). A GRAS-type transcription factor with a specific function in mycorrhizal signaling. *Current Biology,* **22,** 2236-2241.

Gong, Z. Y., Song, X., Chen, G. Y., Zhu, J. B., Yu, G. Q. & Zou, H. S. (2012). Molecular studies of the *Medicago truncatula MtAnn3* gene involved in root hair deformation. *Chinese Science Bulletin,* **57,** 1803-1809.

Govindarajulu, M., Kim, S. Y., Libault, M., Berg, R. H., Tanaka, K., Stacey, G. & Taylor, C. G. (2009). GS52 ecto-apyrase plays a critical role during soybean nodulation. *Plant Physiology,* **149,** 994-1004.

Grandbastien, M. A., Spielmann, A. & Caboche, M. (1989). *TNT1,* a mobile retroviral-like transposable element of tobacco isolated by plant-cell genetics. *Nature,* **337,** 376-380.

Granqvist, E., Wysham, D., Hazledine, S., Kozlowski, W., Sun, J., Charpentier, M., Martins, T. V., Haleux, P., Tsaneva-Atanasova, K., Downie, J. A., Oldroyd, G. E. D. & Morris, R. J. (2012). Buffering capacity explains signal variation in symbiotic calcium oscillations. *Plant Physiology,* **160,** 2300-2310.

Groth, M., Takeda, N., Perry, J., Uchida, H., Draxl, S., Brachmann, A., Sato, S., Tabata, S., Kawaguchi, M., Wang, T. L. & Parniske, M. (2010). *NENA,* a *Lotus japonicus* homolog of *Sec13,* is required for rhizodermal infection by arbuscular mycorrhiza fungi and rhizobia but dispensable for cortical endosymbiotic development. *Plant Cell,* **22,** 2509-2526.

Grynkiewicz, G., Poenie, M. & Tsien, R. Y. (1985). A new generation of Ca^{2+} indicators with greatly improved fluorescence properties. *Journal of Biological Chemistry,* **260,** 3440-3450.

Gu, Y., Li, S. D., Lord, E. M. & Yang, Z. B. (2006). Members of a novel class of Arabidopsis Rho guanine nucleotide exchange factors control rho GTPase-dependent polar growth. *Plant Cell,* **18,** 366-381.

Guo, A. Y., Zhu, Q. H., Chen, X. & Luo, J. C. (2007). GSDS: a gene structure display server. *Yi Chuan,* **29,** 1023-1026.

Haney, C. H. & Long, S. R. (2010). Plant flotillins are required for infection by nitrogen-fixing bacteria. *Proceedings of the National Academy of Sciences of the United States of America,* **107,** 478-483.

Hanson, G. T., Aggeler, R., Oglesbee, D., Cannon, M., Capaldi, R. A., Tsien, R. Y. & Remington, S. J. (2004). Investigating mitochondrial redox potential with redox-

sensitive green fluorescent protein indicators. *Journal of Biological Chemistry,* **279,** 13044-13053.

Harper, J. F., Breton, G. & Harmon, A. (2004). Decoding Ca(2+) signals through plant protein kinases. *Annu Rev Plant Biol,* **55,** 263-88.

Hayashi, T., Banba, M., Shimoda, Y., Kouchi, H., Hayashi, M. & Imaizumi-Anraku, H. (2010). A dominant function of CCaMK in intracellular accommodation of bacterial and fungal endosymbionts. *Plant Journal***,** 141-154.

He, J., Benedito, V. A., Wang, M. Y., Murray, J. D., Zhao, P. X., Tang, Y. H. & Udvardi, M. K. (2009). The *Medicago truncatula* gene expression atlas web server. *Bmc Bioinformatics,* **10**.

He, X., Liu, Y. M., Wang, W. & Li, Y. (2006). Distribution of G-actin is related to root hair growth of wheat. *Annals of Botany,* **98,** 49-55.

Heckmann, A. B., Lombardo, F., Miwa, H., Perry, J. A., Bunnewell, S., Parniske, M., Wang, T. L. & Downie, J. A. (2006). *Lotus japonicus* nodulation requires two GRAS domain regulators, one of which is functionally conserved in a non-legume. *Plant Physiology,* **142,** 1739-1750.

Hellemans, J., Mortier, G., De Paepe, A., Speleman, F. & Vandesompele, J. (2007). qBase relative quantification framework and software for management and automated analysis of real-time quantitative PCR data. *Genome Biol,* **8,** R19.

Herrmann, A. & Felle, H. H. (1995). Tip Growth in root hair cells of *Sinapis alba* L - signficance of internal and external Ca^{2+} and pH. *New Phytologist,* **129,** 523-533.

Hirsch, S., Kim, J., Munoz, A., Heckmann, A. B., Downie, J. A. & Oldroyd, G. E. D. (2009). GRAS proteins form a DNA binding complex to induce gene expression during nodulation signaling in *Medicago truncatula*. *Plant Cell,* **21,** 545-557.

Hoffmann, B., Trinh, T. H., Leung, J., Kondorosi, A. & Kondorosi, E. (1997). A new *Medicago truncatula* line with superior *in vitro* regeneration, transformation, and symbiotic properties isolated through cell culture selection. *Molecular Plant-Microbe Interactions,* **10,** 307-315.

Hofmann, A., Proust, J., Dorowski, A., Schantz, R. & Huber, R. (2000). Annexin 24 from Capsicum annuum - X-ray structure and biochemical characterization. *Journal of Biological Chemistry,* **275,** 8072-8082.

Holdaway-Clarke, T. L., Feijo, J. A., Hackett, G. R., Kunkel, J. G. & Hepler, P. K. (1997). Pollen tube growth and the intracellular cytosolic calcium gradient oscillate in phase while extracellular calcium influx is delayed. *Plant Cell,* **9,** 1999-2010.

Hooijmaijers, C., Rhee, J. Y., Kwak, K. J., Chung, G. C., Horie, T., Katsuhara, M. & Kang, H. (2012). Hydrogen peroxide permeability of plasma membrane aquaporins of Arabidopsis thaliana. *Journal of Plant Research,* **125,** 147-153.

Hunter, S., Jones, P., Mitchell, A., Apweiler, R., Attwood, T. K., Bateman, A., Bernard, T., Binns, D., Bork, P., Burge, S., de Castro, E., Coggill, P., Corbett, M., Das, U., Daugherty, L., Duquenne, L., Finn, R. D., Fraser, M., Gough, J., Haft, D., Hulo, N., Kahn, D., Kelly, E., Letunic, I., Lonsdale, D., Lopez, R., Madera, M., Maslen, J., McAnulla, C., McDowall, J., McMenamin, C., Mi, H., Mutowo-Muellenet, P., Mulder, N., Natale, D., Orengo, C., Pesseat, S., Punta, M., Quinn, A. F., Rivoire, C., Sangrador-Vegas, A., Selengut, J. D., Sigrist, C. J., Scheremetjew, M., Tate, J., Thimmajanarthanan, M., Thomas, P. D., Wu, C. H., Yeats, C. & Yong, S. Y. (2012). InterPro in 2011: new developments in the family and domain prediction database. *Nucleic Acids Res,* **40,** D306-12.

Hussey, P. J., Ketelaar, T. & Deeks, M. J. 2006. Control of the actin cytoskeleton in plant cell growth. *Annual Review of Plant Biology.* Palo Alto: Annual Reviews.

Hwang, J. U., Vernoud, V., Szumlanski, A., Nielsen, E. & Yang, Z. B. (2008). A tip-localized RhoGAP controls cell polarity by globally inhibiting Rho GTPase at the cell apex. *Current Biology,* **18,** 1907-1916.

Hwang, J. U., Wu, G., Yan, A., Lee, Y. J., Grierson, C. S. & Yang, Z. B. (2010). Pollen-tube tip growth requires a balance of lateral propagation and global inhibition of Rho-family GTPase activity. *Journal of Cell Science,* **123,** 340-350.

Imaizumi-Anraku, H., Takeda, N., Charpentier, M., Perry, J., Miwa, H., Umehara, Y., Kouchi, H., Murakami, Y., Mulder, L., Vickers, K., Pike, J., Downie, J. A., Wang, T., Sato, S., Asamizu, E., Tabata, S., Yoshikawa, M., Murooka, Y., Wu, G. J., Kawaguchi, M., Kawasaki, S., Parniske, M. & Hayashi, M. (2005). Plastid proteins crucial for symbiotic fungal and bacterial entry into plant roots. *Nature,* **433,** 527-531.

Inoue, H., Nojima, H. & Okayama, H. (1990). High efficiency transformation of *Escherichia coli* with plasmids. *Gene,* **96,** 23-8.

Ivashuta, S., Liu, J., Liu, J., Lohar, D. P., Haridas, S., Bucciarelli, B., VandenBosch, K. A., Vance, C. P., Harrison, M. J. & Gantt, J. S. (2005). RNA interference identifies a calcium-dependent protein kinase involved in *Medicago truncatula* root development. *Plant Cell,* **17,** 2911-2921.

Jeter, C. R., Tang, W. Q., Henaff, E., Butterfield, T. & Roux, S. J. (2004). Evidence of a novel cell signaling role for extracellular adenosine triphosphates and diphosphates in Arabidopsis. *Plant Cell,* **16,** 2652-2664.

Jones, D. L., Shaff, J. E. & Kochian, L. V. (1995). Role of calcium and other ions in directing root hair tip growth in *Limnobium stoloniferum*.1. Inhibition of tip growth by aluminum. *Planta,* **197,** 672-680.

Jones, K. M., Sharopova, N., Lohar, D. P., Zhang, J. Q., VandenBosch, K. A. & Walker, G. C. (2008). Differential response of the plant *Medicago truncatula* to its symbiont *Sinorhizobium meliloti* or an exopolysaccharide-deficient mutant. *Proceedings of the National Academy of Sciences of the United States of America,* **105,** 704-709.

Jones, K. M. & Walker, G. C. (2008). Responses of the model legume *Medicago truncatula* to the rhizobial exopolysaccharide succinoglycan. *Plant Signaling and Behavior,* **3,** 888-890.

Jones, M. A., Shen, J. J., Fu, Y., Li, H., Yang, Z. & Grierson, C. S. (2002). The Arabidopsis Rop2 GTPase is a positive regulator of both root hair initiation and tip growth. *Plant Cell,* **14,** 763-776.

Jones, M. A., Raymond, M. J., Yang, Z. & Smirnoff, N. (2007). NADPH oxidase-dependent reactive oxygen species formation required for root hair growth depends on ROP GTPase. *Journal of Experimental Botany,* **58,** 1261-1270.

Journet, E. P., El-Gachtouli, N., Vernoud, V., de Billy, F., Pichon, M., Dedieu, A., Arnould, C., Morandi, D., Barker, D. G. & Gianinazzi-Pearson, V. (2001). *Medicago truncatula* ENOD11: A novel RPRP-encoding early nodulin gene expressed during mycorrhization in arbuscule-containing cells. *Molecular Plant-Microbe Interactions,* **14,** 737-748.

Kalo, P., Gleason, C., Edwards, A., Marsh, J., Mitra, R. M., Hirsch, S., Jakab, J., Sims, S., Long, S. R., Rogers, J., Kiss, G. B., Downie, J. A. & Oldroyd, G. E. D. (2005). Nodulation signaling in legumes requires NSP2, a member of the GRAS family of transcriptional regulators. *Science,* **308,** 1786-1789.

Kanamori, N., Madsen, L. H., Radutoiu, S., Frantescu, M., Quistgaard, E. M., Miwa, H., Downie, J. A., James, E. K., Felle, H. H., Haaning, L. L., Jensen, T. H., Sato, S., Nakamura, Y., Tabata, S., Sandal, N. & Stougaard, J. (2006). A nucleoporin is required for induction of Ca^{2+} spiking in legume nodule development and essential for rhizobial and fungal symbiosis. *Proceedings of the National Academy of Sciences of the United States of America,* **103,** 359-364.

Karimi, M., Inze, D. & Depicker, A. (2002). GATEWAY$^{(TM)}$ vectors for Agrobacterium-mediated plant transformation. *Trends in Plant Science,* **7,** 193-195.

Ke, D., Fang, Q., Chen, C., Zhu, H., Chen, T., Chang, X., Yuan, S., Kang, H., Ma, L., Hong, Z. & Zhang, Z. (2012). The small GTPase ROP6 interacts with NFR5 and is involved in nodule formation in *Lotus japonicus*. *Plant Physiology,* **159,** 131-143.

Keller, T., Damude, H. G., Werner, D., Doerner, P., Dixon, R. A. & Lamb, C. (1998). A plant homolog of the neutrophil NADPH oxidase gp91(phox) subunit gene encodes a plasma membrane protein with Ca^{2+} binding motifs. *Plant Cell,* **10,** 255-266.

Kerr, E. M. & Fry, S. C. (2004). Extracellular cross-linking of xylan and xyloglucan in maize cell-suspension cultures: the role of oxidative phenolic coupling. *Planta,* **219,** 73-83.

Kevei, Z., Lougnon, G., Mergaert, P., Horvath, G. V., Kereszt, A., Jayaraman, D., Zaman, N., Marcel, F., Regulski, K., Kiss, G. B., Kondorosi, A., Endre, G., Kondorosi, E. & Ane, J. M. (2007). 3-hydroxy-3-methylglutaryl coenzyme a reductase 1 interacts with NORK and is crucial for nodulation in *Medicago truncatula*. *Plant Cell,* **19,** 3974-3989.

Kiirika, L. M., Bergmann, H. F., Schikowsky, C., Wimmer, D., Korte, J., Schmitz, U., Niehaus, K. & Colditz, F. (2012). Silencing of the Rac1 GTPase MtROP9 in *Medicago truncatula* stimulates early mycorrhizal and oomycete root colonizations but negatively affects rhizobial infection. *Plant Physiology,* **159,** 501-516.

Kim, S. Y., Sivaguru, M. & Stacey, G. (2006). Extracellular ATP in plants. Visualization, localization, and analysis of physiological significance in growth and signaling. *Plant Physiology,* **142,** 984-992.

Kjellbom, P., Snogerup, L., Stohr, C., Reuzeau, C., McCabe, P. F. & Pennell, R. I. (1997). Oxidative cross-linking of plasma membrane arabinogalactan proteins. *Plant Journal,* **12,** 1189-1196.

Klahre, U., Becker, C., Schmitt, A. C. & Kost, B. (2006). Nt-RhoGDI2 regulates Rac/Rop signaling and polar cell growth in tobacco pollen tubes. *Plant Journal,* **46,** 1018-1031.

Klahre, U. & Kost, B. (2006). Tobacco RhoGTPase ACTIVATING PROTEIN1 spatially restricts signaling of RAC/Rop to the apex of pollen tubes. *Plant Cell,* **18,** 3033-3046.

Kobayashi, M., Ohura, I., Kawakita, K., Yokota, N., Fujiwara, M., Shimamoto, K., Doke, N. & Yoshioka, H. (2007). Calcium-dependent protein kinases regulate the production of reactive oxygen species by potato NADPH oxidase. *Plant Cell,* **19,** 1065-1080.

Kost, B., Lemichez, E., Spielhofer, P., Hong, Y., Tolias, K., Carpenter, C. & Chua, N. H. (1999). Rac homologues and compartmentalized phosphatidylinositol 4, 5-bisphosphate act in a common pathway to regulate polar pollen tube growth. *Journal of Biological Chemistry,* **145,** 317-330.

Kost, B. (2008). Spatial control of Rho (Rac-Rop) signaling in tip-growing plant cells. *Trends in Cell Biology,* **18,** 119-127.

Kosuta, S., Hazledine, S., Sun, J., Miwa, H., Morris, R. J., Downie, J. A. & Oldroyd, G. E. D. (2008). Differential and chaotic calcium signatures in the symbiosis signaling

pathway of legumes. *Proceedings of the National Academy of Sciences of the United States of America,* **105,** 9823-9828.

Kosuta, S., Held, M., Hossain, M. S., Morieri, G., MacGillivary, A., Johansen, C., Antolin-Llovera, M., Parniske, M., Oldroyd, G. E. D., Downie, A. J., Karas, B. & Szczyglowski, K. (2011). *Lotus japonicus symRK-14* uncouples the cortical and epidermal symbiotic program. *Plant Journal,* **67,** 929-940.

Kurkdjian, A. C. (1995). Role of the differentiation of root epidermal cells in Nod Factor (from *Rhizobium meliloti*)-induced root hair depolarization of *Medicago sativa*. *Plant Physiology,* **107,** 783-790.

Langhorst, M. F., Jaeger, F. A., Mueller, S., Hartmann, L. S., Luxenhofer, G. & Stuermer, C. A. O. (2008). Reggies/flotillins regulate cytoskeletal remodeling during neuronal differentiation via CAP/ponsin and Rho GTPases. *European Journal of Cell Biology,* **87,** 921-931.

Laohavisit, A., Mortimer, J. C., Demidchik, V., Coxon, K. M., Stancombe, M. A., Macpherson, N., Brownlee, C., Hofmann, A., Webb, A. A. R., Miedema, H., Battey, N. H. & Davies, J. M. (2009). *Zea mays* annexins modulate cytosolic free Ca^{2+} and generate a Ca^{2+}-permeable conductance. *Plant Cell,* **21,** 479-493.

Laohavisit, A., Brown, A. T., Cicuta, P. & Davies, J. M. (2010). Annexins: components of the calcium and reactive oxygen signaling network. *Plant Physiology,* **152,** 1824-1829.

Laohavisit, A., Shang, Z. L., Rubio, L., Cuin, T. A., Very, A. A., Wang, A. H., Mortimer, J. C., Macpherson, N., Coxon, K. M., Battey, N. H., Brownlee, C., Park, O. K., Sentenac, H., Shabala, S., Webb, A. A. R. & Davies, J. M. (2012). Arabidopsis Annexin1 Mediates the Radical-Activated Plasma Membrane Ca2+- and K+-Permeable Conductance in Root Cells. *Plant Cell,* **24,** 1522-1533.

Lefebvre, B., Timmers, T., Mbengue, M., Moreau, S., Herve, C., Toth, K., Bittencourt-Silvestre, J., Klaus, D., Deslandes, L., Godiard, L., Murray, J. D., Udvardi, M. K., Raffaele, S., Mongrand, S., Cullimore, J., Gamas, P., Niebel, A. & Ott, T. (2010). A remorin protein interacts with symbiotic receptors and regulates bacterial infection. *Proceedings of the National Academy of Sciences of the United States of America,* **107,** 2343-2348.

Levy, J., Bres, C., Geurts, R., Chalhoub, B., Kulikova, O., Duc, G., Journet, E. P., Ane, J. M., Lauber, E., Bisseling, T., Denarie, J., Rosenberg, C. & Debelle, F. (2004). A putative Ca^{2+} and calmodulin-dependent protein kinase required for bacterial and fungal symbioses. *Science,* **303,** 1361-1364.

Li, H., Wu, G., Ware, D., Davis, K. R. & Yang, Z. (1998). Arabidopsis Rho-related GTPases: differential gene expression in pollen and polar localization in fission yeast. *Plant Physiology,* **118,** 407-17.

Li, H., Lin, Y., Heath, R. M., Zhu, M. X. & Yang, Z. (1999). Control of pollen tube tip growth by a Rop GTPase-dependent pathway that leads to tip-localized calcium influx. *Plant Cell,* **11,** 1731-42.

Liao, J. Q., Singh, S., Hossain, M. S., Andersen, S. U., Ross, L., Bonetta, D., Zhou, Y. H., Sato, S., Tabata, S., Stougaard, J., Szczyglowski, K. & Parniske, M. (2012). Negative regulation of CCaMK is essential for symbiotic infection. *Plant Journal,* **72,** 572-584.

Lin, D. S., Nagawa, S., Chen, J. S., Cao, L. Y., Chen, X., Xu, T. D., Li, H. J., Dhonukshe, P., Yamamuro, C., Friml, J., Scheres, B., Fu, Y. & Yang, Z. B. (2012). A ROP GTPase-

dependent auxin signaling pathway regulates the subcellular distribution of PIN2 in Arabidopsis roots. *Current Biology,* **22,** 1319-1325.

Liu, P., Li, R. L., Zhang, L., Wang, Q. L., Niehaus, K., Baluska, F., Samaj, J. & Lin, J. X. (2009). Lipid microdomain polarization is required for NADPH oxidase-dependent ROS signaling in *Picea meyeri* pollen tube tip growth. *Plant Journal,* **60,** 303-313.

Liu, W., Chen, A. M., Luo, L., Sun, J., Cao, L. P., Yu, G. Q., Zhu, J. B. & Wang, Y. Z. (2010). Characterization and expression analysis of *Medicago truncatula* ROP GTPase family during the early stage of symbiosis. *Journal of Integrative Plant Biology,* **52,** 639-652.

Lloyd, C. W., Pearce, K. J., Rawlins, D. J., Ridge, R. W. & Shaw, P. J. (1987). Endoplasmic microtubules connect the advancing nucleus to the tip of legume root hairs, but F-actin is involved in basipetal migration. *Cell Motility and the Cytoskeleton,* **8,** 27-36.

Lohar, D. P., Haridas, S., Gantt, J. S. & VandenBosch, K. A. (2007). A transient decrease in reactive oxygen species in roots leads to root hair deformation in the legume-rhizobia symbiosis. *New Phytologist,* **173,** 39-49.

Long, S. R. (1996). Rhizobium symbiosis: Nod factors in perspective. *Plant Cell,* **8,** 1885-1898.

Love, J., Dodd, A. N. & Webb, A. A. R. (2004). Circadian and diurnal calcium oscillations encode photoperiodic information in Arabidopsis. *Plant Cell,* **16,** 956-966.

Ma, W., Smigel, A., Walker, R. K., Moeder, W., Yoshioka, K. & Berkowitz, G. A. (2010). Leaf senescence signaling: The Ca^{2+}-conducting Arabidopsis Cyclic Nucleotide Gated Channel2 acts through nitric oxide to repress senescence programming. *Plant Physiology,* **154,** 733-743.

Madsen, L. H., Tirichine, L., Jurkiewicz, A., Sullivan, J. T., Heckmann, A. B., Bek, A. S., Ronson, C. W., James, E. K. & Stougaard, J. (2010). The molecular network governing nodule organogenesis and infection in the model legume *Lotus japonicus*. *Nature Communications,* **1**.

Maillet, F., Poinsot, V., Andre, O., Puech-Pages, V., Haouy, A., Gueunier, M., Cromer, L., Giraudet, D., Formey, D., Niebel, A., Martinez, E. A., Driguez, H., Becard, G. & Denarie, J. (2011). Fungal lipochitooligosaccharide symbiotic signals in arbuscular mycorrhiza. *Nature,* **469,** 58-63.

Mandon, K., Kaminski, P. A. & Elmerich, C. (1994). Functional analysis of the fixNOQP region of *Azorhizobium caulinodans*. *J Bacteriol,* **176,** 2560-2558.

Marie, C., Barny, M. A. & Downie, J. A. (1992). RHIZOBIUM-LEGUMINOSARUM HAS 2 GLUCOSAMINE SYNTHASES, GLMS AND NODM, REQUIRED FOR NODULATION AND DEVELOPMENT OF NITROGEN-FIXING NODULES. *Molecular Microbiology,* **6,** 843-851.

Marie, C., Plaskitt, K. A. & Downie, J. A. (1994). ABNORMAL BACTEROID DEVELOPMENT IN NODULES INDUCED BY A GLUCOSAMINE SYNTHASE MUTANT OF RHIZOBIUM-LEGUMINOSARUM. *Molecular Plant-Microbe Interactions,* **7,** 482-487.

Marino, D., Andrio, E., Danchin, E. G. J., Oger, E., Gucciardo, S., Lambert, A., Puppo, A. & Pauly, N. (2011). A *Medicago truncatula* NADPH oxidase is involved in symbiotic nodule functioning. *New Phytologist,* **189,** 580-592.

Marsh, J. F., Rakocevic, A., Mitra, R. M., Brocard, L., Sun, J., Eschstruth, A., Long, S. R., Schultze, M., Ratet, P. & Oldroyd, G. E. D. (2007). *Medicago truncatula NIN* is essential for rhizobial-independent nodule organogenesis induced by autoactive calcium/calmodulin-dependent protein kinase. *Plant Physiology,* **144,** 324-335.

McAinsh, M. R., Webb, A. A. R., Taylor, J. E. & Hetherington, A. M. (1995). Stimulus-induced oscillations in guard-cell cytosolic-free calcium. *Plant Cell,* **7,** 1207-1219.

McCormac, A. C., Elliott, M. C. & Chen, D. F. (1998). A simple method for the production of highly competent cells of Agrobacterium for transformation via electroporation. *Molecular Biotechnology,* **9,** 155-9.

Meade, H. M., Long, S. R., Ruvkun, G. B., Brown, S. E. & Ausubel, F. M. (1982). Physical and genetic-characterization of symbiotic and auxotrophic mutants of *Rhizobium meliloti* induced by transposon Tn5 mutagensis *Journal of Bacteriology,* **149,** 114-122.

Messinese, E., Mun, J. H., Yeun, L. H., Jayaraman, D., Rouge, P., Barre, A., Lougnon, G., Schornack, S., Bono, J. J., Cook, D. R. & Ane, J. M. (2007). A novel nuclear protein interacts with the symbiotic DMI3 calcium- and calmodulin-dependent protein kinase of *Medicago truncatula. Molecular Plant-Microbe Interactions,* **20,** 912-921.

Michard, E., Dias, P. & Feijo, J. A. (2008). Tobacco pollen tubes as cellular models for ion dynamics: improved spatial and temporal resolution of extracellular flux and free cytosolic concentration of calcium and protons using pHluorin and YC3.1 CaMeleon. *Sexual Plant Reproduction,* **21,** 169-181.

Michard, E., Lima, P. T., Borges, F., Silva, A. C., Portes, M. T., Carvalho, J. E., Gilliham, M., Liu, L. H., Obermeyer, G. & Feijo, J. A. (2011). Glutamate receptor-like genes form Ca^{2+} channels in pollen tubes and are regulated by pistil D-serine. *Science,* **332,** 434-437.

Middleton, P. H., Jakab, J., Penmetsa, R. V., Starker, C. G., Doll, J., Kalo, P., Prabhu, R., Marsh, J. F., Mitra, R. M., Kereszt, A., Dudas, B., VandenBosch, K., Long, S. R., Cook, D. R., Kiss, G. B. & Oldroyd, G. E. D. (2007). An ERF transcription factor in *Medicago truncatula* that is essential for nod factor signal transduction. *Plant Cell,* **19,** 1221-1234.

Miles, G. P., Samuel, M. A., Jones, A. M. & Ellis, B. E. (2004). Mastoparan rapidly activates plant MAP kinase signaling independent of heterotrimeric G proteins. *Plant Physiology,* **134,** 1332-1336.

Miller, J. B., Pratap, A., Miyahara, A., Zhou, L., Bornemann, S., Morris, R. J. & Oldroyd, G. E. (2013). Calcium/Calmodulin-Dependent Protein Kinase is negatively and positively regulated by calcium, providing a mechanism for decoding calcium responses during symbiosis signaling. *Plant Cell.*

Mitra, R. M., Gleason, C. A., Edwards, A., Hadfield, J., Downie, J. A., Oldroyd, G. E. D. & Long, S. R. (2004). A Ca^{2+}/calmodulin-dependent protein kinase required for symbiotic nodule development: Gene identification by transcript-based cloning. *Proceedings of the National Academy of Sciences of the United States of America,* **101,** 4701-4705.

Miwa, H. (2005). *Calcium signalling in nodulation and mycorrhization* PhD, University of East Anglia.

Miwa, H., Sun, J., Oldroyd, G. E. D. & Downie, J. A. (2006a). Analysis of nod-factor-induced calcium signaling in root hairs of symbiotically defective mutants of *Lotus japonicus. Molecular Plant-Microbe Interactions,* **19,** 914-923.

Miwa, H., Sun, J., Oldroyd, G. E. D. & Downie, J. A. (2006b). Analysis of calcium spiking using a cameleon calcium sensor reveals that nodulation gene expression is regulated by calcium spike number and the developmental status of the cell. *Plant Journal,* **48,** 883-894.

Miyahara, A., Richens, J., Starker, C., Morieri, G., Smith, L., Long, S., Downie, J. A. & Oldroyd, G. E. D. (2010). Conservation in function of a SCAR/WAVE component during infection thread and root hair growth in *Medicago truncatula*. *Molecular Plant-Microbe Interactions,* **23,** 1553-1562.

Miyawaki, A., Llopis, J., Heim, R., McCaffery, J. M., Adams, J. A., Ikura, M. & Tsien, R. Y. (1997). Fluorescent indicators for Ca^{2+} based on green fluorescent proteins and calmodulin. *Nature,* **388,** 882-887.

Miyawaki, A., Griesbeck, O., Heim, R. & Tsien, R. Y. (1999). Dynamic and quantitative Ca^{2+} measurements using improved cameleons. *Proceedings of the National Academy of Sciences of the United States of America,* **96,** 2135-2140.

Molendijk, A. J., Bischoff, F., Rajendrakumar, C. S. V., Friml, J., Braun, M., Gilroy, S. & Palme, K. (2001). *Arabidopsis thaliana* Rop GTPases are localized to tips of root hairs and control polar growth. *Embo Journal,* **20,** 2779-2788.

Monaghan, J. & Zipfel, C. (2012). Plant pattern recognition receptor complexes at the plasma membrane. *Current Opinion in Plant Biology,* **15,** 349-357.

Monshausen, G. B., Bibikova, T. N., Messerli, M. A., Shi, C. & Gilroy, S. (2007). Oscillations in extracellular pH and reactive oxygen species modulate tip growth of Arabidopsis root hairs. *Proceedings of the National Academy of Sciences of the United States of America,* **104,** 20996-21001.

Monshausen, G. B., Messerli, M. A. & Gilroy, S. (2008). Imaging of the Yellow Cameleon 3.6 indicator reveals that elevations in cytosolic Ca^{2+} follow oscillating increases in growth in root hairs of Arabidopsis. *Plant Physiology,* **147,** 1690-1698.

Montiel, J., Nava, N., Cardenas, L., Sanchez-Lopez, R., Arthikala, M. K., Santana, O., Sanchez, F. & Quinto, C. (2012). A *Phaseolus vulgaris* NADPH oxidase gene is required for root infection by rhizobia. *Plant and Cell Physiology,* **53,** 1751-67.

Morieri, G. (2010). *Two Types of Calcium Signalling in Legume-Rhizobia Symbiosis.* PhD, University of East Anglia.

Morieri, G., Martinez, E. A., Jarynowski, A., Driguez, H., Morris, R., Oldroyd, G. E. & Downie, J. A. (2013). Host-specific Nod-factors associated with *Medicago truncatula* nodule infection differentially induce calcium influx and calcium spiking in root hairs. *New Phytologist*, 656-662.

Muday, G. K., Rahman, A. & Binder, B. M. (2012). Auxin and ethylene: collaborators or competitors? *Trends in Plant Science,* **17,** 181-195.

Nagai, T., Sawano, A., Park, E. S. & Miyawaki, A. (2001). Circularly permuted green fluorescent proteins engineered to sense Ca^{2+}. *Proceedings of the National Academy of Sciences of the United States of America,* **98,** 3197-3202.

Nagai, T., Yamada, S., Tominaga, T., Ichikawa, M. & Miyawaki, A. (2004). Expanded dynamic range of fluorescent indicators for Ca^{2+} by circularly permuted yellow fluorescent proteins. *Proceedings of the National Academy of Sciences of the United States of America,* **101,** 10554-10559.

Niebel, F. D., Lescure, N., Cullimore, J. V. & Gamas, P. (1998). The *Medicago truncatula MtAnn1* gene encoding an annexin is induced by nod factors and during the symbiotic interaction with Rhizobium meliloti. *Molecular Plant-Microbe Interactions,* **11,** 504-513.

Oldroyd, G. E., Mitra, R. M., Wais, R. J. & Long, S. R. (2001a). Evidence for structurally specific negative feedback in the Nod factor signal transduction pathway. *Plant Journal,* **28,** 191-199.

Oldroyd, G. E. D., Engstrom, E. M. & Long, S. R. (2001b). Ethylene inhibits the nod factor signal transduction pathway of *Medicago truncatula*. *Plant Cell,* **13,** 1835-1849.

Oldroyd, G. E. D., Murray, J. D., Poole, P. S. & Downie, J. A. 2011. The Rules of Engagement in the Legume-Rhizobial Symbiosis. *In:* Bassler, B. L., Lichten, M. & Schupbach, G. (eds.) *Annual Review Genetics, Vol 45.* Palo Alto: Annual Reviews.

Parniske, M. (2008a). Arbuscular mycorrhiza: the mother of plant root endosymbioses. *Nature Reviews Microbiology,* **6,** 763-775.

Parniske, M. (2008b). Arbuscular mycorrhiza: the mother of plant root endosymbioses. *Nat Rev Microbiol,* **6,** 763-75.

Patil, S., Takezawa, D. & Poovaiah, B. W. (1995). Chimeric plant Calcium/Calmodulin-Dependent Protein-Kinase gene with a neural visinin-like calcium-binding domain. *Proceedings of the National Academy of Sciences of the United States of America,* **92,** 4897-4901.

Peiter, E., Sun, J., Heckmann, A. B., Venkateshwaran, M., Riely, B. K., Otegui, M. S., Edwards, A., Freshour, G., Hahn, M. G., Cook, D. R., Sanders, D., Oldroyd, G. E. D., Downie, J. A. & Ane, J. M. (2007). The *Medicago truncatula* DMI1 protein modulates cytosolic calcium signaling. *Plant Physiology,* **145,** 192-203.

Pellock, B. J., Cheng, H. P. & Walker, G. C. (2000). Alfalfa root nodule invasion efficiency is dependent on *Sinorhizobium meliloti* polysaccharides. *Journal of Bacteriology,* **182,** 4310-4318.

Penmetsa, R. V. & Cook, D. R. (1997). A legume ethylene-insensitive mutant hyperinfected by its rhizobial symbiont. *Science,* **275,** 527-530.

Penmetsa, R. V., Uribe, P., Anderson, J., Lichtenzveig, J., Gish, J. C., Nam, Y. W., Engstrom, E., Xu, K., Sckisel, G., Pereira, M., Baek, J. M., Lopez-Meyer, M., Long, S. R., Harrison, M. J., Singh, K. B., Kiss, G. B. & Cook, D. R. (2008). The *Medicago truncatula* ortholog of Arabidopsis *EIN2*, *sickle*, is a negative regulator of symbiotic and pathogenic microbial associations. *Plant Journal,* **55,** 580-595.

Peret, B., Swarup, R., Jansen, L., Devos, G., Auguy, F., Collin, M., Santi, C., Hocher, V., Franche, C., Bogusz, D., Bennett, M. & Laplaze, L. (2007). Auxin influx activity is associated with *Frankia* infection during actinorhizal nodule formation in *Casuarina glauca*. *Plant Physiology,* **144,** 1852-1862.

Pingret, J. L., Journet, E. P. & Barker, D. G. (1998). *Rhizobium* Nod factor signaling. Evidence for a g protein-mediated transduction mechanism. *Plant Cell,* **10,** 659-672.

Pitts, R. J., Cernac, A. & Estelle, M. (1998). Auxin and ethylene promote root hair elongation in Arabidopsis. *Plant Journal,* **16,** 553-560.

Preisig, O., Anthamatten, D. & Hennecke, H. (1993). Genes for a microaerobically induced oxidase complex in Bradyrhizobium japonicum are essential for a nitrogen-fixing endosymbiosis. *Proc Natl Acad Sci U S A,* **90,** 3309-13.

Rae, A. L., Bonfantefasolo, P. & Brewin, N. J. (1992). Structure and Growth of Infection Threads in the Legume Symbiosis with Rhizobium-Leguminosarum. *Plant Journal,* **2,** 385-395.

Ramu, S. K., Peng, H. M. & Cook, D. R. (2002). Nod factor induction of reactive oxygen species production is correlated with expression of the early nodulin gene *Rip1* in *Medicago truncatula*. *Molecular Plant-Microbe Interactions,* **15,** 522-528.

Rato, C., Monteiro, D., Hepler, P. K. & Malho, R. (2004). Calmodulin activity and cAMP signalling modulate growth and apical secretion in pollen tubes. *Plant Journal,* **38,** 887-97.

Richens, J. (2008). *Infection thread and nodule development in the Medicago truncatula - Sinorhizobium meliloti symbiosis.* PhD, University of East Anglia.

Riely, B. K., Lougnon, G., Ane, J. M. & Cook, D. R. (2007). The symbiotic ion channel homolog DMI1 is localized in the nuclear membrane of *Medicago truncatula* roots. *Plant Journal,* **49,** 208-216.

Riely, B. K., He, H. B., Venkateshwaran, M., Sarma, B., Schraiber, J., Ane, J. M. & Cook, D. R. (2011). Identification of legume RopGEF gene families and characterization of a *Medicago truncatula* RopGEF mediating polar growth of root hairs. *Plant Journal,* **65,** 230-243.

Roberts, N. J., Morieri, G., Kalsi, G., Rose, A., Stiller, J., Edwards, A., Xie, F., Gresshoff, P. M., Oldroyd, G. E. D., Downie, J. A. & Etzler, M. E. (2013). Rhizobial and mycorrhizal symbioses in *Lotus japonicus* require Lectin Nucleotide Phosphohydrolase, which acts upstream of calcium signaling. *Plant Physiology,* **161,** 556-567.

Routray, P., Miller, J. B., Du, L. Q., Oldroyd, G. & Poovaiah, B. W. (2013). Phosphorylation of S344 in the calmodulin-binding domain negatively affects CCaMK function during bacterial and fungal symbioses. *Plant Journal,* **76,** 287-296.

Rubio, M. C., James, E. K., Clemente, M. R., Bucciarelli, B., Fedorova, M., Vance, C. P. & Becana, M. (2004). Localization of superoxide dismutases and hydrogen peroxide in legume root nodules. *Molecular Plant-Microbe Interactions,* **17,** 1294-1305.

Sagi, M. & Fluhr, R. (2001). Superoxide production by plant homologues of the gp91(phox) NADPH oxidase. Modulation of activity by calcium and by tobacco mosaic virus infection. *Plant Physiology,* **126,** 1281-1290.

Saito, K., Yoshikawa, M., Yano, K., Miwa, H., Uchida, H., Asamizu, E., Sato, S., Tabata, S., Imaizumi-Anraku, H., Umehara, Y., Kouchi, H., Murooka, Y., Szczyglowski, K., Downie, J. A., Parniske, M., Hayashi, M. & Kawaguchi, M. (2007). NUCLEOPORIN85 is required for calcium spiking, fungal and bacterial symbioses, and seed production in *Lotus japonicus. Plant Cell,* **19,** 610-624.

Santos, R., Herouart, D., Sigaud, S., Touati, D. & Puppo, A. (2001). Oxidative burst in alfalfa-*Sinorhizobium meliloti* symbiotic interaction. *Molecular Plant-Microbe Interactions,* **14,** 86-89.

Sathyanarayanan, P. V., Siems, W. F., Jones, J. P. & Poovaiah, B. W. (2001). Calcium-stimulated autophosphorylation site of plant chimeric calcium/calmodulin-dependent protein kinase. *Journal of Biological Chemistry,* **276,** 32940-32947.

Schaefer, A., Hoehner, K., Berken, A. & Wittinghofer, A. (2011a). The unique plant RhoGAPs are dimeric and contain a CRIB motif required for affinity and specificity towards cognate small G proteins. *Biopolymers,* **95,** 420-433.

Schaefer, A., Miertzschke, M., Berken, A. & Wittinghofer, A. (2011b). Dimeric plant RhoGAPs are regulated by its CRIB effector motif to stimulate a sequential GTP hydrolysis. *Journal of Molecular Biology,* **411,** 808-822.

Schauser, L., Roussis, A., Stiller, J. & Stougaard, J. (1999). A plant regulator controlling development of symbiotic root nodules. *Nature,* **402,** 191-195.

Schiefelbein, J. W. & Somerville, C. (1990). Genetic-control of root hair development in *Arabidopsis thaliana. Plant Cell,* **2,** 235-243.

Schiefelbein, J. W., Shipley, A. & Rowse, P. (1992). Calcium influx at the tip of growing root-hair cells of *Arabidopsis thaliana. Planta,* **187,** 455-459.

Shaw, S. L. & Long, S. R. (2003a). Nod factor elicits two separable calcium responses in *Medicago truncatula* root hair cells. *Plant Physiology,* **131,** 976-984.

Shaw, S. L. & Long, S. R. (2003b). Nod factor inhibition of reactive oxygen efflux in a host legume. *Plant Physiology,* **132,** 2196-2204.

Shimoda, Y., Han, L., Yamazaki, T., Suzuki, R., Hayashi, M. & Imaizumi-Anraku, H. (2012). Rhizobial and fungal symbioses show different requirements for calmodulin binding to Calcium Calmodulin-Dependent Protein Kinase in *Lotus japonicus*. *Plant Cell,* **24,** 301-21.

Sieberer, B. J., Ketelaar, T., Esseling, J. J. & Emons, A. M. (2005). Microtubules guide root hair tip growth. *New Phytologist,* **167,** 711-719.

Sieberer, B. J., Chabaud, M., Timmers, A. C., Monin, A., Fournier, J. & Barker, D. G. (2009). A nuclear-targeted cameleon demonstrates intranuclear Ca^{2+} spiking in *Medicago truncatula* root hairs in response to rhizobial nodulation factors. *Plant Physiology,* **151,** 1197-1206.

Sieberer, B. J., Chabaud, M., Fournier, J., Timmers, A. C. & Barker, D. G. (2012). A switch in Ca^{2+} spiking signature is concomitant with endosymbiotic microbe entry into cortical root cells of *Medicago truncatula*. *Plant Journal,* **69,** 822-830.

Smit, P., Raedts, J., Portyanko, V., Debelle, F., Gough, C., Bisseling, T. & Geurts, R. (2005). NSP1 of the GRAS protein family is essential for rhizobial Nod factor-induced transcription. *Science,* **308,** 1789-1791.

Smit, P., Limpens, E., Geurts, R., Fedorova, E., Dolgikh, E., Gough, C. & Bisseling, T. (2007). Medicago LYK3, an entry receptor in rhizobial nodulation factor signaling. *Plant Physiology,* **145,** 183-191.

Song, C. J., Steinebrunner, I., Wang, X. Z., Stout, S. C. & Roux, S. J. (2006). Extracellular ATP induces the accumulation of superoxide via NADPH oxidases in Arabidopsis. *Plant Physiology,* **140,** 1222-1232.

Spaink, H. P., Sheeley, D. M., van Brussel, A. A., Glushka, J., York, W. S., Tak, T., Geiger, O., Kennedy, E. P., Reinhold, V. N. & Lugtenberg, B. J. (1991). A novel highly unsaturated fatty acid moiety of lipo-oligosaccharide signals determines host specificity of Rhizobium. *Nature,* **354,** 125-130.

Steinebrunner, I., Wu, J., Sun, Y., Corbett, A. & Roux, S. J. (2003). Disruption of apyrases inhibits pollen germination in Arabidopsis. *Plant Physiology,* **131,** 1638-1647.

Stracke, S., Kistner, C., Yoshida, S., Mulder, L., Sato, S., Kaneko, T., Tabata, S., Sandal, N., Stougaard, J., Szczyglowski, K. & Parniske, M. (2002). A plant receptor-like kinase required for both bacterial and fungal symbiosis. *Nature,* **417,** 959-962.

Strader, L. C., Chen, G. L. & Bartel, B. (2010). Ethylene directs auxin to control root cell expansion. *Plant Journal,* **64,** 874-884.

Sun, J., Miwa, H., Downie, J. A. & Oldroyd, G. E. D. (2007). Mastoparan activates calcium spiking analogous to nod factor-induced responses in *Medicago truncatula* root hair cells. *Plant Physiology,* **144,** 695-702.

Sun, J., Zhang, X., Deng, S. R., Zhang, C. L., Wang, M. J., Ding, M. Q., Zhao, R., Shen, X., Zhou, X. Y., Lu, C. F. & Chen, S. L. (2012). Extracellular ATP signaling is mediated by H_2O_2 and cytosolic Ca^{2+} in the salt response of *Populus euphratica* cells. *Plos One,* **7**.

Sutton, J. M., Lea, E. J. & Downie, J. A. (1994). The nodulation-signaling protein *NodO* from *Rhizobium leguminosarum* biovar *viciae* forms ion channels in membranes. *Proceedings of the National Academy of Sciences of the United States of America,* **91,** 9990-9994.

Swainsbury, D. J. K., Zhou, L., Oldroyd, G. E. D. & Bornemann, S. (2012). Calcium ion binding properties of *Medicago truncatula* Calcium/Calmodulin-Dependent Protein Kinase. *Biochemistry,* **51,** 6895-6907.

Swarbreck, S. M., Colaço, R. & Davies, J. M. (2013). Plant calcium-permeable channels. *Plant Physiology,* **163,** 514-522.

Tadege, M., Wen, J. Q., He, J., Tu, H. D., Kwak, Y., Eschstruth, A., Cayrel, A., Endre, G., Zhao, P. X., Chabaud, M., Ratet, P. & Mysore, K. S. (2008). Large-scale insertional mutagenesis using the Tnt1 retrotransposon in the model legume Medicago truncatula. *Plant Journal,* **54,** 335-347.

Takanashi, K., Sugiyama, A. & Yazaki, K. (2011). Involvement of auxin distribution in root nodule development of *Lotus japonicus*. *Planta,* **234,** 73-81.

Takeda, N., Haage, K., Sato, S., Tabata, S. & Parniske, M. (2011). Activation of a *Lotus japonicus* subtilase gene during arbuscular mycorrhiza is dependent on the common symbiosis genes and two cis-active promoter regions. *Molecular Plant-Microbe Interactions,* **24,** 662-670.

Takeda, N., Maekawa, T. & Hayashi, M. (2012). Nuclear-localized and deregulated Calcium- and Calmodulin-Dependent Protein Kinase activates rhizobial and mycorrhizal responses in *Lotus japonicus*. *Plant Cell,* **24,** 810-822.

Takeda, S., Gapper, C., Kaya, H., Bell, E., Kuchitsu, K. & Dolan, L. (2008). Local positive feedback regulation determines cell shape in root hair cells. *Science,* **319,** 1241-1244.

Takezawa, D., Ramachandiran, S., Paranjape, V. & Poovaiah, B. W. (1996). Dual regulation of a chimeric plant serine/threonine kinase by calcium and calcium/calmodulin. *Journal of Biological Chemistry,* **271,** 8126-32.

Tang, W. Q., Brady, S. R., Sun, Y., Muday, G. K. & Roux, S. J. (2003). Extracellular ATP inhibits root gravitropism at concentrations that inhibit polar auxin transport. *Plant Physiology,* **131,** 147-154.

Tanimoto, M., Roberts, K. & Dolan, L. (1995). Ethylene is a positive regulator of root hair development in *Arabidopsis thaliana*. *Plant Journal,* **8,** 943-948.

Tao, L. Z., Cheung, A. Y. & Wu, H. M. (2002). Plant Rac-like GTPases are activated by auxin and mediate auxin-responsive gene expression. *Plant Cell,* **14,** 2745-2760.

Tirichine, L., Imaizumi-Anraku, H., Yoshida, S., Murakami, Y., Madsen, L. H., Miwa, H., Nakagawa, T., Sandal, N., Albrektsen, A. S., Kawaguchi, M., Downie, A., Sato, S., Tabata, S., Kouchi, H., Parniske, M., Kawasaki, S. & Stougaard, J. (2006). Deregulation of a Ca^{2+}/calmodulin-dependent kinase leads to spontaneous nodule development. *Nature,* **441,** 1153-1156.

Trinh, T. H., Ratet, P., Kondorosi, E., Durand, P., Kamate, K., Bauer, P. & Kondorosi, A. (1998). Rapid and efficient transformation of diploid *Medicago truncatula* and *Medicago sativa* ssp falcata lines improved in somatic embryogenesis. *Plant Cell Reports,* **17,** 345-355.

Uhrig, J. F., Mutondo, M., Zimmermann, I., Deeks, M. J., Machesky, L. M., Thomas, P., Uhrig, S., Rambke, C., Hussey, P. J. & Hulskamp, M. (2007). The role of Arabidopsis SCAR genes in ARP2-ARP3-dependent cell morphogenesis. *Development,* **134,** 967-977.

van Batenburg, F. H. D., Jonker, R. & Kijne, J. W. (1986). *Rhizobium* induces marked root hair curling by redirection of tip grwoth: a computer simulation. *Physiologia Plantarum,* **66,** 476-480.

Van den Bosch, K. A. & Stacey, G. (2003). Summaries of legume genomics projects from around the globe. Community resources for crops and models. *Plant Physiology,* **131,** 840-865.

Venkateshwaran, M., Riely, B. K., Peiter, E., Otegui, M., Sun, J., Heckmann, A. B., Lougnon, G., Edwards, A., Freshour, G., Hahn, M. G., Sanders, D., Oldroyd, G. D., Downie, A. J., Cook, D. R. & Ane, J. (2008). The putative ion channel DMI1 localizes to the nuclear envelope and regulates nuclear calcium spiking during early symbiotic signaling. *Phytopathology,* **98,** S163-S163.

Venkateshwaran, M., Cosme, A., Han, L., Banba, M., Satyshur, K. A., Schleiff, E., Parniske, M., Imaizumi-Anraku, H. & Ane, J. M. (2012). The recent evolution of a symbiotic ion channel in the legume family altered ion conductance and improved functionality in calcium signaling. *Plant Cell,* **24,** 2528-2545.

Very, A. A. & Davies, J. M. (2000). Hyperpolarization-activated calcium channels at the tip of Arabidopsis root hairs. *Proceedings of the National Academy of Sciences of the United States of America,* **97,** 9801-9806.

Wais, R. J., Galera, C., Oldroyd, G., Catoira, R., Penmetsa, R. V., Cook, D., Gough, C., Denarie, J. & Long, S. R. (2000). Genetic analysis of calcium spiking responses in nodulation mutants of *Medicago truncatula*. *Proceedings of the National Academy of Sciences of the United States of America,* **97,** 13407-13412.

Walker, S. A. & Downie, J. A. (2000). Entry of *Rhizobium leguminosarum* bv. viciae into root hairs requires minimal nod factor specificity, but subsequent infection thread growth requires *nodO* or *nodE*. *Molecular Plant-Microbe Interactions,* **13,** 754-762.

Walker, S. A., Viprey, V. & Downie, J. A. (2000). Dissection of nodulation signaling using pea mutants defective for calcium spiking induced by nod factors and chitin oligomers. *Proceedings of the National Academy of Sciences of the United States of America,* **97,** 13413-13418.

Wang, Y. F., Munemasa, S., Nishimura, N., Ren, H. M., Robert, N., Han, M., Puzorjova, I., Kollist, H., Lee, S., Mori, I. & Schroeder, J. I. (2013). Identification of Cyclic GMP-Activated Nonselective Ca2+-Permeable Cation Channels and Associated CNGC5 and CNGC6 Genes in Arabidopsis Guard Cells. *Plant Physiology,* **163,** 578-590.

Weerasinghe, R. R., Collings, D. A., Johannes, E. & Allen, N. S. (2003). The distributional changes and role of microtubules in Nod factor-challenged Medicago sativa root hairs. *Planta,* **218,** 276-287.

Weerasinghe, R. R., Bird, D. M. & Allen, N. S. (2005). Root-knot nematodes and bacterial Nod factors elicit common signal transduction events in *Lotus japonicus*. *Proceedings of the National Academy of Sciences of the United States of America,* **102,** 3147-52.

Wu, G., Li, H. & Yang, Z. B. (2000). Arabidopsis RopGAPs are a novel family of Rho GTPase-activating proteins that require the Cdc42/Rac-interactive binding motif for Rop-specific GTPase stimulation. *Plant Physiology,* **124,** 1625-1636.

Wu, J., Steinebrunner, I., Sun, Y., Butterfield, T., Torres, J., Arnold, D., Gonzalez, A., Jacob, F., Reichler, S. & Roux, S. J. (2007). Apyrases (nucleoside triphosphate-diphosphohydrolases) play a key role in growth control in arabidopsis. *Plant Physiology,* **144,** 961-975.

Wu, Y. X., Zhao, S. J., Tian, H., He, Y. Q., Xiong, W., Guo, L. & Wu, Y. (2013). CPK3-phosphorylated RhoGDI1 is essential in the development of Arabidopsis seedlings and leaf epidermal cells. *Journal of Experimental Botany,* **64,** 3327-3338.

Wymer, C. L., Bibikova, T. N. & Gilroy, S. (1997). Cytoplasmic free calcium distributions during the development of root hairs of *Arabidopsis thaliana*. *Plant Journal,* **12,** 427-439.

Xie, F., Murray, J. D., Kim, J., Heckmann, A. B., Edwards, A., Oldroyd, G. E. D. & Downie, A. (2012). Legume pectate lyase required for root infection by rhizobia. *Proceedings of the National Academy of Sciences of the United States of America,* **109,** 633-638.

Xu, T. D., Wen, M. Z., Nagawa, S., Fu, Y., Chen, J. G., Wu, M. J., Perrot-Rechenmann, C., Friml, J., Jones, A. M. & Yang, Z. B. (2010). Cell Surface- and Rho GTPase-Based Auxin Signaling Controls Cellular Interdigitation in Arabidopsis. *Cell,* **143,** 99-110.

Yang, G. H., Gao, P., Zhang, H., Huang, S. J. & Zheng, Z. L. (2007). A mutation in MRH2 kinesin enhances the root hair tip growth defect caused by constitutively activated ROP2 Small GTPase in Arabidopsis. *Plos One,* **2,** 12.

Yano, K., Yoshida, S., Muller, J., Singh, S., Banba, M., Vickers, K., Markmann, K., White, C., Schuller, B., Sato, S., Asamizu, E., Tabata, S., Murooka, Y., Perry, J., Wang, T. L., Kawaguchi, M., Imaizumi-Anraku, H., Hayashi, M. & Parniske, M. (2008). CYCLOPS, a mediator of symbiotic intracellular accommodation. *Proceedings of the National Academy of Sciences of the United States of America,* **105,** 20540-20545.

Yokota, K., Fukai, E., Madsen, L. H., Jurkiewicz, A., Rueda, P., Radutoiu, S., Held, M., Hossain, M. S., Szczyglowski, K., Morieri, G., Oldroyd, G. E., Downie, J. A., Nielsen, M. W., Rusek, A. M., Sato, S., Tabata, S., James, E. K., Oyaizu, H., Sandal, N. & Stougaard, J. (2009). Rearrangement of actin cytoskeleton mediates invasion of *Lotus japonicus* roots by *Mesorhizobium loti*. *Plant Cell,* **21,** 267-84.

Yoo, K. S., Ok, S. H., Jeong, B. C., Jung, K. W., Cui, M. H., Hyoung, S., Lee, M. R., Song, H. K. & Shin, J. S. (2011). Single Cystathionine beta-Synthase Domain-Containing Proteins Modulate Development by Regulating the Thioredoxin System in Arabidopsis. *Plant Cell,* **23,** 3577-3594.

Zhang, Y. & McCormick, S. (2007). A distinct mechanism regulating a pollen-specific guanine nucleotide exchange factor for the small GTPase Rop in *Arabidopsis thaliana*. *Proceedings of the National Academy of Sciences of the United States of America,* **104,** 18830-5.

Zhou, X., Chandrasekharan, M. B. & Hall, T. C. (2004). High rooting frequency and functional analysis of GUS and GFP expression in transgenic Medicago truncatula A17. *New Phytologist,* **162,** 813-822.